



MINISTRY OF EDUCATION AND RESEARCH
National University of Science and Technology
Politehnica Bucharest
Doctoral School of
Industrial Engineering and Robotics

Mariana-Cristiana M. IACOB

PhD THESIS

Material Extrusion-based Additive Manufacturing of Foot Orthoses: Customization, Innovative Materials, and Mechanical Characterization

SUMMARY

Scientific supervisor,
Prof. Eng. Diana POPESCU, PhD

Table of Contents

Foreword	3
Chapter 1. Introduction. Medical aspects. Literature review	4
Section 1. Rationale. Structure and objectives of the doctoral thesis.	4
Section 2. Medical aspects. Anatomy of the foot and gait analysis.	5
Section 3. Foot orthoses	7
Conclusions and Contributions	9
Chapter 2. Customized insole design	10
Section 1. 3D Scanning	10
Section 2. Design of the insoles	11
Conclusions, contributions, and dissemination	13
Chapter 3. Design and fabrication of equipment for flexural fatigue testing of insoles	13
Section 1. Study of existing equipment for insole testing.....	13
Section 2. Design of a device dedicated to fatigue testing of insoles	14
Section 3. Prototyping the device dedicated to flexural fatigue testing of insoles.....	18
Conclusions and contributions	19
Chapter 4. Design and manufacture of a device for measuring plantar pressure	20
Section 1. Comfort and its evaluation methods.....	20
Section 2. Plantar pressure data acquisition	21
Conclusions and Contributions	23
Chapter 5. Investigations on the manufacturing of 3D printed insoles from PCL	24
Section 1. AM through MEX with PCL.....	24
Section 2. Manufacturing of PCL Insoles	25
Conclusions and Contributions	26
Chapter 6. Investigations on the manufacturing of 3D printed insoles from PCL	26
Section 1. AM through MEX with TPU	26
Section 2: Printability of low Shore A hardness TPU filaments in the context of custom insole production.....	29
Conclusions and Contributions	32
Chapter 7. Investigations on the manufacturing of 3D printed insoles from	33
Section 1. AM through MEX with varioShore	33
Section 2. Comparative study of the flexural fatigue behavior of insoles made of different TPUs	36
Section 3: Study of customized insoles made from varioShore.....	43
Conclusions and contributions	53
Chapter 8. Results, contributions, conclusions and directions for further research	54
Bibliography	57

Foreword

My first encounter with the world of 3D printing occurred during my master's studies. During this time, I gained valuable knowledge about Additive Manufacturing technology and the types of materials used in various fields, developing a deep passion for 3D printing and the multitude of innovative applications which can be developed. The dynamic evolution and extensive opportunities of Additive Manufacturing based on material extrusion process continued to capture my interest throughout my studies, naturally leading me to pursue my dissertation in this field.

My motivation to use 3D printing in daily life to improve and ease people's life has guided me to explore the application in the orthotics field. In doing so, I discovered how this technology can play an essential role in advancing and developing this domain where personalization is crucial.

The doctoral program has included the preparation, presentation, and completion of exams, as well as the development of scientific reports. The work was also focused on proposing and developing customized foot orthoses produced through material extrusion-based process, investigating new materials and process parameter settings, designing custom insoles based of foot 3D scanning. Additionally, it involved the development of a dedicated prototype system for flexural fatigue testing of the orthoses and a system based on sensors for reading peak plantar pressures. Moreover, seven scientific articles have been published, four of which were as the first author (three in ISI-indexed journals: one in Q1, one in Q2, and one in Q4, and one in a BDI-indexed journal), along with two ISI-indexed articles in Q1 and Q2 journals, and one article as a co-author in the ICMA S conference proceedings. The development and completion of this thesis would not have been possible without the help and support of exceptional individuals.

In this regard, I would like to express my deep gratitude to *Prof. Eng. PhD. Diana Popescu* for her coordination, support, and constant help offered over the years, both in my studies and personal life. Her willingness to share her expertise, experience, and passion for Additive Manufacturing has profoundly impacted my professional, academic, and personal development. She has been a true source of inspiration and motivation, encouraging me to pursue my passions and curiosities.

At the same time, I would like to extend my sincere thanks to the members of the coordination committee: *Assoc. Prof. Eng. PhD. Florin Baci*, *Assoc. Prof. Eng. PhD. Radu Parpală*, *Lecturer Eng. PhD. Tudor George Alexandru* and *Lecturer Eng. PhD. Constantin Stochioiu*, for their valuable suggestions and advice throughout my doctoral studies, as well as for their involvement and contributions to the scientific articles I had the honor of collaborating on with them. I also owe special thanks to the members of the Department of Robotics and Production Systems and the Department of Materials Strength within the Faculty of Industrial Engineering and Robotics, for their solid support, useful advice over the years.

I would also like to thank *Eng. PhD. Petcu Daniel*, a specialist in podiatry, and *Prof. PhD. MD. Rodica Marinescu* from University of Medicine and Pharmacy Carol Davila of Bucharest, for their involvement and expertise. I would also like to express my gratitude to *Assoc. Prof. Eng. PhD. Cosmin Mihai Cotruș* for his collaboration in the preparation of the scientific articles.

I would especially like to express my deep appreciation to my family and friends for their continuous support and constant encouragement throughout my development, standing by me from the very first stages of this journey.

Mariana-Cristiana Iacob

Chapter 1. Introduction. Medical aspects.

Literature review

Section 1. Rationale. Structure and objectives of the doctoral thesis.

According to the International Federation of Podiatrists and the Podiatry Association [1,2], podiatry is the medical branch specialized in the study, prevention, diagnosis, and treatment of deformities, pathologies, and injuries of the foot, as well as foot-related structures. It is directly connected to the overall health of the body through the use of orthopedic footwear and foot orthoses (also known as insoles).

The market for insoles is experiencing significant growth [3], driven by factors such as increasing awareness of the importance of foot health and its direct impact on well-being. The rising prevalence of foot conditions, such as plantar fasciitis, arthritis, diabetes, and musculoskeletal disorders, significantly contributes to this growth. These conditions are primarily caused by the sedentary lifestyles, an aging population, and obesity. For instance, approximately 422 million people globally suffer from diabetes, with most cases occurring in low-income countries. Diabetes is directly responsible for around 1.5 million deaths annually [4]. Additionally, about 1.71 billion people worldwide live with musculoskeletal disorders, often due to demanding work conditions and performance requirements. According to recent reports, the global demand for orthopedic insoles was estimated at \$1.541.2 billion in 2020, with a projected increase to approximately \$2.8 billion by 2026, reflecting a compound annual growth rate of 5.3% between 2021 and 2026.

Additionally, the increase in investments and the intensification of research and development activities in the field have significantly contributed to this market expansion. Investments from both the public and private sectors, along with the involvement of market leaders, particularly stimulated the growth in North America [5]. In Europe, research and development activities, as well as the growing number of manufacturers involved in product manufacturing, are the key drivers of market development [3]. Through the topic addressed in this doctoral thesis and the dissemination of its results, an importance has been placed on including Romania among the contributors to this field by focusing on the use of 3D printing with innovative materials for the customization of insoles. This research is essential for providing innovative and efficient solutions tailored to the increasingly complex and personalized needs of users.

The scientific literature presents a variety of studies highlighting the importance of insoles and their effects on foot conditions in daily activities [6], demonstrating their effectiveness in reducing pain, preventing injuries during running or walking [7] and improving balance in elderly individuals [8]. Insoles have been studied in the context of various disorders such as diabetic peripheral neuropathy [9], where it has been shown that they can reduce the risk of plantar ulcers [10]. They also provide benefits for those affected by flat feet [11], and contribute to the development of systems for diagnosing and rehabilitating foot diseases [12]. Insoles play an important role in maintaining foot health by providing support and comfort. Thus, studies have been conducted to develop insoles for individuals who spend long periods standing [13] or for those engaged in sports activities [14,15].

Advances in material development, digitalization, development of computer-aided design tools, advances in the existing manufacturing processes, and emergence of new manufacturing technologies have all led to the production of more efficient and high-performing podiatric products. Among these new technologies is Additive Manufacturing (AM, also known as 3D printing – 3DP), which has significantly impacted the industry by offering expanded possibilities in terms of material selection and customization options [16,17]. The literature in the field emphasizes the numerous advantages of using AM, the most notable and studied being the ability to create "custom orthotics down to the last detail" [18]. The customization process of insoles begins with a

3D scan of the patient's foot, which is then processed to generate the necessary 3D digital models for 3D printing. Additionally, the digital models of the foot can be enhanced by incorporating information about plantar pressure maps, which are unique to each individual, further personalizing the product.

In the context, the main objective of the doctoral thesis can be formulated as the investigation of customized 3D-printed foot orthotics made by material extrusion (MEX) process using innovative materials, focusing on insoles' comfort, hardness, mechanical strength, and plantar pressure associated with infill variability. This objective required the integration of several skills, including the dedicated design of orthotics, optimization of MEX process parameters, the use of novel materials that have not been previously explored for the field, as well as the evaluation of plantar pressures and their correlation with process parameter values. Achieving this main objective not only that addresses individual needs for insole customization but also contributes to streamlining the production process by reducing manufacturing time and enhancing the quality of the final product. Additionally, the approaches proposed in this thesis offer new and adaptable solutions for treating various podiatric conditions by using materials that can be configured to achieve variable hardness, optimized according to the specific pathology of each patient. This flexibility in material properties enhances the effectiveness of the orthoses in meeting the personalized therapeutic requirements of users.

In addition to this general objective, specific objectives were formulated and achieved:

- **OS1:** Study of foot anatomy and evaluation methods of plantar pressure in healthy versus pathological feet, based on literature data;
- **OS2:** Systematic analysis of the literature on the use of AM in the production of customized insoles;
- **OS3:** Creation of customized designs for insoles based on 3D scanning data, and conducting comparative analyses regarding equipment, software, and post-processing of scans;
- **OS4:** Designing customized insoles using specialized software applications;
- **OS5:** Development of equipment for testing the fatigue life of insoles through bending;
- **OS6:** Development of a sensor-based device for measuring the peak plantar pressure;
- **OS7:** Study of the printability of various categories of materials (rigid polymers, elastomers) for MEX, with the aim of evaluating their use in the manufacturing of customized insoles;
- **OS8:** Analysis of the behavior of elastomeric materials with different Shore A hardness to create insoles that provide comfort and mechanical strength;
- **OS9:** Investigation of the behavior of elastomeric materials with variable Shore A hardness to optimize the properties of the insoles;
- **OS10:** Production of 3D printed insoles with variable hardness, adjusting process parameters to ensure customization;
- **OS11:** Evaluation of the comfort of MEX insoles through usability tests.

Section 2. Medical aspects. Anatomy of the foot and gait analysis.

1.1. Anatomy of the foot and gait analysis

The locomotor system enables the performance of activities and tasks through movement, with the foot, as part of this system, serving as the extremity of the lower limbs and being responsible for supporting the body's weight. The foot has a complex structure consisting of bones, connective elements (ligaments, joints), and muscles. The foot's skeleton is divided into three main segments: the front, middle, and back. The front segment contains fourteen phalanges (the bones of the toes) and five metatarsal bones. The biomechanics of the foot involves movements such as flexion, extension, abduction, adduction, and rotation, which work together to facilitate complex motion.

Plantar pressure is defined as the force exerted by the foot on the support surface per unit area of the sole during walking or in a static position [19]. This parameter provides valuable insights into weight distribution and foot function. Plantar pressure can vary due to several factors, such as the type of physical activity, footwear, the shape and structure of the foot, and the presence of foot conditions or deformities. Therefore, the study of plantar pressure (Fig. 1.1) is instrumental in diagnosing and treating various foot conditions, as well as in developing custom orthotics that alleviate patient discomfort and prevent injuries.

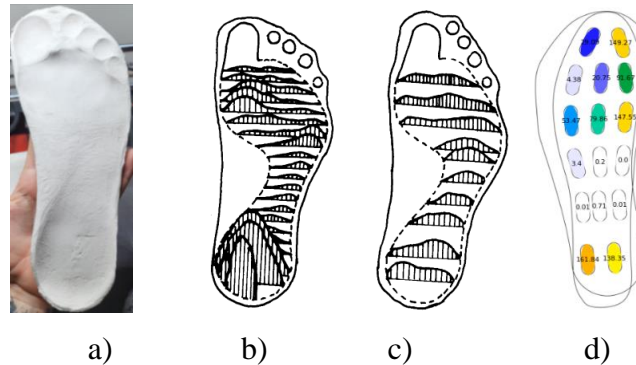


Fig.1.1.1. Plantar pressure: a) footprint [20]; b) pressure map on support surface [19]; c) pressure map on preformed surface [19]; d) plantar pressure map of a healthy foot [21].

1.2. Foot diseases

The normal foot is defined as a foot that, during movement, does not exhibit stresses that exceed the values considered normal in its proximal joints or anatomical structure [19]. In contrast, there are foot conditions that represent organic or functional changes caused by diseases, trauma, or lifestyle choices. The most common local foot conditions include toe deformities (hammer toes), hallux valgus, plantar warts, hyperkeratosis (calluses), plantar fasciitis (painful heel), and Morton's neuroma. Various foot pathologies require the use of orthotics to improve daily activities, alleviate pain, and reduce functional disorders during walking. Among these are flexible flatfoot [22] and rigid flatfoot [23], cavus foot [24], diabetic foot, heel spur, and plantar fasciitis. Neuropathic ulcers are among the most common complications of the diabetic foot, and occur in areas with high plantar pressure, characterized by a central red area and surrounding thickened skin. Ischemic ulcers [25] can also develop on the dorsum of the foot, on the toes, and between them, they are painful and have a red margin with a central area that is yellowish or necrotic. Neuroischemic ulcers [19] are caused by vascular conditions and the onset of neuropathy, which can lead to gangrene and amputations.

1.3. Plantar pressures associated with healthy and pathological feet

The plantar pressure exerted by the foot on the supporting surface, both during movement and stationary activities, is not uniformly distributed across the entire sole [41,42]. Certain areas, such as the heel and the forefoot region near the toes, typically experience the highest pressure values due to biomechanical and physiological factors related to weight distribution, toe movement, or the initial contact of the heel with the ground during walking, as well as the push-off phase during gait, etc. [28].

Existing studies have identified differences in plantar pressure between healthy feet and those affected by various pathologies, such as flat feet or high arches. For example, in [29], a study was conducted on three groups of participants, with average weights of 70 kg for those with normal feet, 69 kg for those with high arches, and 72 kg for those with flat feet. The plantar pressure in the heel area for high-arched feet ranged from 400 to 411 kPa, which was higher than the plantar pressure observed in normal feet. In the case of flat feet, the plantar pressures varied between 336 and 349 kPa, which were lower than that of normal feet, which recorded values of 370 to 378 kPa. Other

significant differences were observed in the hallux area, which exhibited a similar behavior to that described earlier. Thus, for high-arched feet, the recorded values were approximately 280 kPa, for flat feet 523 kPa, and for normal feet 378 kPa.

Research also includes analyses of plantar pressure for diabetic feet affected by calluses [30] or diabetic neuropathy [31]. The study in [30] was conducted on a sample of individuals with weights ranging from 60 to 80 kg. In all groups, plantar pressure showed significant variations.

Section 3. Foot orthoses

1.4. Definition and classification of insoles

Orthoses are external medical devices that support, align, correct, or enhance the biomechanical function of certain body parts, especially joints and limbs.

In the case of foot orthoses (also known as insoles, orthotic insoles, shoe inserts, or plantar supports), these are inserted inside shoes to correct the posture and align the foot, absorb shocks, evenly distribute weight, improve sports performance, align the spine, and treat various foot conditions, contributing to the correction of some of the aforementioned foot anomalies [32].

The manufacturing of insoles provides significant opportunities to create more comfortable, affordable, and durable products. Their therapeutic effectiveness depends on the comfort, adaptability, and durability provided. New technologies, such as 3DP, allow for the development of customized insoles which will gradually replace conventional methods. This transition reflects a similar evolution seen in the field of orthotics for the upper limbs [33], highlighting the potential of AM technology in improving orthopedic treatments.

Figure 1.2 presents a classification of insoles according to different criteria.

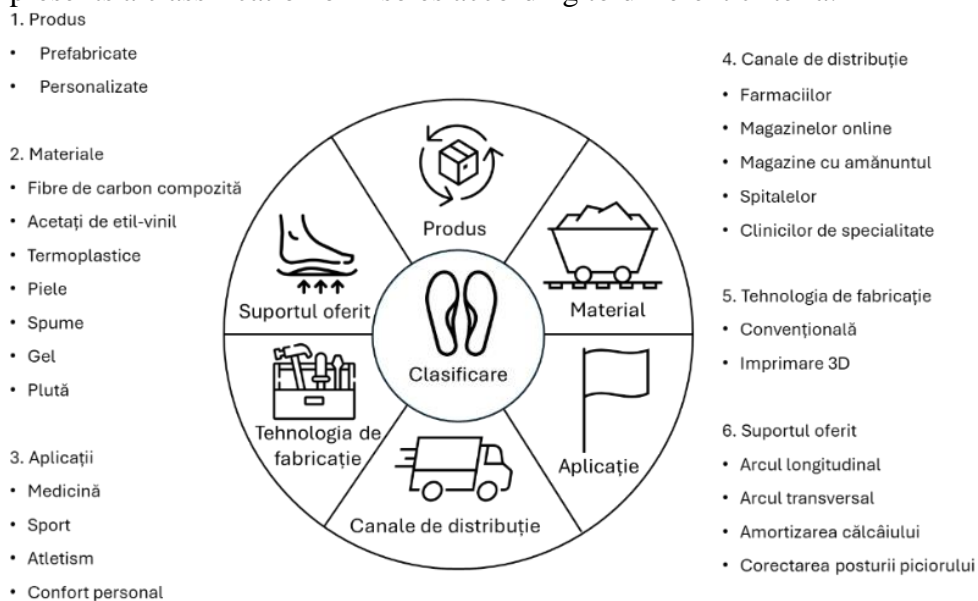


Fig.1.2. Classification of insoles

For the patients with diabetic foot, where foot stability is compromised due to joint damage and the plantar arch [34], customized insoles and appropriate footwear are essential to ensure the protection of these insensate feet [35], reducing the risk of severe complications.

In the case of cavus feet, customized insoles have proven effective in reducing pain by redistributing plantar pressure across the entire support surface [36].

Recent studies, detailed in section 1.6, have shown that 3D-printed insoles can provide biomechanical correction and pain reduction, along with high durability [37], opening the possibility for MEX process to be a reliable alternative to the conventional methods, even surpassing them through the customization of shape and hardness in different areas.

1.5. Manufacturing of insoles

1.5.1. Conventional methods for manufacturing insoles

The first stage in the conventional insole manufacturing involves a detailed evaluation and measurement of the foot to identify the specific needs of the patient, including length, width, and possible structural or alignment issues. In the second stage, based on measurements, an insole’s model is created either in the form of a physical mold or as digital model obtained by 3D scanning.

In the case of using a physical model, wet plaster strips are applied to the foot to contour its shape. The person for whom the mold is being made must remain still for 5-10 minutes until the plaster strips harden. After the mold has hardened, it is removed from the foot and left to dry completely for 24 hours, and then sent to a laboratory for processing and insole production. In contrast, using a digital model through 3D scanning generates a file with the 3D model of the foot. This method allows for the digital storage of 3D models, facilitating the repeated production of insoles [38]. Additionally, the use of a computer-aided design program for insole design, based on pre-programmed templates, simplifies the creation of customized insole models [39].

1.5.2. Manufacturing insoles through AM Technology

The review of literature in the field has shown that insoles are manufactured using AM through the following processes: MEX [40–44]; Stereolithographic - SLA [45]; Selective Laser Sintering - SLS [46–51]. Among these processes, MEX is the most frequently used due to the low cost of equipment (3D printers) and feedstock. Additionally, the range of elastomeric materials available is wider for MEX than for the other mentioned processes. Furthermore, varying hardness in different areas of the insoles can be achieved more easily through MEX. For this reason, the insoles studied in the doctoral thesis were exclusively manufactured through MEX, and the choice of materials was considered a defining criterion in the conducted research. Based on typical materials for MEX, in accordance with the objectives OS7-OS10, several types of materials were investigated and mechanically characterized for the manufacture of insoles: PCL (polycaprolactone), thermoplastic polyurethane (TPU) with different Shore A hardness values, and thermoplastic elastomer with variable density (varioShore).

1.5.3. Comparative analysis of insole manufacturing processes

Insoles manufacturing processes described are compared based on several criteria (Table 1.1).

Table 1.1. Comparison of insole manufacturing methods: traditional vs. MEX

Criteria	Conventional methods	MEX
Production stages	It involves several stages, including mold making, casting, and finishing, all of which are time-consuming. [52]	3D printing layer by layer, without the need for molds. [53]
Customization	Requires the manual creation of custom molds, which can lead to variations in quality and accuracy. [52]	Detailed customization through digital modeling, quickly adjustable. [52]
Durability	Less consistent process due to potential human errors. [52]	Consistency, with high precision due to automated control [52]
Production Time	Production is slow, with many steps and manual finishing, which can take weeks. [52,54]	3D printing significantly reduces production time. [52,54]
Complexity	Complex and influenced by the technician's experience [52,54]	Simplified process, controlled by software and printer technology [52,54]
Accuracy	Precision can vary due to human errors and casting. [52]	Offers very high precision due to digital modeling. [52]
Quality	Material variety and processes can lead to inconsistencies. [52]	Uniformity and consistent quality due to automated control. [52]
Material	Traditional materials such as EVA, polyurethane, and foams. [55]	Utilizes advanced materials, including TPU and other elastomers. [55]

Flexibility	Materials are less adaptable and require post-production adjustments. [55]	High flexibility in adjusting materials according to patient needs. [55]
Storage: Stability and durability	Stable materials, but susceptible to deformation and aging. [55]	Modern materials like TPU exhibit high durability [55]
Storage: Sensitivity to environmental factors	Sensitive to moisture, extreme temperatures, and UV light; can undergo physical changes. [55]	Materials used in MEX can be sensitive to moisture and extreme temperatures. [55]
Storage: Space	Requires large storage space for insoles and molds. [55]	Reduces the need for space due to direct production based on the digital model. [55]
Costs	High costs due to equipment and manual labor. [52,54]	Initial costs may be higher, but long-term efficiency is increased. [52]
Economy	Costs vary significantly based on complexity and production volume [52,54]	Savings achieved through waste reduction and process automation. [52]

1.6. Systematic review of the literature on 3D printed insoles

The literature systematic review in the field was conducted in 2021, and subsequently updated in 2024. Scientific articles in English language were searched in the following electronic databases: Clarivate Web of Knowledge, PubMed, and Scopus, using relevant keywords. Out of a total of 192 identified works, 57 relevant articles were retained after eliminating redundancies and reviewing abstracts. Studies focusing on smart insoles with sensors, the development of new materials for insoles, or those related to 3D printed shoes were excluded. The remaining 57 articles were analyzed to identify common pathologies, types of manufacturing processes, materials, designs, methods of collecting data about the foot, the presence of clinical trials, the number of insoles tested, and evaluations of efficacy. The results are presented in detail in the full length manuscript of the doctoral thesis.

Daryabor et al. [56] published a systematic review and meta-analysis on 3D-printed insoles for flat feet, analyzing ten studies with 225 patients, all treated with customized insoles, with favorable comfort-related results. Xu et al. compared conventional insoles and 3D-printed counterparts among 80 subjects with flatfoot, concluding that 3D-printed insoles are more effective in redistributing plantar pressure and improving comfort [57] Mo et al. [58] conducted a comparative study on runners with excessive pronation, finding no significant biomechanical differences but highlighting a preference for 3D-printed insoles in terms of comfort. Walker et al. investigated the comfort of 3D-printed insoles with variable hardness, showing an advantage over those with uniform hardness [59]. Channasanon et al. evaluated 3D-printed orthoses with variable hardness, finding that they reduce pressure on the heel [60]. Articles in the field also study the influence of infill patterns and density on comfort, such as gyroid structures [61], body-centered cubic structures [62], triply periodic surfaces [63–66], topologically optimized structures [67] and spiderweb-like structures for thermal comfort [68]. FEA method was used in four studies [69–72] for simulating the behavior of insoles under compression, comparing internal structures adapted to plantar pressures. This numerical approach reduces the number of physical tests and shortens the development time.

Conclusions and Contributions

Contributions:

- Systematic analysis of the literature on 3D-printed insoles, identifying trends in foot pathologies studied, exploring the range of materials, and mechanical testing of insoles, which are specific objectives within the doctoral thesis.
- Systematization of data regarding maximum plantar pressure in different areas of the foot, depending on pathology.
- Identification of research niches related to mechanical behavior, the use of numerical analyses, and range of materials for insoles.

Chapter 1 conclusions:

- Foot conditions such as hammer toes, plantar warts, and painful heels affect quality of life, while pathologies like flat feet, cavus, or diabetic feet require insoles for relief.

- Insoles, whether made by traditional methods or 3D-printed, support the foot and redistribute the plantar pressure. 3DP allows for the manufacturing of complex shapes and variable hardness, eliminating the manual steps and slow adjustments of conventional methods. The literature review showed that 3D-printed insoles are at least as effective as traditional ones in redistributing pressure and improving comfort.

- The specialized literature highlights the interest in using 3DP for insole manufacturing, due to the flexibility offered by methods like MEX, which allow the use of various elastomeric filaments and hardness adjustments.

- The thesis emphasizes the need for further research on mechanical resistance and proposes the exploration of new materials adapted to specific plantar pressures.

Chapter 2. Customized insole design

Section 1. 3D Scanning

2.1. 3D Scanning – General aspects

3D scanning is a process of capturing the shape and dimensions of a physical object, creating a digital 3D model that replicates the real object. Equipment varies in their resolution and the distance between the recorded points at a specific scanning distance. The resolution of a 3D scanner is limited by the density of points in the point cloud, meaning that features smaller than the distance between these points will not be captured accurately.

Scanners used to capture the shape of the human body are non-contact devices, including laser scanners, structured light scanners, modular light scanners, and medical scanners [73]. In the case of CT or MRI equipment, 2D sections are usually generated in DICOM format. Laser or light 3D scanners generate a precise point cloud, which can be used for various analyses, feature inspection, surface evaluation, and rapid prototyping.

2.2. 3D Scanning of users' feet for customization of insoles

Depending on equipment availability and the required resolution, three portable scanners were used in the thesis research: Artec Eva Lite (Artec 3D, Luxembourg), Mini 1, and Range 2 (RevoPoint 3D Technologies, China), all based on structured light scanning technology.

Fig.2.1 presents the scanning results using Artec Lite for both feet of a healthy subject, as well as the data processing steps to obtain a viable 3D model. The scanning duration for each foot with Artec Lite was 1 to 1½ hours, with time proportional to the number of captures needed for good resolution in the final 3D model. The acquired data was processed in the dedicated application, Artec Studio 17 Professional.

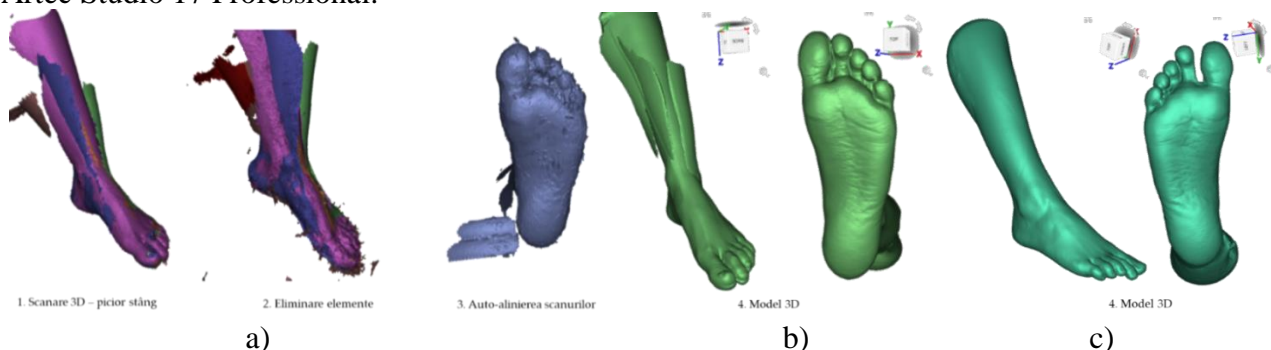


Fig.2.1. 3D Scanning with Artec Lite: a) Post-processing of scans; b) Left foot; c) Right foot.

In comparison, using the RevoPoint Range 2, the scanning duration for each foot was shorter than with Artec Lite, approximately 15-20 minutes per foot. The dedicated Revo Scan 5 software was used to remove unnecessary elements, fill in gaps, and smooth the surfaces, with the reduction of the number of elements also being necessary (Fig. 2.2).

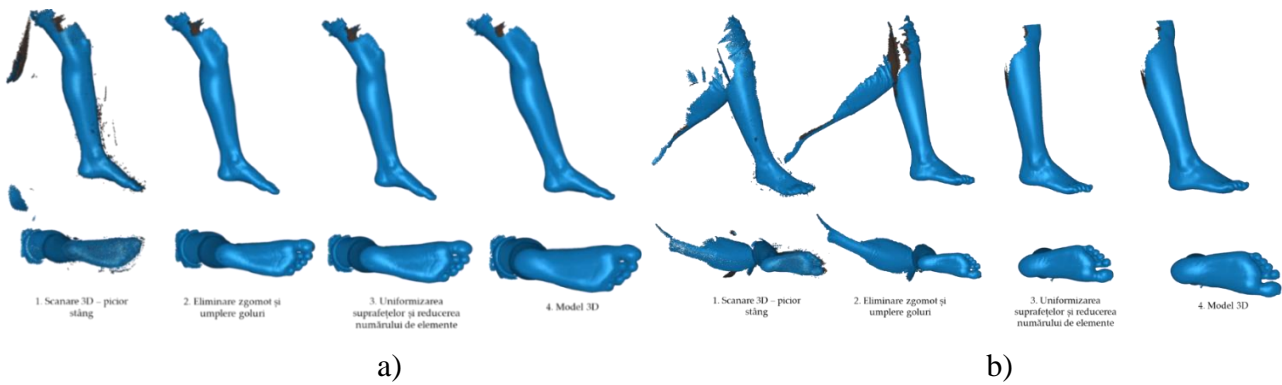


Fig.2.2. 3D Scanning with RevoPoint Mini 3D: a) Left foot; b) Right foot.

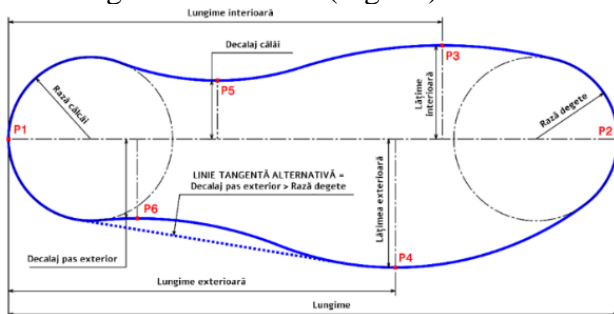
Section 2. Design of the insoles

2.3. Customized insole design using dedicated software applications and 3D CAD software

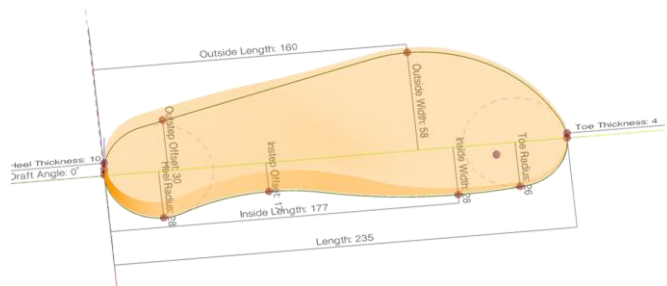
The choice of type and shape of an insole depends on factors such as the presence and type of foot pathology, individual anatomy, type of footwear and activities performed. The research in this doctoral thesis was focused on comfort insoles for individuals spending extended periods standing. These insoles aim to improve cushioning, support the plantar arch, and have customized hardness for comfort. Fig.2.3 illustrates the workflow in Gensole through which the 3D models of the insoles were produced. These steps are part of the personalization process, ensuring not only a perfect fit on the user's foot but also precise delineation of pressure areas. Subsequently, these pressure zones were adjusted in the slicer, using variable densities and fill patterns to optimize comfort (by adjusting hardness) and functionality of the insoles.

AceSole3D is another program dedicated to the custom design of 3D printed insoles (Fig.2.4).

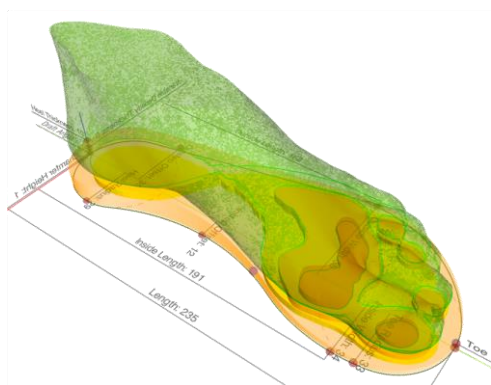
As a general 3D CAD program, the capabilities of Autodesk Fusion 360 were tested for modeling custom insoles (Fig.2.5).



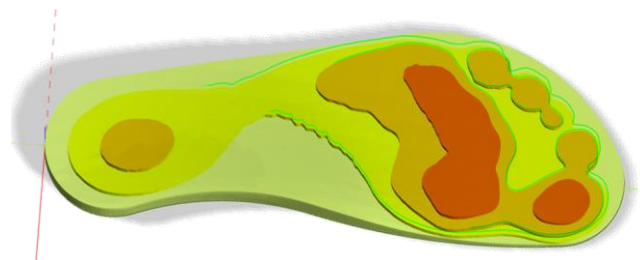
1. Parametrized profile (translation and adaptation based on [74])



2. Personalization of input data



3. Alignment of the 3D Scan with the generated insole



4. Display of pressure points



5. Adjustment of foot arch height

6. Final 3D model of the insole

Fig.2.3. Workflow in Gensole for designing a customized insole

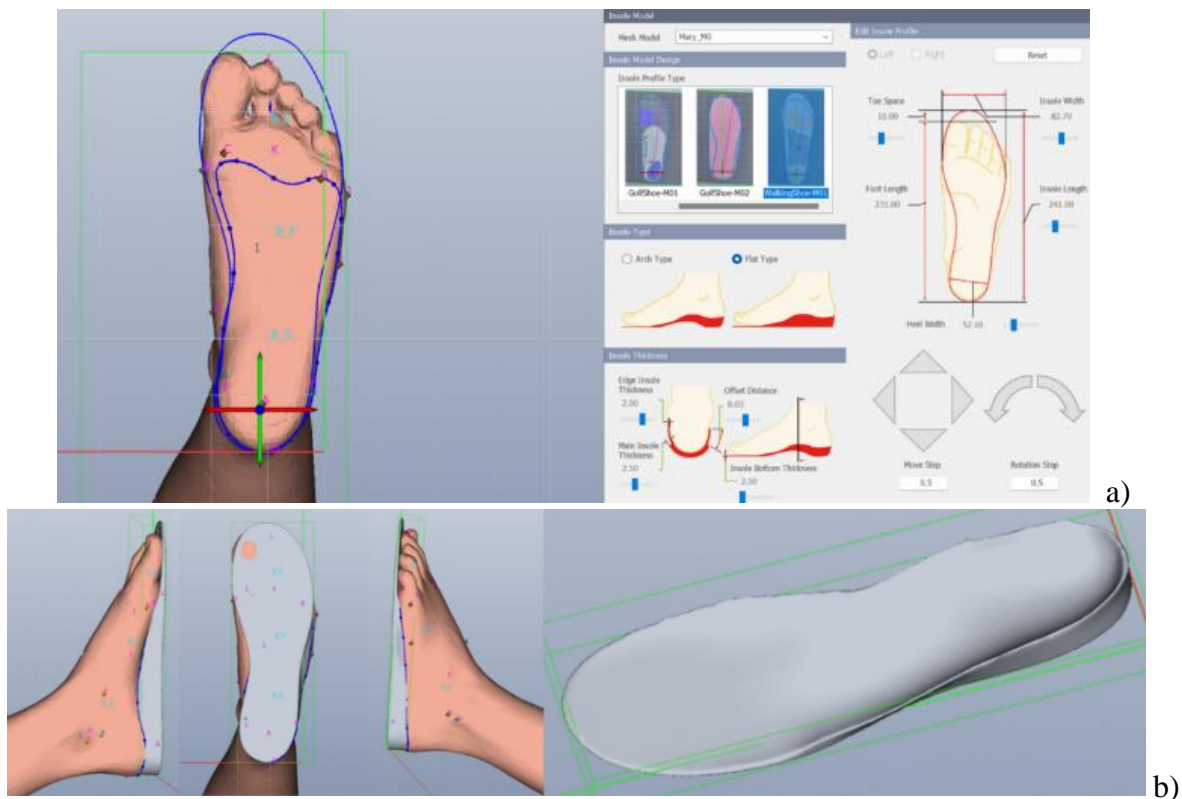


Fig.2.4. Customization in AceSole 3D: a) Parameter selection; b) 3 D Model generation.

Using software such as Gensole, AceSole 3D, and Autodesk Fusion 360, three comfort insole designs were created, fabricated, and utilized (Fig. 2.6), as follows:

- Design 1: 7 mm height and flat foot seating area;
- Design 2: 8 mm height in the metatarsophalangeal, heel, and plantar arch areas, serving as a supportive insole;
- Design 3: 6 mm height and flat foot seating area.

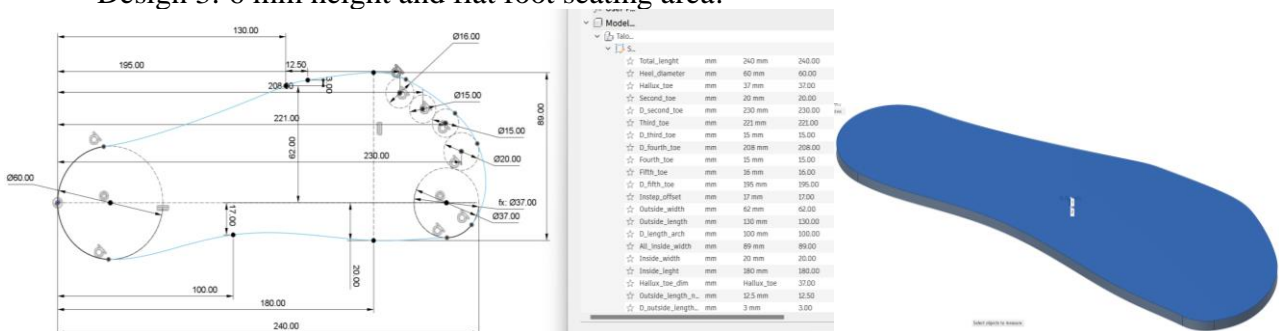


Fig.2.5. Generation of the 3D model of the insole starting from a parametric sketch in Fusion 360

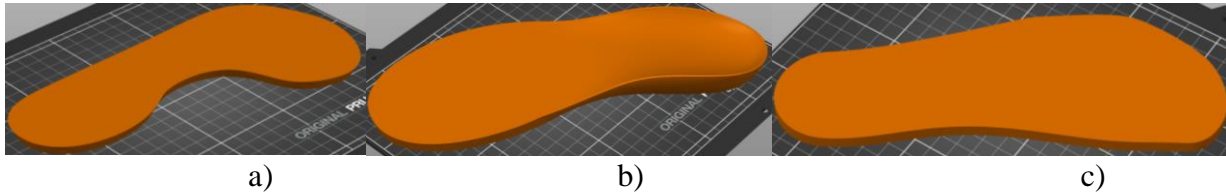


Fig.2.6. Comfort insole designs used: a) Design 1; b) Design 2; c) Design 3.

Conclusions, contributions, and dissemination

Contributions:

- Comparison of three 3D scanning devices from diverse perspectives including accessibility, weight and ease of use, precision, dedicated software friendliness, data scans' post-processing.
- Optimization of the scanning and post-processing processes for 3D foot models.
- Implementation and evaluation of various programs for the design of customized insoles.
- Development of a customized workflow for insole design.
- Generation of three distinct insole designs.

Chapter 2 conclusions:

- Research has demonstrated the effectiveness of using 3D scanning technology and computer-aided design in creating custom insoles, resulting in accurate models of users' feet.
- Contactless 3D scanning allowed for precise capture of foot shapes, essential for customization. Portable scanners provided superior resolution and precision while being easy to use.
- Software applications like Gensole, AceSole3D, and Fusion 360 offered options for developing customized insoles, optimized for user needs.
- The designs created aimed to enhance comfort, support the arch, and distribute plantar pressure for users who spend long hours standing.
- The use of high-resolution scanners and advanced software generated a large volume of data, complicating the post-processing stage.

Chapter 3. Design and fabrication of equipment for flexural fatigue testing of insoles

Section 1. Study of existing equipment for insole testing

No specific equipment dedicated to flexural fatigue testing of insoles was identified, only for outsoles and shoes. An analysis was conducted on shoes testing devices for understanding the functioning of the existing solutions and identifying modalities to design and fabricate equipment specifically for insoles, considering both functionality and cost-effectiveness, as well as execution time. Documenting a variety of fatigue testing systems provided the foundation for developing similar equipment, in-house. In this context, an efficient design was proposed, with component drawings detailed in the annexes of the doctoral thesis, ensuring reproducibility for further research.

3.1. Analysis of existing equipment

The following section presents two of the most relevant examples of testing equipment, used as models in the development of the device described in the thesis.

1. SATRA Performance Footwear Testing [75] – is a professional device designed to evaluate the performance and durability of footwear. The device consists of components that simulate the movements and forces exerted on footwear during use (Fig.3.1).

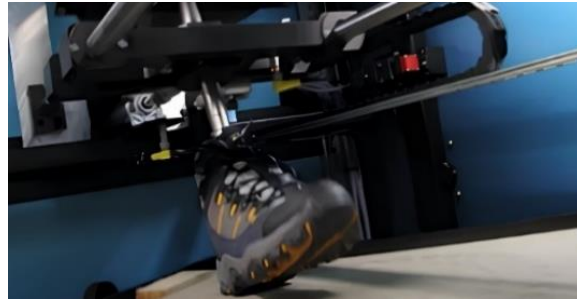


Fig.3.1. SATRA Footwear durability testing equipment [75]

2. Whole Shoes Flexing Tester GT-KA01-2B [76] – is equipment for testing the durability of footwear by simulating walking (Fig.3.2.).



Fig.3.2. GT-KA01-2B Footwear durability testing machine [76]

Section 2. Design of a device dedicated to fatigue testing of insoles

3.2. 3D modeling of the device

The design of the device considered two essential aspects: an analysis of walking, described in Chapter 1, and the requirements from ISO 17707:2005 [77]. The standard defines methods for testing the flexural resistance of insoles, indicating that their support surface should be inclined at a maximum angle of 45° relative to the support plane. Thus, the design focused on this requirement while ensuring the following essential functions: (1) Fatigue stress on insoles - The device must simulate real-life conditions by applying repetitive stress on the insoles to evaluate their durability; (2) Counting load-unload cycles - The device must measure the number of cycles to which the insoles are subjected, determining long-term performance and fatigue life; (3) Allow repeated flexing cycles along the natural flex line corresponding to the metatarsophalangeal area; (4) Be compatible with a wide range of insole sizes, from those for children to adult men; (5) Allow the application of a set pressure in the metatarsophalangeal area to simulate the pressure exerted by body weight on the insoles; (6) Be cost-effective (using wood, 3D-printed parts, standard mechanical components); (7) Include a counter for the flex cycles; (8) Implement a control program that combines insoles' flexion and resting phases.

To ensure the device efficiency, a detailed study of the insole fixation methods was conducted, considering application specifications and plantar pressures in the toe and heel areas, as identified in Chapter 1. The variable sizes of insoles required the development of a custom clamping system to ensure stable and precise fixation, essential for obtaining accurate and reproducible results. The main components of the insole clamping system (Fig. 3.3) are: (1) front support area (corresponding to the toes), (2) front clamping system, (3) hinge connecting the support surface to the clamping system, (4) insole support surface, and (5) heel clamping system. This testing stand was designed with two workstations to reduce the time needed for tests and increase the testing capacity. However, due to financial reasons, the physical prototype included only one workstation.

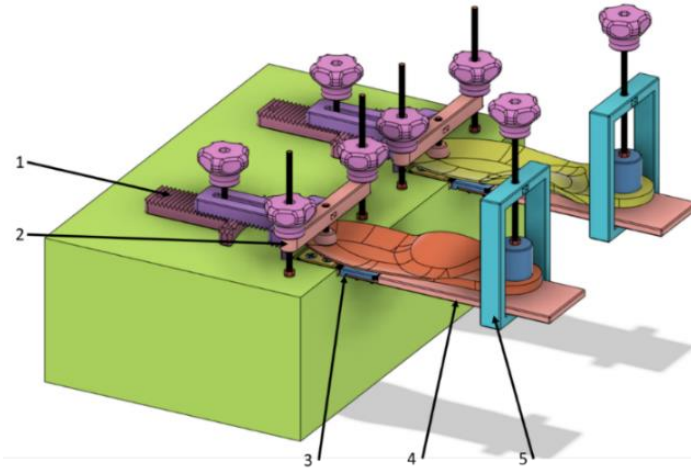


Fig.3.3. Insole clamping system in the device

The motion system of the testing stand (Fig. 3.4) used the crank principle, identified as a solution in other equipment presented in Section 1, which converts rotation movement into translation. The movement is generated by a DC motor (1), equipped with a disc (2) mounted on its output shaft, secured with a square nut (3) and a screw (4). This rotational motion is transferred to the connecting rod assembly (5), which is attached to the disc (2) via a screw (6), nut (7), and washer (8), thus forming a crank. To physically produce the stand's components, several manufacturing drawings were created using the Autodesk Fusion 360 computer-aided design software, starting from the 3D virtual model of the stand (Fig. 3.5).

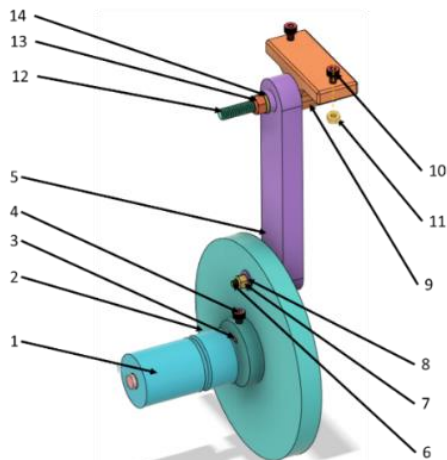


Fig.3.4. Motion system of the device

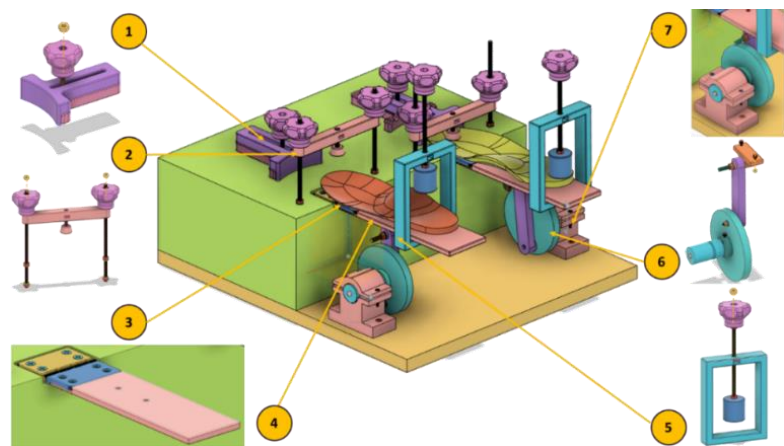


Fig.3.5. Testing stand – digital prototype

3.3. Dimensional accuracy in manufacturing objects through MEX

Many of the components of the device were designed for 3DP to reduce costs. The stand was designed for screw-based detachable assemblies, maintaining the integrity of the parts after repeated disassembles. The dimensional accuracy of the holes for fastening, influenced by 3DP parameters, is essential. Literature offers limited information on the influence of parameters such as layer thickness, printing speed and perimeters [78], extrusion temperature, bed temperature, and material flow rate [79–82], as well as the effect of ultraviolet (UV) radiation on the behavior of plastics like PLA and PET-G [83–85] on the holes' accuracy. For this study, a test piece was designed with 14 through holes of variable diameters ($\text{\O}6$ mm, $\text{\O}8$ mm, and $\text{\O}10$ mm) to [78].

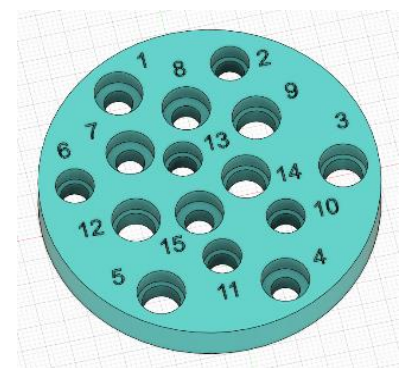


Fig.3.6. Test part

Table 3.2 presents the average values of the hole diameters, as well as information regarding the printing time for each specimen (provided by Prusa slicer). The average diameter for each group of diameters was calculated based on caliper measurements for each of the twelve test pieces.

Table 3.1. Constant and variable process parameters [77]

Constant process parameters		Item	Variable process parameters		
			Perimeters	Layer height (mm)	Print speed (mm/s)
Nozzle diameter	0.4 mm	1	2	0.2	30
Flow material	100%	2	2	0.2	50
Fan speed	100%	3	2	0.2	65
Nozzle temperature	215°C	4	3	0.2	30
Bed temperature	60°C	5	3	0.2	50
Infill density	15%	6	3	0.2	65
Infill pattern	Gyroid	7	2	0.32	30
Extrusion width	0.45 mm	8	2	0.32	50
Bottom/top layers	2	9	2	0.32	65
		10	3	0.32	30
		11	3	0.32	50
		12	3	0.32	65

Table 3.2. Measurement results of specimen hole diameters [77]

Specimen	10 mm– Average diameter values	8 mm– Average diameter values	6 mm– Average diameter values	Printing time	Error (mm)
1	9.866	7.873	5.876	2h 44 min	0.134
2	9.864	7.868	5.844	2h 26 min	0.136
3	9.837	7.840	5.824	2h 25 min	0.163
4	9.800	7.803	5.816	3h 7 min	0.200
5	9.812	7.809	5.785	2h 42 min	0.188
6	9.826	7.778	5.762	2h 36 min	0.174
7	9.784	7.750	5.753	2h	0.216
8	9.774	7.727	5.734	1h 51 min	0.226
9	9.758	7.728	5.688	1h 48 min	0.242
10	9.734	7.698	5.681	2h 12 min	0.266
11	9.718	7.683	5.639	1h 58 min	0.282
12	9.708	7.667	5.630	1h 54 min	0.292

To investigate the statistical significance of the effects of the process parameters on each analyzed diameter, an ANOVA analysis was performed (DF: degrees of freedom; SS: sum of squares; MS: mean square error). The results presented in Table 3.3 showed that for each diameter, the most important influencing factor is the layer thickness, followed by the number of perimeters and the printing speed. In the case of the largest diameter, the p-value indicated that the printing speed does not significantly influence the accuracy of the 10 mm holes. However, the printing speed does influence the accuracy of the 8 mm and 6 mm diameter holes, although it is less relevant than the layer thickness and the number of perimeters.

Among the three variable parameters chosen for the study, it was observed that the layer height is the most influential parameter, followed by the number of perimeters and the printing speed. The printing speed does not have a significant impact on the final product, but it does affect the printing time. Thus, the best quality/time ratio is chosen (Fig. 3.7).

The experiment confirmed the conclusions of Hernandez et al. [86], who observed that a larger contour thickness (0.4 mm and 1.6 mm) and a higher printing speed increase the dimensional deviation of the holes, similar to the conclusions of the current study for three different diameters. Additionally, the trends regarding the correlation between layer height and dimensional accuracy were consistent with the results of Herath et al. [87] and Zhu et al. [88].

Table 3.3. ANOVA results for the measured specimens, by diameter category [77]

Item	DF	SS	MS	F-value	p-value
Analysis of variance for holes with a diameter of 10 mm					
Perimeters	1	0.006769	0.006769	39.1	0
Extrusion width	1	0.02332	0.02332	134.7	0
Printing speed	2	0.0004	0.0002	1.16	0.368
Error	7	0.001212	0.000173		
Total	11	0.031701			
R2: 96.18%	R2 adjusted: 93.99%				
Analysis of variance for holes with a diameter of 8 mm					
Perimeters	1	0.010092	0.010092	143.83	0
Extrusion width	1	0.04296	0.04296	612.26	0
Printing speed	2	0.001597	0.000799	11.38	0.006
Error	7	0.000491	0.00007		
Total	11	0.055141			
R2: 99.11%	R2 adjusted: 98.60%				
Analysis of variance for holes with a diameter of 6 mm					
Perimeters	1	0.013736	0.013736	180.29	0
Extrusion width	1	0.05096	0.05096	668.85	0
Printing speed	2	0.006189	0.003094	40.61	0
Error	7	0.000533	0.000076		
Total	11	0.071419			
R2: 99.25%	R2 adjusted: 98.83%				

The results showed that the printing speed is the least influential factor, which is relevant as it directly affects the time and cost of printing. Additionally:

- Specimen 1 had the best quality, with the most precise holes.
- Specimen 2 provided the best balance between quality and time, with printing taking 18 minutes less than Specimen 1, without significantly compromising quality.

The research in this chapter has been disseminated in the article [77]

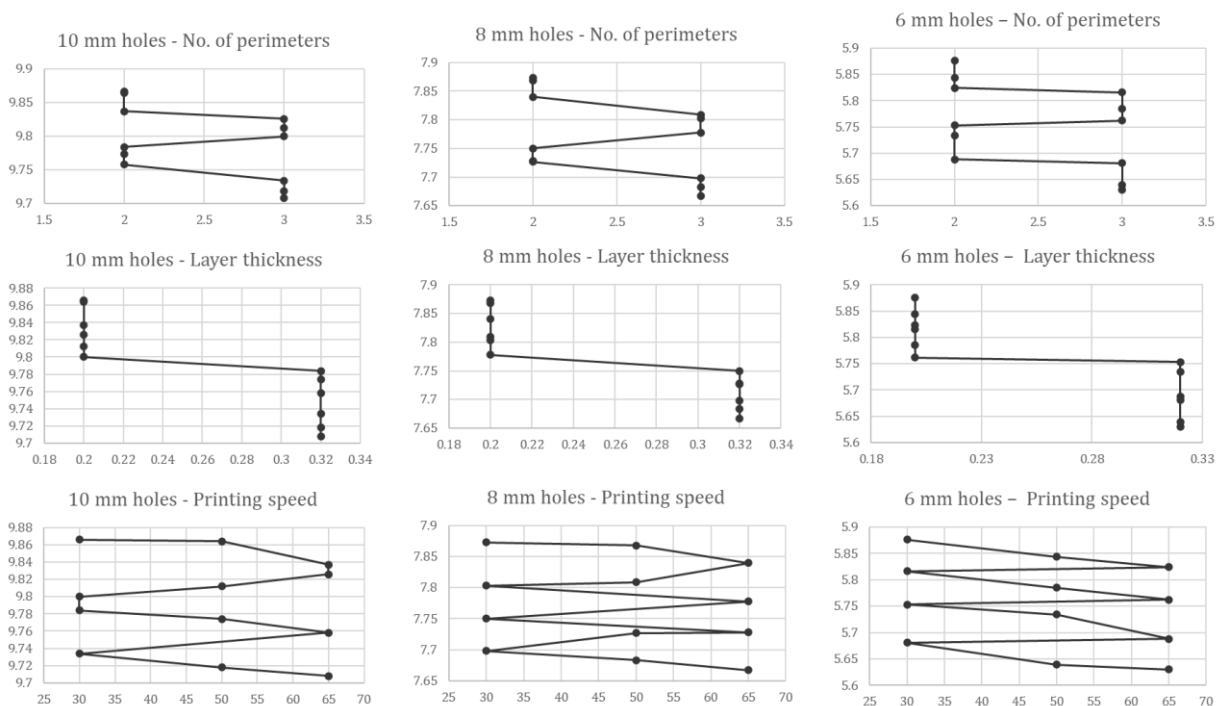


Fig.3.7. Influence of process parameters over holes' accuracy

Section 3. Prototyping the device dedicated to flexural fatigue testing of insoles

3.4. Implementation of the hardware

The process of building the physical prototype of the device, starting from the 3D CAD model, included the following steps:

1. Selection of materials;
2. Acquisition and/or processing of materials;
3. Assembly the parts.

The assembly process and material details are summarized below:

1. Testing stand frame – made of wooden panels
2. Front support mechanism for the insole, made of PLA using MEX (Fig.3.8.)
3. Clamping mechanism for the insole in the toe area – made of PLA using MEX and fixed to the frame (Fig.3.9.).



Fig.3.8. Assembly of the support mechanism – front



Fig.3.9. Assembly of the base plate, handles, and last

4. Hinge, initially manufactured from PLA, after which a commercial variant was chosen to ensure the durability and long-term reliability of the testing stand;
5. Seating surface of the insole, 3D printed from PLA;
6. Insole clamping mechanism – rear, made from PLA and PETG;
7. Driving mechanism of the testing stand – made from 3D-printed components and assembled with screws. The disc that interconnects motor and connecting rod is an essential component that requires high dimensional precision for the passing holes. In the development of this part, data obtained from the study on the dimensional accuracy of 3D-printed holes was used [78].
8. Motor clamping-fixing system, manufactured through 3D printing from PLA, ensuring a precise and stable integration of the motor into the structure of the stand (Fig. 3.10.), then mounted on the wooden frame of the testing stand with the help of wood screws.

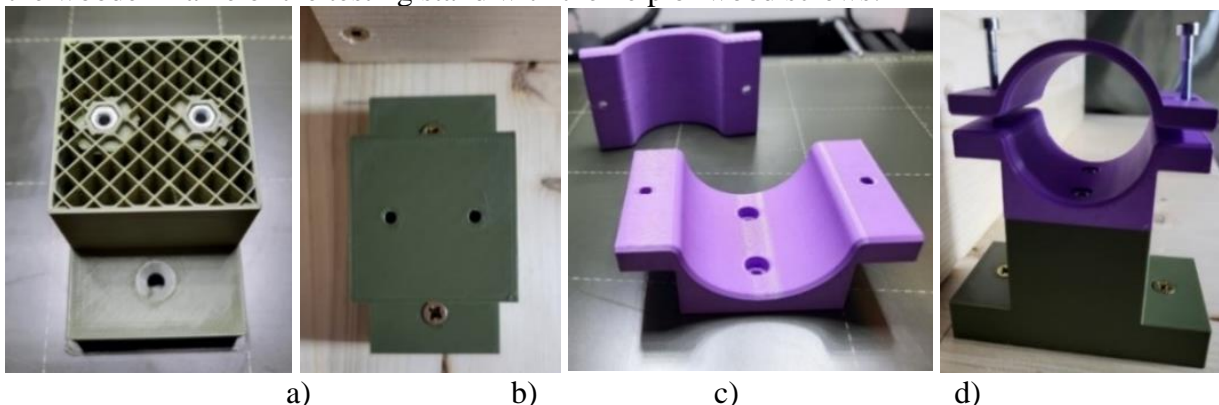


Fig.3.10. Motor support V2: a) Embedding nuts in the fixed part; b) Mounting of the fixed part; c) Mobile part; d) Assembly of the motor clamping-fixing system of the stand.

3.5. Implementation of the control and command system

1. *Development of the basic program:* The testing stand was initially tested using the motor to assess its operational impact on the prototype components. The motor was connected to a 12V power source, both with and without the test piece mounted. Following the test, areas on the motor support (the moving parts) that required additional stiffening were identified. These were redesigned and reinforced according to the new dimensions of the motor and in relation to the fixed part of the support (Fig. 3.11). The motor performs a complete loading-unloading cycle with each rotation, lifting the insole surface to 45° (loading) and returning it to 0° (unloading). Although initially a code was needed to control the inclination, this functionality was then integrated into the design. The connecting rod achieved max angle of 45° relative to the support plane (Fig. 3.12).

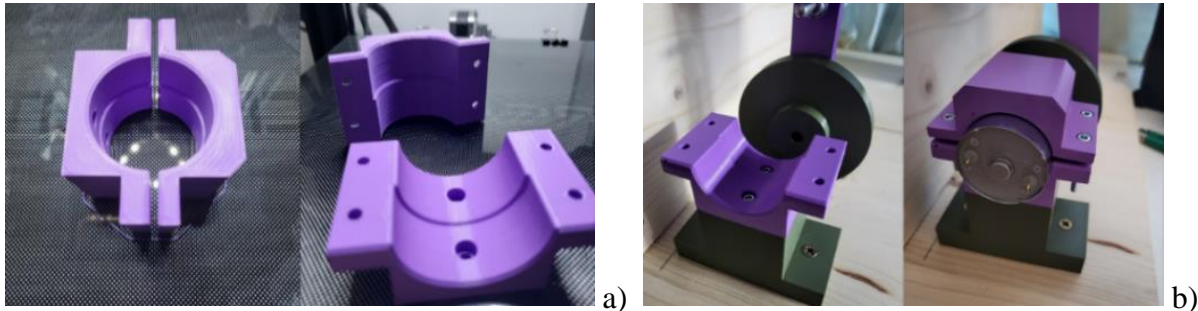


Fig.3.11. Motor support: a) 3DP of the moving parts – V3; b) Assembly of the moving parts V3.



Fig.3.12. Support surface at 0° and at 45° relative to the support plane.

2. *General functions implementation of the stand:* The testing stand was powered through an electrical circuit initially consisting of the following components: 1 x Arduino Uno board; 1 x 12V power supply; 1 x DC motor - Polulu 19:1 gear motor; 1 x toggle switch.

The program for the testing stand was developed in Arduino IDE and tested on the Creality V1.1.3 board.

Conclusions and contributions

Contributions:

- Constructive-functional analysis of existing equipment for testing the fatigue life of shoes and shoe soles;
- Determining the influence of process parameters on the dimensional accuracy of holes obtained directly through MEX;
- Designing and implementing a fatigue testing stand for the insoles flexion around the metatarsophalangeal area;
- Integrating 3DP technology for the fabrication of equipment components;
- Developing a control program for the testing device.

Chapter 3 conclusions:

- The insole testing stand was efficient and compliant with ISO 17707:2005 standards, performing repeated flexion movements of the insoles. The equipment provided precise and reproducible test results, allowing for the evaluation of fatigue life under usage conditions similar with a real scenario;

- 3DP offered flexibility and efficiency in the production of customized parts. Research showed that the dimensional accuracy of the fastening holes primarily depends on the layer thickness, while the numbers of perimeters and printing speed have lesser effect. Optimal results were achieved using a layer height of 0.2 mm and two perimeters;
- 3DP enabled the production of durable and precise components, such as holes intended for fastening, which maintained their exact dimensions during testing conditions. Additionally, aging treatment showed limited effect on the accuracy of these holes;
- The developed control program allowed for the automation and efficient monitoring of tests. The system accurately counted the loading-unloading cycles and confirmed compliance with the code and motor commands;
- The custom 3D-printed trigger proved an effective solution for counting the flexion cycles, ensuring accurate monitoring of the testing process and reducing errors in cycle counting.

Chapter 4. Design and manufacture of a device for measuring plantar pressure

Section 1. Comfort and its evaluation methods

4.1. Analysis of existing studies

The comfort of insoles can be defined as the state of well-being felt by users at the foot level, manifesting both as a physical sensation and as a psychological state, often combining both aspects simultaneously [89]. This definition mainly implies subjective aspects that complicate the precise and consistent evaluation of comfort. However, there are also objective methods for evaluating comfort. While subjective assessment relies on user feedback regarding their experience and perceived sensations, objective assessment uses tools and techniques to measure characteristics such as peak plantar pressure, plantar pressure distribution, and material hardness.

In the thesis, two methods were used to evaluate 3D-printed insoles' comfort:

- The *subjective evaluation* was based on a customized questionnaire in which users rated various aspects of insole comfort (hardness, flexibility, support sensation) on a scale from 1 to 5, where 1 indicates the lowest level of comfort, and 5 the highest. The questionnaire was designed to identify comfort issues and then optimize the parameters of MEX process.
- The *objective evaluation* focused on measuring plantar pressure, providing data on the distribution of forces exerted on the foot. There are a variety of devices and techniques for measuring plantar pressure, including resistive sensors, microcapsules, projection devices, capacitive transducers, and pedoscopes. These techniques can be divided into two main categories:
 - *Qualitative evaluation* provides visual images of pressure distribution on the plantar surface during bipodal or unipodal support. It allows for direct observation of the contact area and pressure distribution, facilitating the identification of areas with excessive pressure. This category includes: plantar imprinting, the pedoscope, the pedobarograph, and 2D and 3D scanners.
 - *Quantitative techniques* for evaluating plantar pressure are used to obtain precise data on the distribution of forces exerted on the surface of the foot. These techniques use sensor-equipped devices to accurately measure plantar pressure.

The solutions for measuring plantar pressure are divided into several categories: devices for measuring bare foot pressure, in-shoe devices, devices placed between the support surface and the shoe (sole-shoe), and devices for measuring shear forces and/or vertical forces.

In the doctoral thesis, in-shoe devices were used, in which pressure sensors are integrated into thin and flexible silicone insoles. These devices exclusively measure vertical forces, providing information about the impact of various interventions on insole comfort. The data collected are associated with the infill structure values of the insole. Thus, for evaluating plantar pressure, two types of devices were used:

- A professional in-shoe system Pedar (Novel, Germany) that measured the pressure distribution, thus allowing to monitoring foot-shoe local loads. The equipment is equipped with insoles featuring capacitive sensors that capture pressure variations exerted on the plantar surface;
- An in-house developed system, designed to provide an economical solution while maintaining essential functionality for pressure analysis.

Section 2. Plantar pressure data acquisition

4.2. Development of the data acquisition equipment

The measurement of peak plantar pressures was carried out with an insole with 16 sensors covered by a transparent silicone layer (Fig. 4.1. a), similar to the one in [90]. According to the manufacturer's specifications, the pressure sensors have the capability to measure weights ranging from 500g to 10kg [91]. In addition to the insole, the system included an Arduino Mega board equipped with an ATmega 2560 microcontroller and 16 analog inputs to connect all the pressure sensors (Fig. 4.2 b). Additionally, it features a flexible printed circuit board with 20 pins and a 1.0 mm pitch, wires, a project board, and 470 k Ω resistors (Fig. 4.2.c-d).

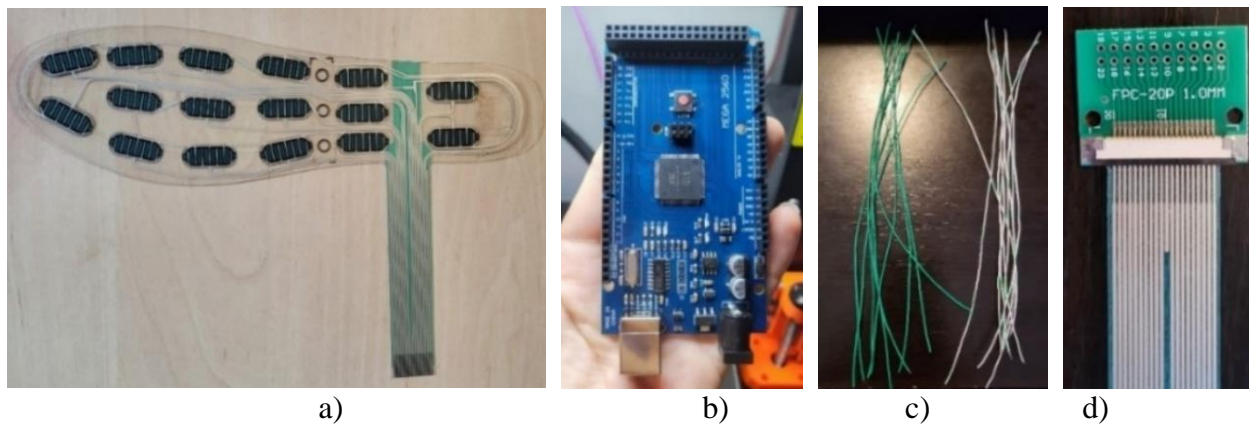


Fig.4.1.1. Components: a) plantar support with sensors; b) Arduino Mega; c) wires; d) FPC

The first stage involved connecting the sensor-equipped insole to the flexible printed circuit. Each of the 16 sensors was assigned a specific trace and a corresponding pin on the circuit, and the insole was configured with 16 analog inputs. Wires and resistors were connected to each line, numbering the wires according to the corresponding sensor (Fig. 4.2. a). The wires were then inserted into a project board (Fig. 4.2. b), and the resistors were placed and connected to 0V/ground and the 12V power source. Subsequently, the connection wires to the Arduino board were added (Fig. 4.2. c), with an example illustrated in Fig. 4.2. d. The Arduino was connected to a computer and powered up, preparing the system for data collection from the sensors (Fig. 4.2. e).

To ensure stability and a fixed position for the sensor-equipped insole, it was necessary to design and 3D print a frame made of PETG. The template covering the frame does not come into direct contact with the electronic insole but is positioned 0.2 mm away from it to avoid any unwanted influence on the measurements. To ensure uniform pressure on the sensors, a 3D printed pad made of TPU Filaflex 70A, with a 100% infill density, was used (Fig. 4.2. f).

The system programming involved the use of two platforms: Visual Studio Code for developing the graphical interface and Python as the programming language, along with Arduino IDE for reading and transforming data from the sensors.

In the first testing phase, a code was created in Arduino IDE designed to check each sensor. The next step involved creating a program to convert the data collected from the sensors into plantar pressure values. Since the sensors do not exhibit a linear increase in values, calibration was necessary using weights of 500g, 1500g, 3000g, and 4500g.

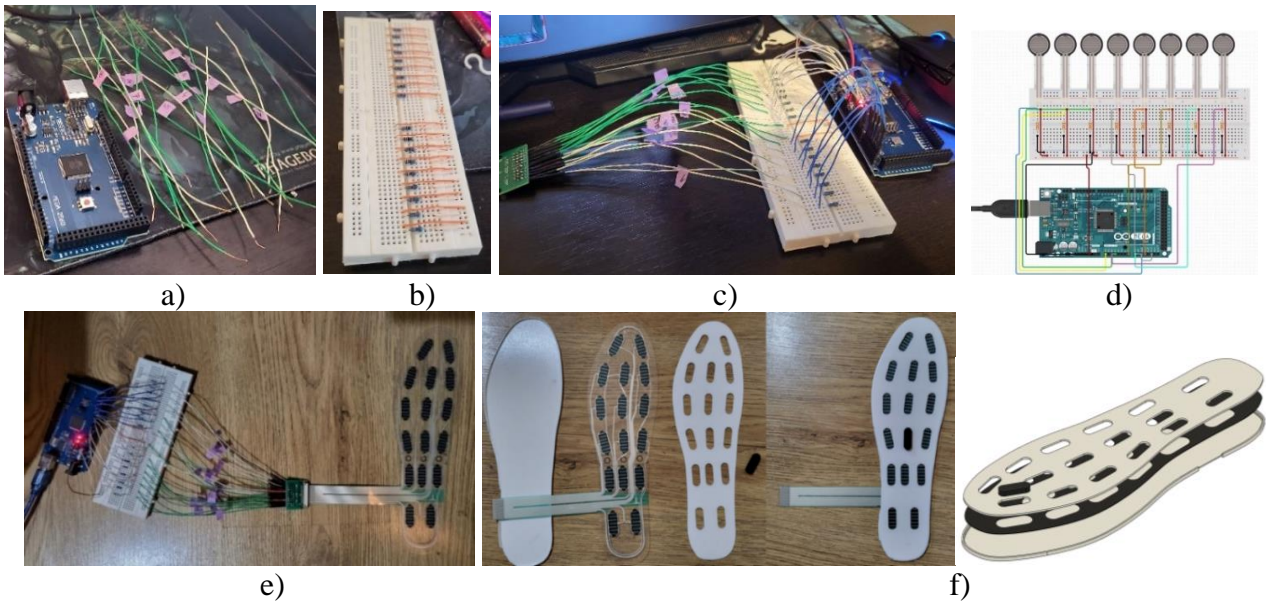


Fig.4.2. Connecting components: a) creating and numbering wires; b) project board; c) assembly of components; d) general schematic; e) the complete system for measuring maximum plantar pressures; f) the frame together with the template and the pad for reading the data.

The development of the user interface code supposed establishing the connection between the interface and the data transmitted by Arduino. To facilitate sensors' identification, a graphical representation reflecting the corresponding positions of the sensors on the insole was created in the interface. This visual representation allowed for real-time monitoring of plantar pressure for each specific area of the foot, ensuring a detailed and intuitive evaluation of the data.

The initial tests, conducted for two users with different mass and foot sizes (Fig. 4.3), facilitated the display of data in an accessible and intuitive format, thereby contributing to a better interpretation of the information collected from the sensors. During these tests, certain sections of the program code which required further development were also identified.

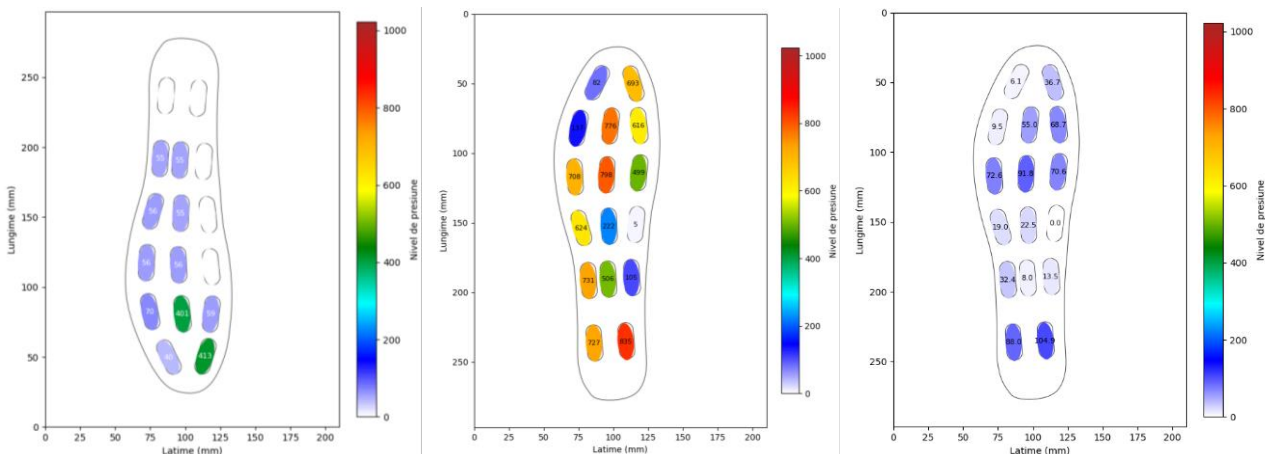


Fig.4.3. Interface tests for the sensor insole

Following tests, a significant difference was observed between the width of the sensor insole and that of the custom insoles, hence the necessity to add of the contour of the custom insole in the user interface for accurate visualization. The measured values were calibrated using mathematical functions and transformed into plantar pressure values in the Arduino code. After testing several calibration methods, individual calibration of each sensor was chosen using exponential functions, which provided more precise results.

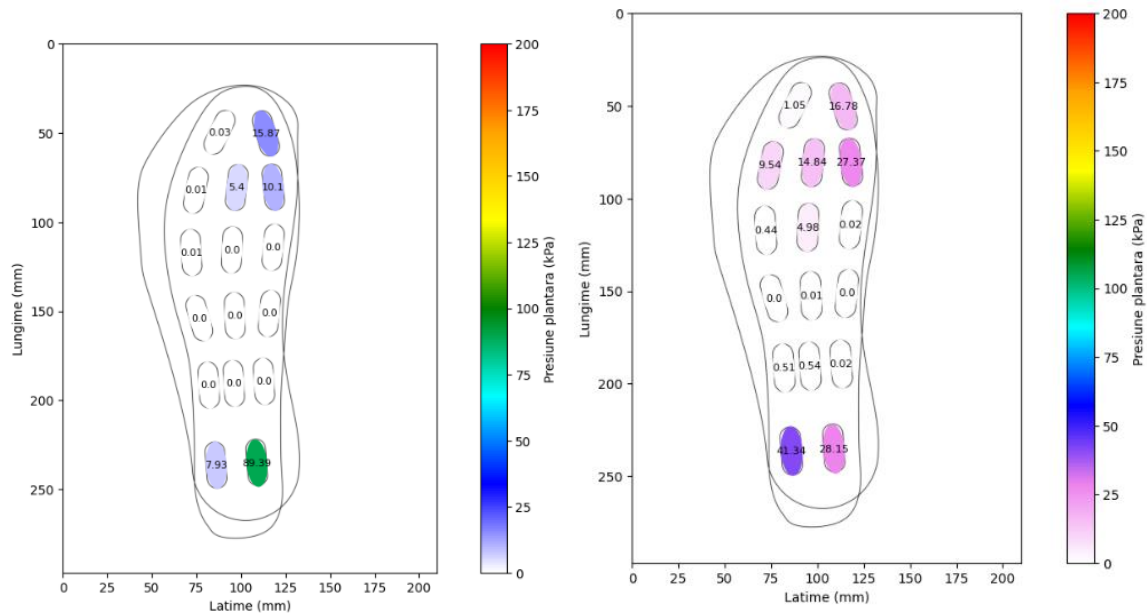


Fig.4.4. Measurement interface after calibration with calibration curve

The exponential calibration function covered a wide range of values, allowing for the interpretation of data. This function encompassed a large range, with recorded values for 500g being around ~80 (raw reading from the Arduino board) and for 4500g around ~112.5. These values were integrated into a Python-based user interface, allowing for adjustments to the density and infill pattern of the insoles to improve pressure redistribution and comfort (Fig. 4.4).

A limitation of the study was that the system developed for measuring maximum plantar pressure, although cost-effective and accessible compared to specialized equipment like the professional Pedar system [16], currently cannot assess plantar pressure during dynamic activities such as walking or running. The system only collected data on static pressure, making it useful for designing insoles intended for individuals who stand for long periods.

Conclusions and Contributions

Contributions:

- Development of an in-house system for measuring plantar pressure – insole with sensors;
- Individual calibration of sensors using advanced mathematical functions;
- Development of a customized visual interface for monitoring plantar pressure.

Chapter 4 conclusions:

- Cost-effectiveness and accessibility - the system uses an insole with 16 pressure sensors integrated with an Arduino Mega board, providing an affordable and functional financial solution suitable for applications with limited budgets, without compromising data quality.
- Calibration and accuracy - by switching to exponential functions instead of polynomial ones, more precise and consistent results were obtained, reducing systemic errors and improving plantar pressure measurement.
- Data integration and visualization - the system is integrated into a visual interface developed in Python, facilitating real-time monitoring and optimizing insole comfort by adjusting the density and infill pattern.
- Limitations and applications - the system is effective for measuring static pressure, but cannot assess plantar pressure during dynamic activities, making it more suitable for users who stand for long periods of time.
- Improvement perspectives - expanding functionality through the integration of advanced sensors and dynamic calibration would increase the system's applicability and measurement accuracy.

Chapter 5. Investigations on the manufacturing of 3D printed insoles from PCL

Section 1. AM through MEX with PCL

5.1. Polycaprolactone: properties, applications and AM through MEX

The literature review in Chapter 1 highlighted several materials suitable for manufacturing insoles through MEX, including both soft materials for comfort and rigid materials for support. Poly(ϵ -caprolactone) (PCL) was identified as a promising candidate due to its biocompatibility and biodegradability, being one of the few fully biodegradable synthetic polymers [92,93]. PCL is frequently used in medical applications and has the advantage of being thermoplastic at low temperatures, the target being to use it for customization through insoles' thermoforming.

The 3D printer used for calibrating and optimizing the PCL profile was the Creality Ender 3 with an enclosed chamber, E3D Revo extruder, and a borosilicate glass bed. Before producing the samples, the 3D printer's software was updated to allow the extruder to operate at temperatures below 170°C, considering that PCL requires lower temperatures for printing. The parameters were then adjusted (Table 5.1), and the results of the modifications were visually analyzed.

Several test parts were produced with different configurations of parameters (Fig. 5.1).



Fig.5.1. Calibration tests

Following the analysis of the samples, it was found that the best results were achieved with the following parameters: variable printing temperature (80°C for the first layer and 75°C for subsequent layers), bed temperature of 45°C for the first layer and 50°C for the remaining layers, material flow rate of 1 mm³/s, and printing speed of 10 mm/s. No significant differences in the dimensions of the parts were observed between printing speeds of 10 mm/s and 20 mm/s. Additionally, thicker samples were also 3D printed, and the optimal bed temperature identified in the tests with lines C proved unsuitable for thicker samples. These samples exhibited a tendency to detach from the platform and deform (Fig. 5.2.).

Table. 5.1. Variable process parameters used for 3DP PCL samples

Parameter	Bed temperature [°C]	Nozzle temperature [°C]	Printing speed [mm/s]	Flow material [mm ³ /s]
Values	25 – room temperature	70	10	
	30	80 → 75	20	0.9
	45	80	30	1
	45 → 50	100	40	1.1
	50	110	50	1.4

A significant issue in 3DP with PCL is the accumulation of material on the print nozzle during the process. Due to slow cooling, the material can deposit in other areas of the part, causing defects. To improve adhesion and minimize these defects, it was decided to disable cooling for the first four layers, after which cooling was automatically activated to 100%.

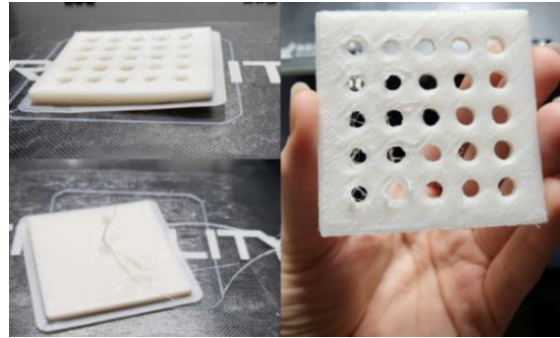


Fig.5.2. Sample detachment and deformation

5.2. Behavior of PCL under different stresses

The samples were subjected to thermoforming tests to verify the hypothesis that PCL can be modified according to the footprint. For example, the sample with holes was exposed to hot water at 53°C for 1 minute, after which it was deformed. Initially, the part showed slight cracks; however, following additional tests conducted at a temperature of 55°C, it completely broke (Fig. 5.3).

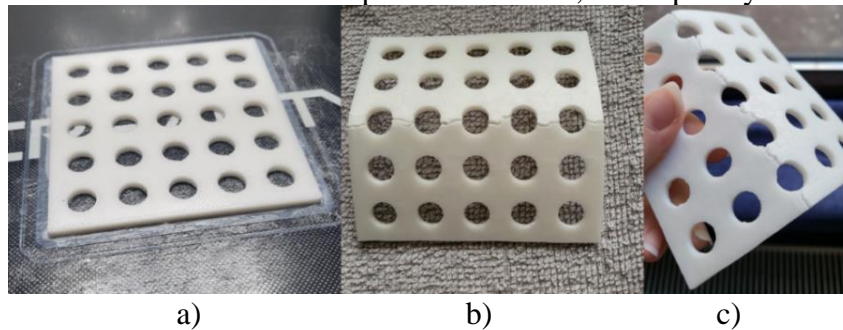


Fig.5.3. Sample with holes: a) 3D-printed sample located on the printer bed; b) sample after the first thermoforming; c) sample after the second thermoforming.

Section 2. Manufacturing of PCL Insoles

5.3. Establishing infilling parameters for the 3D printing of insoles

Considering that the insoles should have variable infill densities in different areas, this stage focused on setting process parameters related to infill density. The test specimens included cubes with a side length of 20 mm and simple shapes of various sizes, similar to the dimensions of the insoles. The process parameters used are detailed in Table 5.2.

Table 5.2. Process parameters

Constant parameters	Values (layer 1 → layer 2)	Variable parameters	Values
Bed temperature [°C]	45 → 50	Infill density	10% 20% 30% 40%
Nozzle temperature [°C]	80 → 75		
Print speed [mm/s]	20		
Flow material [mm ³ /s]	1		
Infill pattern	Gyroid		
Perimeters	0		
Fan speed	0% → 100% (layer 4)		

The PCL samples were tested for manual compression, highlighting differences in behavior based on infill density. The 10% infill sample underwent plastic deformation under low force, while the 20% infill sample exhibited moderate deformation under a mass of 50 kg, maintaining its flexibility. The 30% infill sample did not experience significant deformation, remaining rigid. A similar sample, V2, was tested at 30% and 40% densities, finding that while it was elastic at 30% density, the 40% sample showed brittleness and broke upon manual bending.

Following tests, it was noticed that PCL exhibits brittle behavior at a sample height of 5 mm, suitable for a supportive insole. This brittleness led to the sample breaking under stress, limiting its use for the intended application. A complete insole printed with optimal settings, designed as described in Chapter 2 and generated with the Gensole program [74], showed areas of variable rigidity, with deformations in the thinner regions and rigidity in the thicker ones (Fig. 5.4).



Fig.5.4. Insole made of PCL

Conclusions and Contributions

Contributions:

- Analysis of the suitability of PCL for manufacturing custom insoles through MEX.
- Calibration of process parameters for 3D printing of PCL.
- Testing the thermoformability of 3D-printed PCL.

Chapter 5 conclusions and challenges:

- PCL presents challenges for MEX due to slow cooling and difficult adhesion to the 3D printer bed. Adjusting parameters such as extruder temperature, bed temperature, and printing speed is essential to ensure defect-free parts.
- The first layer requires good adhesion to the printer bed and using a borosilicate glass bed necessitated additional methods to ensure this adhesion.
- Optimal parameters for simple parts did not always apply to more complex pieces, requiring adjustments and additional testing.
- PCL becomes sticky at high temperatures, limiting its applicability under variable temperature conditions.
- Density and thickness influence the behavior of PCL: thick parts become rigid and susceptible to breakage, while thin parts are elastic, but deform more easily.
- PCL does not meet the performance and durability requirements for custom insoles, exhibiting issues with deformability and resistance to dynamic stresses, highlighting the need to explore other materials.

Chapter 6. Investigations on the manufacturing of 3D printed insoles from PCL

Section 1. AM through MEX with TPU

6.1. Establishing process parameters for printing TPU filaments with different shore a hardness

TPU filaments with different Shore A hardness levels were analyzed to evaluate their ability to meet the specific requirements for manufacturing custom insoles through MEX. The analyzed filaments include: Filaflex with hardness levels of 60A, 70A, 82A, and PolyFlex 90A (Table 6.1). The literature review presented in Chapter 1 revealed that not all these filaments have been studied comparatively, which limits podiatry specialists in selecting the optimal material for each patient based on their pathology and plantar pressure distribution.

Table 6.1. Producers' specifications for the studied TPU materials

Material	Material density [g/cm ³]	Shore A hardness [HA]	Material elongation at break [%]
Filaflex 60A [94]	1.07	63	950
Filaflex 70A [95]	1.08	70	900
Filaflex 82A [96]	1.12	82	650
PolyFlex 90A [97]	1.12	90	586

Considering that TPU is characterized by very high elasticity and a high elongation at break, the manufacturing process through MEX is considerably complex. In the case of standard low-cost 3D printers, fabrication may even become impossible without significant technical adjustments. In this context, the doctoral thesis aimed to identify and document the technical solutions and process parameters that would allow the production of customized insoles on standard 3D printers without requiring costly modifications, thus addressing specific objectives OS7-OS9. For manufacturing all the TPU samples in the thesis, the Original Prusa i3 Mk3S+ printer (Prusa Research, Czech Republic) was used, equipped with an E3D Revo 6 extruder, and Prusa Slicer as slicing software.

6.1.1. Preparatory steps for TPU manufacturing by MEX

a) Filament preparation

TPU is hygroscopic and quickly absorbs moisture from the environment, requiring the filament to be dried before 3DP. The drying time varies inversely with the material's hardness. For instance, Filaflex 70A filament underwent a 12h dehydration process, followed by continuous dehydration during printing. Without proper dehydration, TPU undergoes polymer chain breakage during extrusion, significantly affecting the quality of 3D-printed parts (Fig. 6.1).



Fig.6.1. Filaflex 70A

b) 3D Printer preparation

Printing TPU requires the use of a Direct Drive extruder, which reduces the risk of clogging due to the material's high elasticity. E3D Revo 6 extruder ensured a smooth path for the filament, preventing blockages. In comparison, a standard nozzle extruder may not be as precisely machined on the inside, exhibiting irregularities and/or roughness in the filament path.

c) Material path preparation

Due to its high adhesion, TPU can cause blockages during printing. To prevent this, the filament must "flow" freely without being guided through tubes that could lead to kinks. The filament spool was placed above the 3D printer on a special holder to facilitate an even flow and prevent blockages (Fig. 6.2).

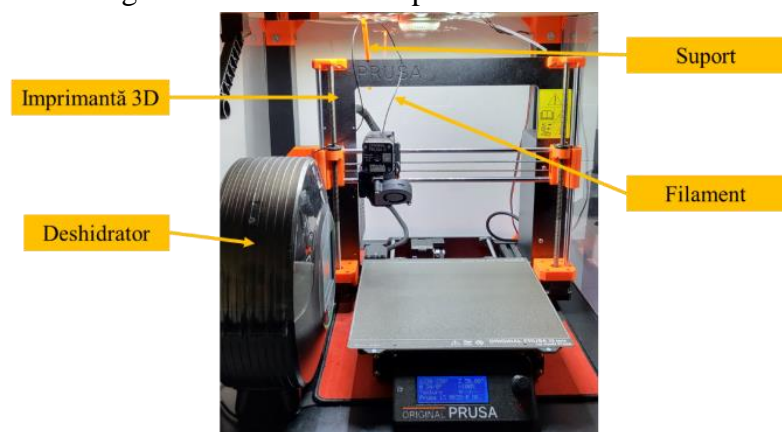


Fig.6.2. The configuration used

d) Print program preparation

Based on the manufacturer's recommendations (Table 6.2.), specific parameters for the 3D printer were calibrated, as described for PCL in Chapter 5. This step is essential to ensure optimal printing and achieve high-quality results by adapting the printer settings (i.e. printing profiles) to the specific requirements of each material.

Tabel 6.2. Manufacturer Recommendations Regarding Process Parameters

Material	Nozzle temperature [°C]	Bed temperature [°C]	Printing speed [mm/s]
Filaflex 60A	215 - 235	21	20 – 30
Filaflex 70A	215 - 235	0 – 40	20 - 40
Filaflex 82A	215 - 235	0	20 - 60
PolyFlex 90A	210 - 230	25 – 60	30 - 60

6.1.2. Filaflex 60A and Filaflex 70A

Filaflex 60A TPU [94] and Filaflex 70A TPU [95] from Recreus (Spain) are elastomers with significantly lower hardness compared to standard TPU variants used in 3DP. With Shore A hardness of 60 and 70, these materials are extremely flexible, and their printing presented a significant challenge. The potential issues that may arise when printing with these highly flexible materials were identified as follows:

- *Filament clogging in the extruder*: occurs when the filament is not correctly inserted into the hotend, causing blockages due to gaps that may remain between the drive wheels and filament entry hole.
- *Excessive friction inside the extrusion nozzle*: results from the thermal expansion of the filament and the material's high adhesion inside the nozzle. Friction intensifies when hardened steel nozzles with higher roughness are used or when there is insufficient cooling in the transition zone (barrel) guiding the material to the nozzle for extrusion.
- *Pressure inside the hotend* – a smaller nozzle diameter increases pressure inside the hotend, which can lead to extrusion problems. Therefore, the nozzle diameter must be inversely proportional to the pressure generated within the hotend.

These issues caused numerous challenges in printing TPU Shore 60A and 70A filaments, requiring detailed investigation of multiple hardware and software settings for defect-free parts.

Calibration tests were conducted using nozzles with diameters of 0.4 mm and 0.6 mm. To calibrate the material extrusion flow, rectangular specimens and cubes with dimensions of 30 mm x 20 mm x 0.65 mm and 10 mm x 10 mm x 10 mm were used, similar to those for PCL printing, to optimize 3D printing for each type of TPU analyzed.

1. 0.4 mm Nozzle

Printing TPU with a 0.4 mm nozzle requires thorough material dehydration because, inside the nozzle, pressure increases, and the presence of moisture in the material causes filament clogging right at the extruder's entry. Additionally, too low a printing temperature can cause the filament to clog at the very beginning of the printing process (Fig.6.3.a), while too high a temperature can damage the filament or the surface of the 3D-printed part due to polymer degradation at excessive nozzle temperatures (Fig.6.3.b).

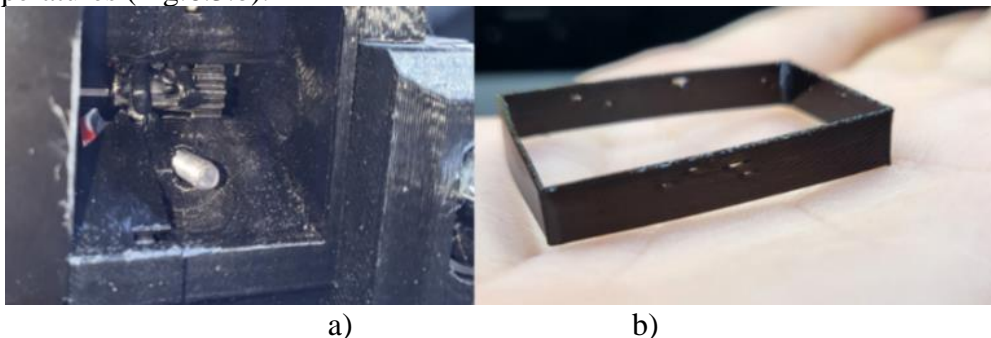


Fig.6.3. Filaflex 60A 0.4 mm nozzle: a) 215°C – filament clogging; b) 235°C – low-quality surfaces.

Based on these observations and through careful calibration of the extrusion temperature, along with adapted cooling (ventilation) for the small size of the parts, the calibration samples for the 0.4 mm nozzle were produced with very good quality and precision. The recorded deviations were

± 0.05 mm for the rectangular specimens and ± 0.1 mm for the cubes, both for Filaflex 60A and Filaflex 70A.

2. 0.6 mm Nozzle

Calibration for the 0.6 mm nozzle was simpler, thanks to the experience gained in overcoming the difficulties encountered with the 0.4 mm nozzle. The same calibration samples were used to check if there was any significant difference in the material flow required for extrusion when switching from the 0.4 mm to the 0.6 mm diameter nozzle, and whether the optimal temperatures identified previously were also applicable for this nozzle. Filament blockages were less frequent due to the larger nozzle diameter, which allows for reduced pressure inside the print head.

Table 6.3. Process parameters used for printing TPU Filaflex 60A and 70A

Material	Nozzle temperature [°C]	Bed temperature [°C]	Printing speed [mm/s]	Flow material [%]	Fan speed [%]
Filaflex 60A	The first layer: 230 Following: 225	0	20	100	50 Disabled for the first 3 layers
Filaflex 70 A	228				

6.1.3. Filaflex 82A & PolyFlex 90A

Filaflex 82A TPU from Recreus (Spain) [96] and PolyFlex 90A TPU from Polymaker (China) [97] are other elastomers used in 3DP, designed to maintain flexibility without affecting extrusion speed, according to manufacturers' specifications. These materials have Shore hardness of 82A, respectively 90A, and are notable for their UV resistance. The calibration process for these materials was simpler, without special adjustments, the same calibration steps described in the previous section being followed. The process parameters used are detailed in Table 6.4.

Table 6.4. Process parameters used for printing

Material	Nozzle temperature [°C]	Bed temperature [°C]	Extrusion/printing speed [mm/s]	Material flow [%]
Filaflex 82A	240	40	20	115
PolyFlex 90A	215	The first layer:40 Following layers: 0	30	98

Section 2: Printability of low Shore A hardness TPU filaments in the context of custom insole production

6.2. Insoles from Filaflex 60A and Filaflex 70A

A flat insole model was designed with Gensole (Chapter 2) to enhance the user comfort. The insole has 6 mm thickness, selected to provide support and effective cushioning while maintaining the shape's integrity inside footwear. 3D scans taken with Artec Eva Lite were used to personalize the insole, also considering the uneven distribution of the plantar pressure, as will be explained further. The adjustments for higher plantar pressure areas were made in Prusa Slicer, allowing the density and fill pattern to be customized in the targeted zones. Parameter modifications were incorporated into the G-code using modifier bodies (Fig.6.4).

1. Evaluation of plantar pressure distribution

To correctly establish the process parameters and identify areas of high plantar pressure, a foot imprinting method in clay was used, prior to the functionality of the insole with sensors described in Chapter 4. This approach allowed for a customized fit adapted to the foot's contours, with the depth of the clay imprint providing data on plantar pressure. Two molds were created for each foot, 3D printed from PETG, ensuring an even distribution of clay. After imprinting, the molds were heated to 60°C for 3 hours, then the solidified clay was fully cured at 150°C for 30 minutes. The resulting imprints were 3D scanned with RevoPoint Mini 3D and processed with Revo Scan 5 software (Fig.6.5).

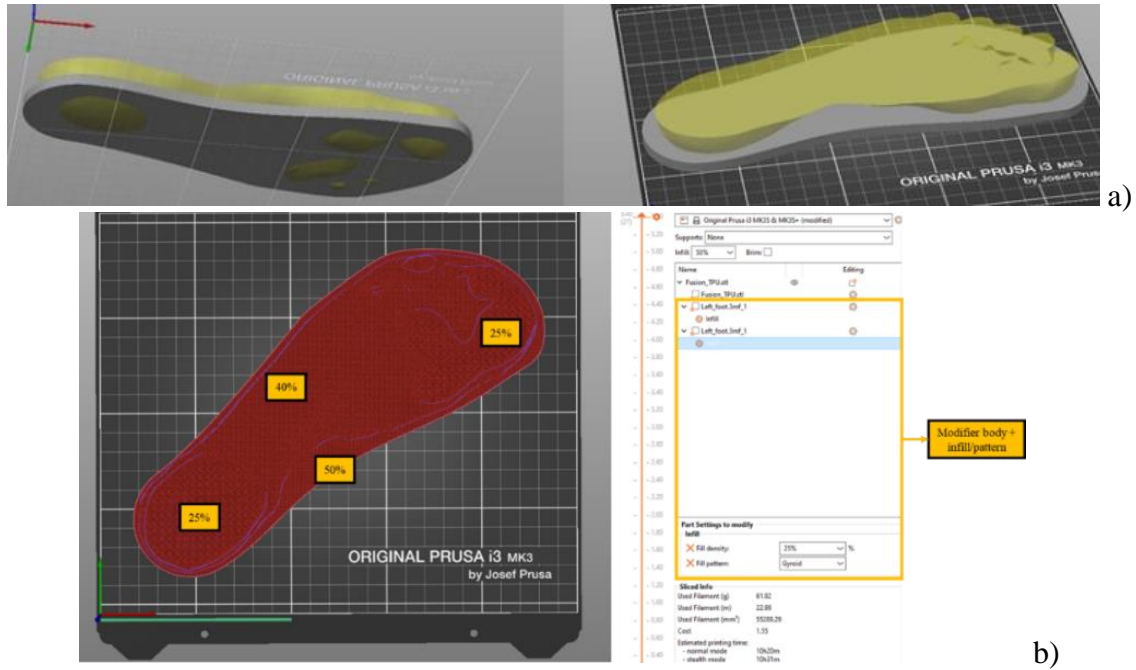


Fig.6.4. Prusa Slicer: a) *Modifier body*; b) *Mesh modifier*.



Fig.6.5. Evaluation of maximum plantar pressure: a) 3D modeling of the molds; b) 3D-printed molds; c) clay formation; d) clay curing shapes; e) hardened clay; f) scans of the foot imprints.

2. Determining the hardness of 3D-printed insoles

The goal of this step was to correlate the hardness values of test samples with the determined plantar pressures to set the infill density values for the insoles based on these pressures. This approach aimed to optimize the internal structure by adjusting the infill density so to provide adequate support in high-pressure areas and comfort in low-pressure areas. To determine the hardness of the insoles created with different process parameter configurations from Table 6.5, eight parallelepiped specimens with dimensions of 40 mm x 40 mm x 6 mm were 3D-printed (Fig. 6.6). The hardness of these specimens was measured using Shore A durometer. The obtained values were correlated with the results of the plantar pressure evaluation previously determined using the

clay model, allowing for the customization of the infill density of the insoles, thus adapting them to the specific pressure values recorded for each area of the user's/patient's foot.



Fig.6.6. Filaflex 60A – specimens and measurement with shore A durometer

The hardness was calculated as the average of 10 random points measured on each specimen. The infill patterns used were gyroid and cubic, with densities of 30%, 40%, 50%, and 60%.

Tabel 6.5. Process parameters used for producing insoles with Filaflex 60A

Dimensions [mm x mm x mm]	No. Crt.	Infill pattern	Infill density [%]	Weight [g]	Shore A hardness
40 x 40x 6	1	Cubic	30	2.89	8.6
	2		40	3.10	10.3
	3		50	3.71	20.75
	4		60	4.42	26.55
	5	Gyroid	30	3.40	15.65
	6		40	3.97	24.65
	7		50	4.50	28.85
	8		60	5.19	35.85

3. Process parameters for 3D Printing TPU insoles

The digital models of the foot impressions, obtained through the steps outlined earlier, were post-processed for thickness analysis. SolidWorks 2022 (Dassault Systèmes, France) was used for this purpose (Fig. 6.7.a). From the analysis, it was observed that the most significant deformation for the right foot insole was 9.47 mm, and for the left foot insole, it was 9.6 mm, both occurring in the heel area. The toe region also recorded higher plantar pressure, although the metatarsophalangeal area exhibited lower pressure (the yellow zones). However, this area is subjected to cyclic bending stresses. The blue zones indicate very low plantar pressure in the arch region. Fig. 6.7.b) shows the pressure graphs for the right and left foot insoles.

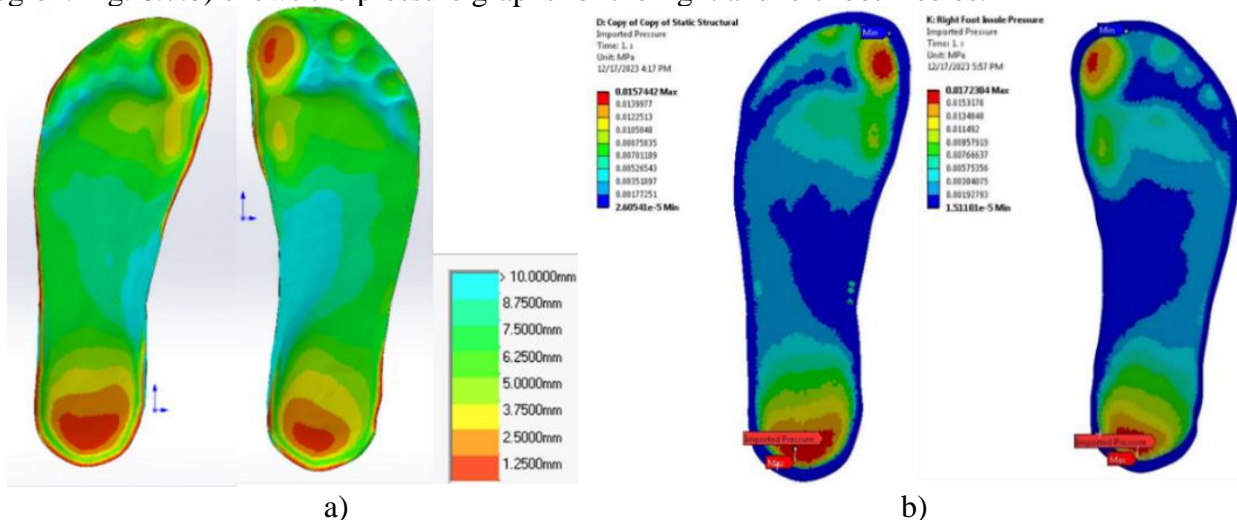


Fig.6.7. Analysis of impressions: a) Thickness analysis with SolidWorks vs. b) Plantar pressure realized with ANSYS for the left and right foot insoles.

A linear approximation was derived to describe the relationship between the measured displacement and the elastic constant. The external data interface from ANSYS Workbench 19.0 was utilized for visualization purposes. In both cases, the maximum pressure was concentrated in the areas of the big toe and the heel. A significant difference of 8.7% was observed between the two graphs, and this behavior aligns with the aspects presented in the previous section.

4. 3D Printing of the insoles

Table 6.6 presents the process parameters used for 3DP the TPU 60A and 70A insoles. The infill densities were customized based on the evaluation of plantar pressures and hardness values (Table 6.5). Thus, two specimens were created for each foot, which were subsequently tested for comfort.

Specimen 1 was 3D-printed with constant 25% infill, while Specimen 2 featured variable infill: the areas marked in green had 40% infill, while those with higher pressure (the red zones in Fig. 6.7.a) had a density of 50% (Fig. 6.8.).



Fig.6.8. Filaflex 60A, left foot insole (25%, 40%, and 50% infill)

Table. 6.6. Process parameters for Filaflex 60A TPU insoles 3D printing

Process parameters	Values
Nozzle temperature [°C]	The first layer: 230; Following: 225
Bed temperature [°C]	0
Printing speed[mm/s]	20, full last layer; 25
Flow material [%]	1.03
Layer height [mm]	0.2
Bottom/top layers	3/2
Infill density and pattern	Specimen 1: Gyroid, 50%
	Specimen 2: Gyroid 25% High plantar pressure, 40% and 50% lowest plantar pressure

5. User experience evaluation

The insoles were tested during normal walking, standing still, and jumping in place for one hour by a healthy user whose footprints were used as a model. The conclusion is that the user prefers the comfort provided by Specimen 2, although Specimen 1 was also considered comfortable.

Conclusions and Contributions

Contributions:

- TPU filaments with different Shore A hardness (Filaflex 60A TPU, Filaflex 70A TPU, Filaflex 82A TPU, and PolyFlex 90A TPU) were analyzed and tested to identify the most suitable solutions for the production of custom insoles.
- In the absence of literature data regarding the printability and behavior of these filaments, the presented printing and optimization methodology constitutes an original contribution to the field.
- Process parameters for TPU on standard 3D printers have been optimized:
 - Through a trial-and-error approach, optimal process parameters for TPU printing were identified and calibrated, ensuring good quality parts on low-cost 3D printers.
 - Tests included adjusting printing temperature, printing speed, cooling, and material flow to overcome challenges encountered with very flexible TPUs, such as those with hardness values of 60A and 70A.

- Customization of the infill density of the insoles was achieved using the clay imprinting method.
- The influence of infill density on the hardness of TPU insoles was evaluated.
- The 3D printing of custom insoles and their evaluation:
 - The manufactured insoles were tested by a healthy user to assess their comfort and performance in everyday use. The evaluation indicated that insoles with variable infill density provided superior comfort in areas with high pressure.
 - Two specimens were produced for each foot, and the observed differences in comfort and hardness levels demonstrated the effectiveness of the proposed methodology.

Chapter 6 conclusions:

Filaflex 60A and 70A highlight the challenges associated with these highly flexible filaments, which require careful adjustment of process parameters to avoid blockages in the extruder and degradation of surface quality. The optimal printing temperatures are 230°C for Filaflex 60A and 228°C for 70A, and calibrations are essential for precision. In contrast, printing with Filaflex 82A and PolyFlex 90A is more straightforward. Filaflex 82A prints at 240°C, offering superior quality, while PolyFlex 90A can also be printed at 215°C. Both materials ensure good inter-layer adhesion and stability during printing, making them preferable for applications requiring a balance between flexibility and durability.

Chapter 7. Investigations on the manufacturing of 3D printed insoles from Section 1. AM through MEX with varioShore

7.1. Establishing process parameters for 3D printing with varioShore

Among the filaments incorporating foaming technology, available options on the market include: Colorfabb LW-PLA and Colorfabb varioShore TPU. While LW-PLA has been a subject of interest in current literature [98,99], varioShore TPU is significantly less investigated and has a high potential for comfort applications, particularly in the context of insole manufacturing [100,101]. While ABS is frequently used for producing custom surgical guides [102], PLA is often employed for orthoses [103] to maintain joint rigidity, while flexible filaments are recommended for custom insoles for various conditions, such as diabetic foot [104].

The literature analysis not only allowed for the collection of information on how process parameters related to internal structure affect compressive strength and hardness, but also revealed the lack of data regarding the calibration process for TPU [105], particularly for varioShore TPU filament [106]. These gaps indicated the need for further research to optimize the printing process and develop precise guidelines for the use of varioShore TPU in comfort applications.

Process parameters such as printing temperature, printing speed, fan speed, or material flow have a significant impact on the degree of foaming of the filament, thus influencing the hardness and compressive strength of the printed parts [107]. TPU filaments with active blowing agents are sensitive to printing temperature. Under the influence of heat, these agents generate voids in the material, thus creating a porous structure that modifies the hardness and mass of the print [107,108]. Fig.7.1. shows the influence of these agents, with investigations performed using SEM (Scanning Electron Microscopy) at the Faculty of Materials Science at Politehnica București, using the Pro-X microscope (Phenom-World, NL). At 190°C, pore expansion is minimal or nonexistent (Fig. 7.2 a). At 220°C, pores have a spherical shape (Fig. 7.2 b), suggesting a medium degree of foaming, while at 240°C, the pores become smaller and more oval or flattened, indicating a greater degree of foaming (Fig. 7.2 c) [109].

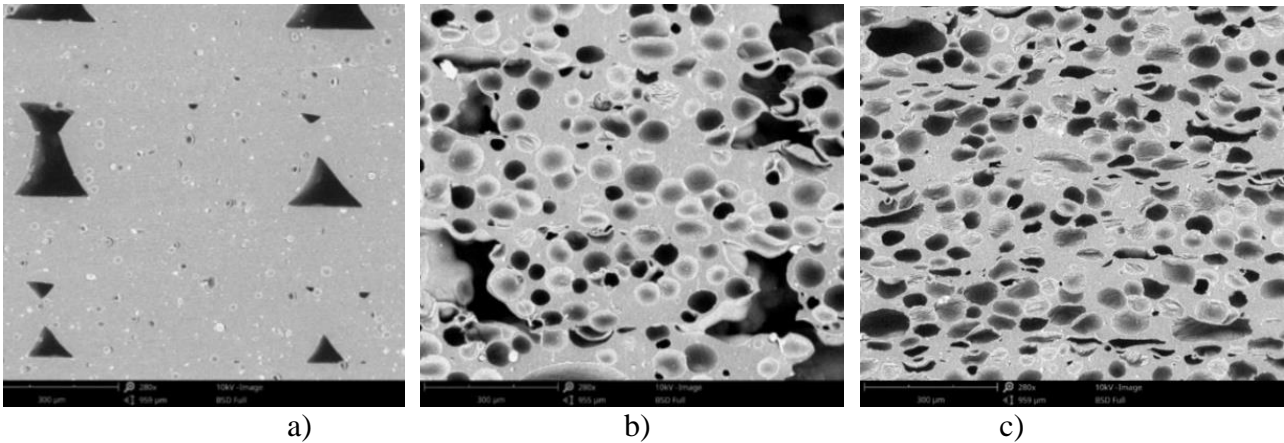


Fig.7.1. Porous structures of cylindrical specimens – SEM Results: a) Specimen 190°C; b) Specimen 220°C; c) Specimen 240°C.

In Fig. 7.2, the porous structure of a parallelepiped specimen with density of 18%, 3D printed at 190°C and 220°C, highlights the differences between the two analyzed temperatures. The transition from 190°C to 220°C was achieved using G-code, specifically the command M104 S220, while the material flow was adjusted from 125% to 60% via the command M221 S48. At the interface between the two zones, noticeable differences in color and pore density can be observed. At 220°C, the foaming agent is activated, resulting in a porous structure, whereas at 190°C, foaming is minimal or nonexistent. The pores at 190°C measure approximately 33.5 μm (Fig. 7.2.a), while at 220°C, their sizes increase to around 223.5 μm due to the merging of multiple pores. In another area (Fig. 7.2 b), the pores at 190°C exhibit a maximum diameter of about 72.5 μm, whereas in Fig. 7.2 c, at 220°C, the pores reach sizes of approximately 206 μm.

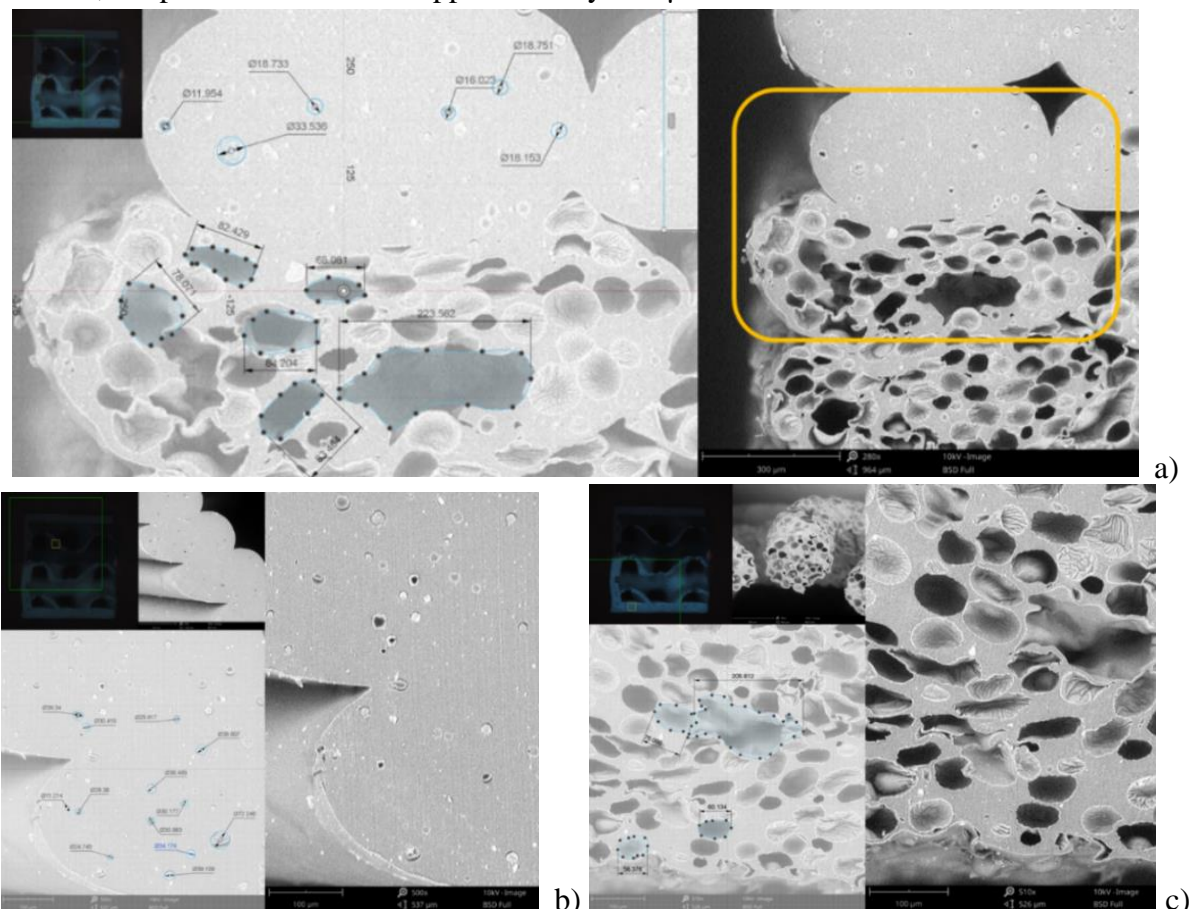


Fig.7.2. Specimen parallelepiped – 18% density: a) 190°C and 220°C; b) 190°C; c) 220°C.

1. Calibration of the printer for varioShore filaments

In the first phase, varioShore filament was 3D printed with the default settings of the profile provided by the Prusa slicer. The extrusion temperature was set to 220°C, and the initial flow rate was set to 85%. Subsequently, an additional test was conducted in which the flow rate was tuned to 58%, according to the reference values from [101]. Considering that the obtained results matched those reported in [101], a fine-tuning incremental adjustment process was applied to achieve the desired dimensions. The main goal of this stage was to reduce flow rate deviations, thus ensuring uniform and precise extrusion throughout the manufacturing process.

Material flow calibration was performed for all temperatures listed in Table 7.1:

- Printing calibration specimens: specimens were produced using the temperature settings established for each test configuration;
- Measuring the dimensions and width of the extruded line;
- Material flow calibration: material flow was adjusted based on the measured dimensions to meet the desired specifications of the printed parts. The samples that achieved the best dimensional values are presented in Fig. 7.3.



Fig.7.3. Material flow calibration tests

Table 7.1. Process parameters used for 3D printing with varioShore

Specimen	Variable parameters	Constant parameters (10x10x10mm)	Constant parameters (30x20x10mm)
	Nozzle temperature [°C]		
1	190	Filament diameter: 1.75 mm Bed temperature: 50°C Infill density: 30% Infill pattern: linear Perimeters: 2 Top/bottom layers: 2 layers Line width: 0.65 mm Layer height: 0.2 mm Printing speed: 35 mm/s No adhesive	Filament diameter: 1.75 mm Bed temperature: 50°C Infill density: 0% Infill pattern: none Perimeters: 1 Top/bottom layers: 0 layers Line width: 0.65 mm Layer height: 0.2 mm Printing speed: 35 mm/s No adhesive
2	195		
3	200		
4	205		
5	210		
6	220		
7	230		
8	235		
9	240		
10	250		

Thus, the necessary values for the material flow rate as a function of temperature for the used printer were obtained. The information presented in this section of the thesis constitutes a detailed calibration methodology intended to serve as a guide for the necessary adjustments for each specific equipment.

At 190°C, the material flow behaved as expected, maintaining the typical characteristics for a TPU filament Shore 92A. However, at 220°C, the activation of the foaming agent led to an increase in the porosity of the extruded material, resulting in a larger volume. This expansion of the material requires an adjustment of the flow rate to restore extrusion accuracy and ensure compliance with the desired specifications. The parameter calibration was followed by the manufacturing of several varioShore insoles and testing their fatigue life in comparison to insoles with a similar design but made from the filaments analyzed in Chapter 6.

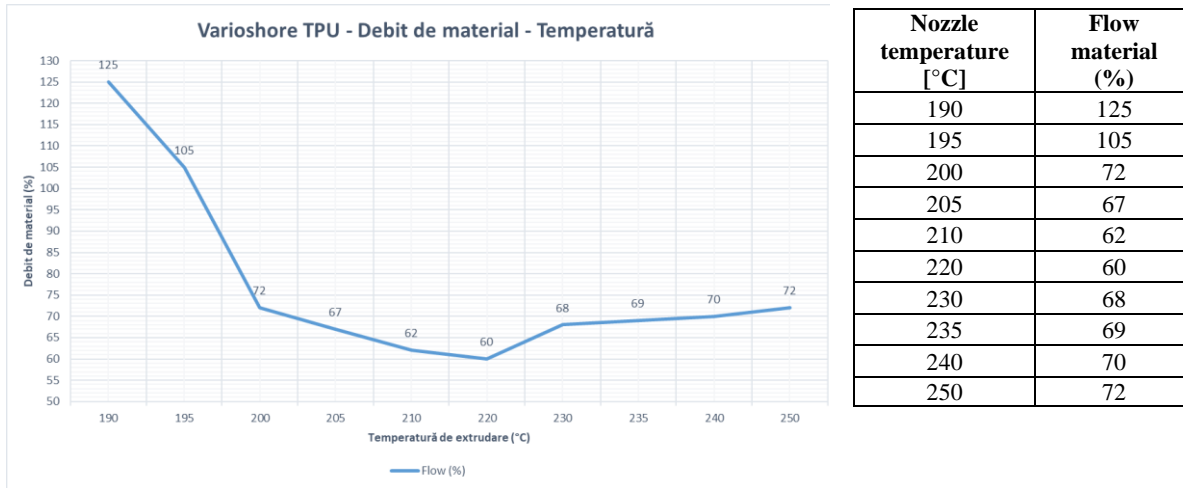


Fig.7.4. Flow material – temperature curve

Section 2. Comparative study of the flexural fatigue behavior of insoles made of different TPUs

7.2. Design, 3D printing, and testing of customized comfort insoles

7.2.1. Insole design

The materials used for 3DP this insole are Filaflex 60A, Filaflex 70A, Filaflex 82A (blue and black), PolyFlex 90A, and varioShore TPU – Fig. 7.5. a) The second insole design (Fig. 7.5. b) has a height of 8 mm in the metatarsophalangeal area, in the heel and arch areas, and was printed with Filaflex 82A, PolyFlex 90A, and varioShore TPU filaments.



Fig.7.5. 3DPrinted comfort insoles: a) Design 1; b) Design 2.

7.2.2. Fabrication of insoles using MEX

The process parameters used for insoles with Filaflex 60A, 70A, 82A, and PolyFlex 90A are shown in Table 7.2. Table 7.3 contains the process parameters for insoles printed from varioShore.

varioShore was used to manufacture two insoles (Fig. 7.6) by adjusting the extrusion temperature to 190°C and 220°C, respectively. These temperatures correspond to the lowest level of foam activation (equivalent to the highest hardness) and the highest level of foam activation (equivalent to the lowest hardness), as presented in the previous chapter. A color difference is observed, indicating the two hardness levels of the material. Thus, one insole (varioShore 1) was entirely printed at 220°C, while the second insole (varioShore 2) had the first five layers printed at 190°C and the remaining layers at 220°C. Design 1 was created using the varioShore 1 and 2

settings, while Design 2 was printed using the varioShore 2 settings. The infill densities of the insoles were uniform across the entire support surface.

Tabel 7.2. 3D printing process parameters for the Filaflex and PolyFlex insoles

Material	Printer settings	Parameter settings
Filaflex 60A	Bed temperature: First layer: 30 °C Other: 0 °C Nozzle temperature: 215 °C Flow rates: 100%	Layer thickness: 0.3 mm Top/bottom layers: 1 Minimum shell thickness top/bottom: 0.7 mm/0.5 mm Perimeters: 1 Infill densities: 25% Infill pattern: Gyroid Printing speed: 15 mm/s Fan speed: 30% Disabled for the first 4 layers, full at layer 6
Filaflex 70A	Bed temperature: First layer: 40 °C Other: 0 °C Nozzle temperature: 228 °C Flow rates: 78%	Layer thickness: 0.3 mm Top/bottom layers: 1 Minimum shell thickness top/bottom: 0.7 mm/0.5 mm Perimeters: 1 Infill densities: 25% Infill pattern: Gyroid Printing speed: 15 mm/s Fan speed: 30% Disabled for the first 4 layers, full at layer 6
Filaflex 82A	Bed temperature: 40 °C Nozzle temperature: 240 °C Flow rates: 115%	Layer thickness: 0.3 mm Top/bottom layers: 1 Minimum shell thickness top/bottom: 0.7 mm/0.5 mm Perimeters: 1 Infill densities: 20%, 25%, 40% in different zones of the insoles Infill pattern: Gyroid Printing speed: 20 mm/s Fan speed: 50% Disabled for the first 4 layers, full at layer 6
PolyFlex 90A	Bed temperature: 215 °C Nozzle temperature: 40 °C Flow rates: 98%	Layer thickness: 0.3 mm Top/bottom layers: 1 Minimum shell thickness top/bottom: 0.7 mm/0.5 mm Perimeters: 1 Infill densities: 20%, 50% in different zones of the insoles Infill pattern: Gyroid Printing speed: mm/s Fan speed: min. 30% - max. 50% Disabled for the first 4 layers, full at layer 6

Tabel 7.3. 3D printing process parameters for the varioShore insoles

Material	Fixed parameters	Variable parameters
varioShore 1	Bed temperature: 50 °C Layer thickness: 0.3 mm Top/bottom layers: 1 Minimum shell thickness top/bottom: 0.7 mm/0.5 mm Perimeters: 1 Infill pattern: Gyroid Printing speed: 35 mm/s First layer printing speed: 10 mm/s Fan speed: 60% Disabled for the first 4 layers, full at layer 6	Nozzle temperature: 220 °C Flow rates: 60% Infill density: 25%
varioShore 2		Nozzle temperature: 190 °C (the first 1.4 mm) & 220 °C Flow rates: 110% & 60% Infill density: 20%

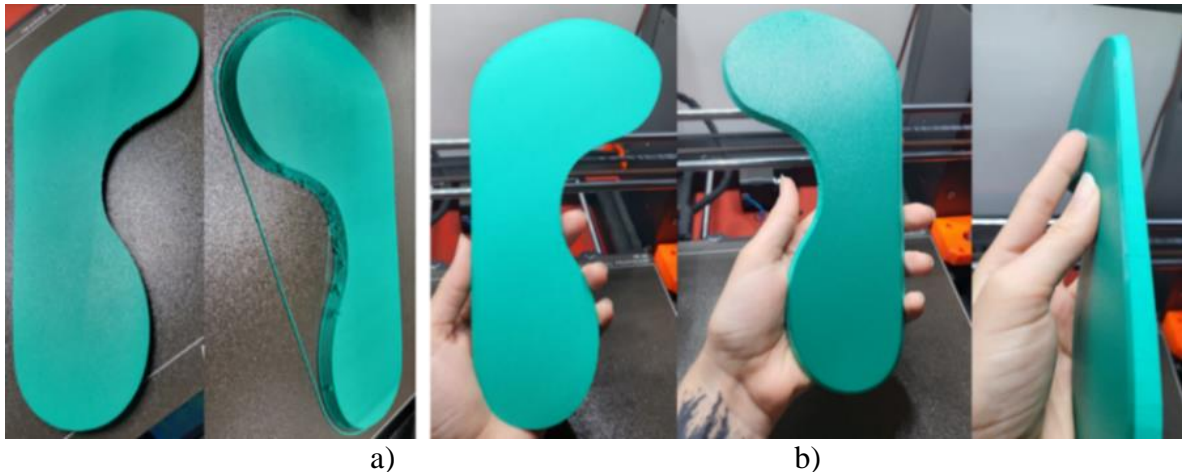


Fig.7.6. varioShore insoles: a) At 220°C; b) At 190°C and 220°C.

A direct relationship was observed between the extruded material flow and the printing temperature, which required the calibration of these parameters to prevent printing errors. At 190°C and a flow rate of 1.25, difficulties were encountered in extruding the material due to its softness and its tendency to heat quickly in the extruder, while reducing the printing speed led to filament deformation. Tests demonstrated that a material flow rate of 1.1 provided satisfactory results, although small defects were observed at 220°C, especially when adjusting the layer placement angle. The settings necessary for printing the insoles were made by modifying the G-code directly from the slicing software, introducing new lines of code to optimize the printing process.

7.2.3. Fatigue testing of insoles

The fatigue testing of the insoles was conducted on the experimental setup presented in Chapter 3. Additionally, the insoles were tested by a healthy user specialized in podiatry. In all cases of bench testing, the insoles were subjected to sets of 7,000 cycles (this value being the daily medical recommendation [110]), followed by visual evaluation and monitoring of distinctive sounds generated by the degradation of the internal structure when pressed with a finger. The test simulated the daily wear and tear of insoles, alternating periods of fatigue stress with rest periods. In the absence of any signs of degradation, the tests were stopped after 700,000 cycles (steps).

The insoles were tested as follows:

1. Design 1:

- Filaflex 60A – flexural fatigue on the testing device;
- Filaflex 70A – flexural fatigue on the testing device;
- Filaflex 82A (blue) – daily use followed by flexural fatigue on the testing device;
- PolyFlex 90A - flexural fatigue on the testing device;
- varioShore 1 – flexural fatigue on the testing device;
- varioShore 2– flexural fatigue on the testing device;

2. Design 2:

- Filaflex 82A (black) – daily use;
- PolyFlex 90A - flexural fatigue on the testing device;
- varioShore – flexural fatigue on the testing device;

7.2.4. Daily wear testing

Two of the insoles (Filaflex 82A black, design 1, and Filaflex 82A blue, design 2) were subjected to wear through daily use by the user. The Filaflex 82A black insole underwent approximately 200,000 steps, after which it was stored on a shelf for almost a year before being tested for fatigue on the test stand. Similarly, for design 2 made from Filaflex 82A blue, the insole was worn for 423,452 steps over 203 days/7,000 steps per day. After 310,000 steps, the Filaflex

82A blue, design 2 insole was evaluated with the professional Pedar system (Novel GmbH, Germany), and the data were compared with the original shoe insoles (Fig. 7.7).



Fig.7.7. In-Shoe Pedar pressure measurement system: a) 3D printed blue Filaflex 82A insoles (left); b) Original shoe insoles (right).

7.2.5. Measuring the hardness of 3D printed insoles

The hardness of the 3D printed TPU insoles was measured with a type A durometer, by taking measurements at several points on their surface (Fig. 7.8) and calculating the arithmetic mean of the values obtained. Immediately after the insoles were manufactured, their hardness was measured at 30 points. After the insoles were tested for fatigue through bending, another 30 measurements were taken in the most stressed areas of the insoles. The second hardness measurement was conducted approximately 36-48 h after the stand testing.

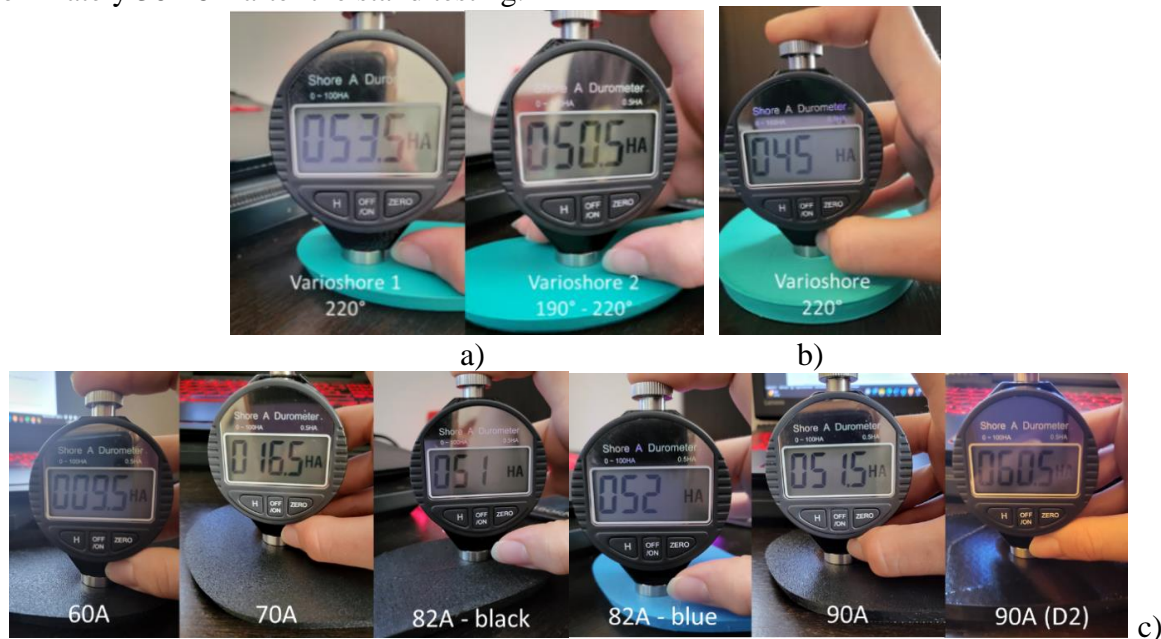


Fig.7.8. Hardness measurement of varioShore insoles: a) Design 1; b) Design 2; c) Other materials.

The initial measurement points were selected to cover the entire surface of the insole, while for the tested insoles, the points focused more on the areas in contact with the stand grips (the forefoot and heel areas). The final measurements were taken after subjecting the insoles to one or both fatigue methods. According to the ISO-7619-1-2004 standard [111], the measurement time for each point with the type A durometer was 3 seconds. The hardness values at the 30 points were used to calculate the initial average hardness of the insole (m_i) and the average hardness after the bending fatigue tests (m_a), as well as the deviation from the mean, allowing for an assessment of the variance in the set of numbers compared to the mean.

7.2.6. Results and discussion

Figures 7.9–7.11 show images of the insoles after testing, sectioned to see any changes in the internal gyroid structure. The exterior surfaces remained intact for both the insoles tested under real conditions and those tested for bending fatigue on the dedicated stand. Except for the insole made from Filaflex 82A black, Design 1, which was tested under real wear conditions and later on the test stand, no other insole showed defects within the internal structure during stand testing. For the Filaflex 82A black insole, Design 1, the internal structure failed after approximately 7,000 cycles on the test stand, with layer delamination observed (Fig. 7.11). The hypothesis was that degradation resulted from summer wear (high temperatures and sweat) and aging, considering the insole was tested after nearly a year of uncontrolled storage on a shelf. However, further studies are needed to confirm or disprove this hypothesis.

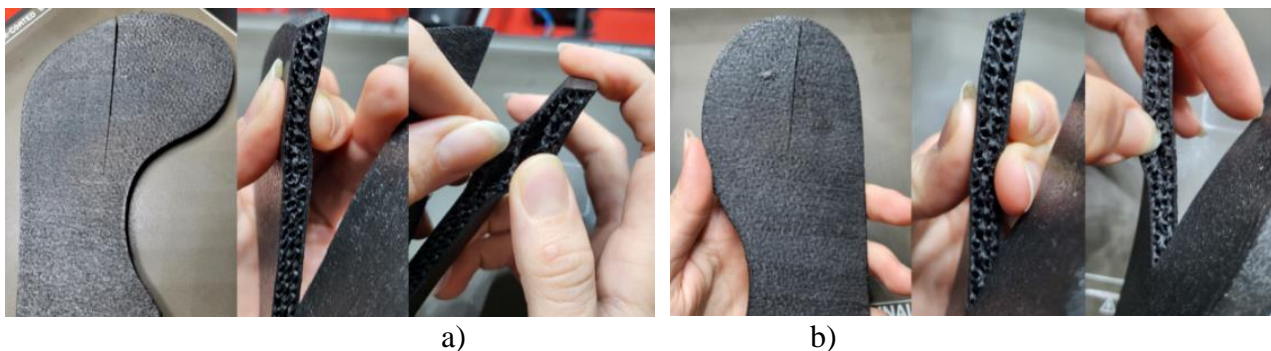


Fig.7.9. Insole made from Filaflex 82A, black (tested under normal conditions, followed by stress testing on the dedicated stand): a) Forefoot area; b) Heel area.

Fig. 7.11 presents the evolution of the external surface of the insole made from varioShore 1, design 1, after a specific number of test cycles. In the heel area, the marks faded quickly between test cycles, leaving only friction marks from the mentioned grips on the surface. In the forefoot area, the marks left by the grips were deeper due to the double pressure compared to the heel area (175.6 kPa). However, over time, their intensity significantly reduced, although they did not completely disappear.

In comparison, the compression marks on the insoles made from Filaflex and PolyFlex TPU were less prominent. This observation was confirmed by the user during comfort tests, who reported that the deformations, perceived as a reduction in stiffness, appeared more quickly on the varioShore insoles than on the others. The same behavior was observed on the insole made from Filaflex 82A, blue, design 1, as well as on the right foot insole from Filaflex 82A, blue, design 2, after 1,423,452 steps. However, the left foot insole, which had a 24% infill density in the metatarsal area, did not degrade. Thus, it was concluded that further research should focus on variable infill, with higher density in stressed areas.



Fig.7.10. The insole varioShore 1 show no degradation of the internal structure.



Fig.7.11. The evolution varioShore 1 insole after: a) 3D printing; b) 7,000 cycles; c) 42,000 cycles; d) 63,000 cycles; e) 98,000 cycles; f) 48 hours after testing.

Pressure measurements using the *in-Shoe Pedar system* (Fig. 7.12.), conducted at the Faculty of Mechanics and Mechatronics from Politehnica București and Pedorthic Art, showed a decrease in peak pressure when wearing the insoles. This means that the 3D-printed TPU insoles can distribute plantar pressure effectively. Compared to the original insole of the footwear, the 3D-printed insole made from Filaflex 82A, blue, Design 2, reduced the maximum pressure observed in the forefoot area from 250 kPa to 207 kPa (a 17% reduction) for the left foot (with a 24% infill density) and from 305 kPa to 280 kPa (a 9% reduction) for the right foot (with a 20% infill density). These values are lower than those reported by Birke et al. [112] for PORON insoles designed for flat feet.

For the insoles tested under real conditions, the residual deformation after 1,000,001 steps was approximately 55% (4.4 mm out of 8 mm) for the highest infill density and 31.2% (2.5 mm out of 8 mm). In the literature dedicated to the physical properties of materials used for diabetic insoles, residual deformation is reported to range between 10% and 42% after 80,000 cycles [113].

In addition to fatigue testing and hardness measurements, the insoles were also evaluated for comfort. As mentioned in Chapter 4, users answered a questionnaire after wearing the insoles for 15 minutes. This comfort evaluation can only be correlated with the cushioning sensation, as the testing period was too short to assess aspects related to moisture and heat transfer, which remain open subjects for future studies.

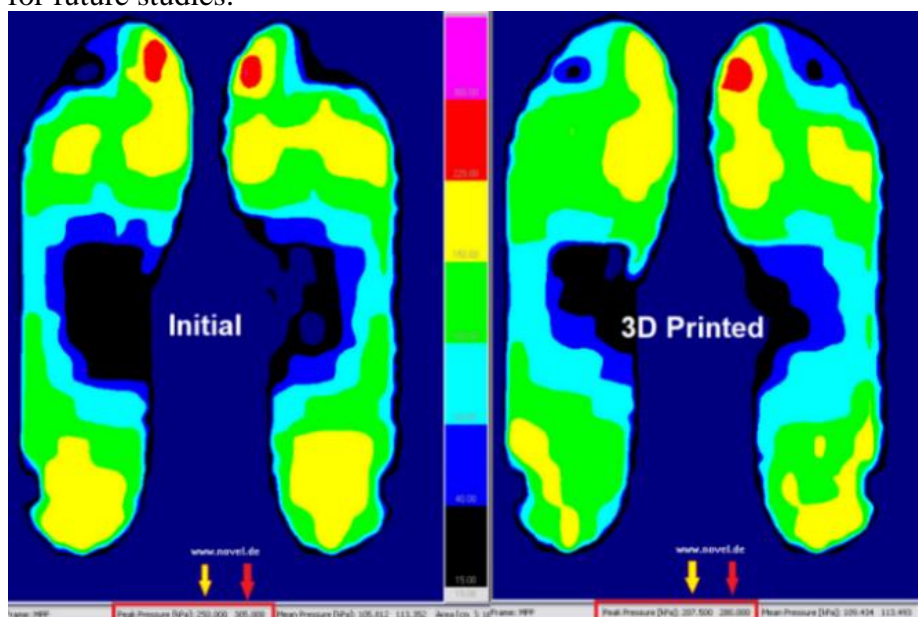


Fig.7.12. in-Pedar results for blue Filaflex 8A insoles design 2

Table 7.4 summarizes the most important test results, including Shore A hardness and comfort evaluation (Likert scale from 1 – least comfortable to 5 – most comfortable). Fig. 7.13 graphically represents the Shore A hardness values for each tested insole.

Table 7.4. Hardness and comfort tests results

Specimen	Hardness before testing (HA)	Hardness after testing (HA)	Type of damage	Number of cycles until damage	Total number of cycles	Comfort
Filaflex 60A design 1	3.5 – 12.5	2.5 – 11	Compression & rubbing marks	No damage of the infill structure	700,000	2
Filaflex 70A design 1	13.5 – 19.5	11 - 16	Compression & rubbing marks	No damage of the infill structure	700,000	4
Filaflex 82A black design	49-58.5	44 – 55.5 (damaged area)	Internal structure	Around 7,000 cycles until cracks were heard (interior structure failure)	500,000 following 200,000 steps in daily use	1
Filaflex 82A blue design 1	51.5 - 58	51 – 58	Slight compression marks	No damage of the infill structure	700,000	1
PolyFlex 90A design 1	49 – 59.5	46.5 - 57	No damage	No damage of the infill structure	700,000	2
VarioShore 1 design 1	53 - 60	50.5 – 58.5	Compression & rubbing marks	No damage of the infill structure	700,000	2
VarioShore 2 design 1	50 - 55	50 - 54	Compression & rubbing marks	No damage of the infill structure	700,000	5
PolyFlex 90A design 2	56.5 – 63.5	56.5 – 64.5	Compression & rubbing marks	No damage of the infill structure	700,000	2
VarioShore design 2	43 – 50	46 - 46	Compression marks	No damage of the infill structure	700,000	3

Table 7.5 presents the hardness values measured immediately after 3D printing and after testing. The insole made from PolyFlex 90A, design 1, showed the smallest deviation, with a difference of +0.03 between the two measurements. The largest deviation was observed in the insoles made from Filaflex 70A, with a difference of +0.45 from the initial value, followed by varioShore 1 (design 1 and 2) with -0.44 and +0.44.

Regarding changes in hardness after the insole testing (minimum and maximum values), it was observed that the insoles least affected by bending fatigue were those made from Filaflex 82A (blue), PolyFlex 90A, and varioShore 2. The most affected were Filaflex 60A and Filaflex 70A.

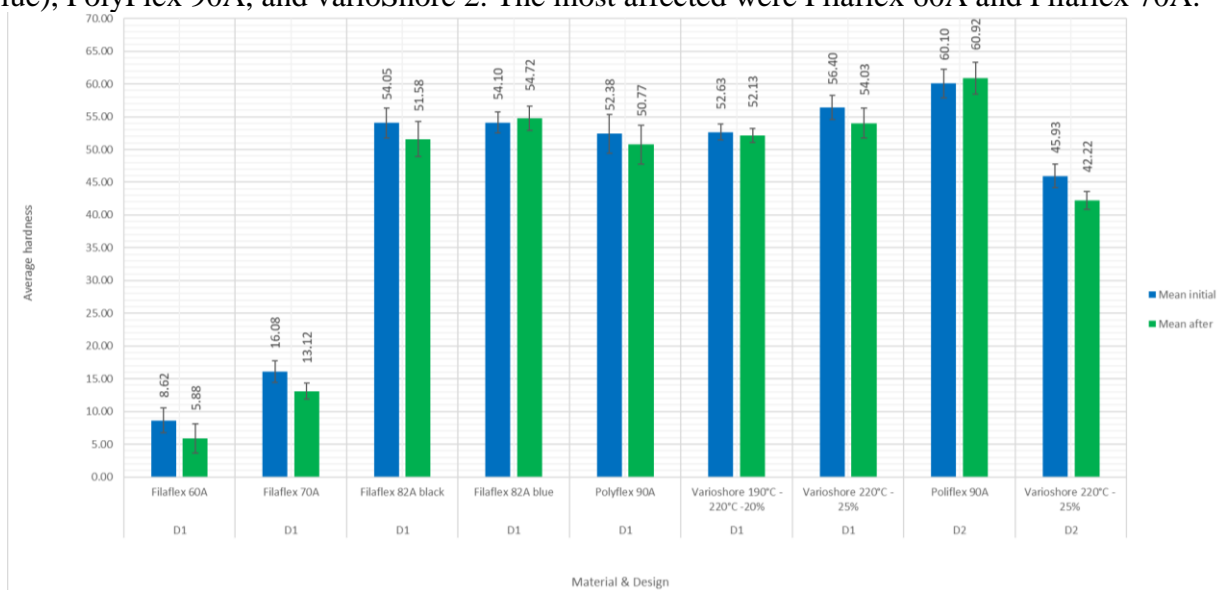


Fig.7.13. Shore A hardness results: initial – immediately after 3D printing (blue); after – post testing (green)

Tabel 7.5. Standard deviation initial (SD_i) and after tests (SD_a)

Material	Design	SD_i	SD_a	$SD_a - SD_i$
Filaflex 60A	D1	1.89	2.21	0.32
Filaflex 70A	D1	1.68	1.23	-0.45
Filaflex 82A black	D1	2.30	2.65	0.35
Filaflex 82A blue	D1	1.61	1.85	0.24
PolyFlex 90A	D1	2.93	2.96	0.03
varioShore 190°C - 220°C -20%	D1	1.22	1.07	-0.15
varioShore 220°C - 25%	D1	1.83	2.27	0.44
PolyFlex 90A	D2	2.18	2.44	0.25
varioShore 220°C - 25%	D2	1.80	1.36	-0.44


From the perspective of comfort, varioShore 1 stands out due to its elasticity, providing cushioning for body weight. This insole has a minimal deviation from the initial measurement of -0.15, with a hardness of approximately 52A. Based on the data from this comparative study, it was concluded that varioShore is a more suitable and versatile material for insole manufacturing applications. Section 3 of this chapter focuses on the compression testing of this material, as well as the testing of insoles using the sensor-equipped insole developed in Chapter 4.

Section 3: Study of customized insoles made from varioShore

7.3. The effect of 3D Printing parameters on varioShore hardness

Table 7.6 presents the investigated process parameters, with three cylindrical specimens fabricated for each configuration, each having a diameter of 29 mm and a height of 12.5 mm. These specimens were measured with a durometer for hardness analysis and subjected to standardized mechanical compression tests for such materials. The hardness of the specimens was measured using the Shore A durometer.

Tabel 7.6. Specific parameters for cylindrical specimens

Specimen	Variable process parameters	Fixed parameters
	<i>Printing temperature:</i> Levels: 190 °C, 220 °C, 240 °C	Bed temperature: 0 °C Flow rates: 110%, 72%, 60% Layer thickness: 0.2 mm Top/bottom layers: 4 Perimeters: 0 Printing speed: 35 mm/s Fan speed: 70% Disable for the first 4 layers, full speed at layer 6
	<i>Infill density:</i> Levels: 10%, 15%, 20%, 25%, 30%, 35%	
	<i>Infill pattern:</i> Levels: gyroid, honeycomb	

The measurements were taken at ten different points on the surface of the specimens, with hardness variation recorded as an effect of the infill density. The average hardness value for each specimen was calculated and compared with the hardness of the parts with 100% density, which served as a reference.

From the hardness measurements at the ten points, the minimum, maximum, arithmetic mean, and standard deviation were calculated to assess the variation within the set of measured values relative to their average. For the specimens with a 25% infill density, it was observed that the honeycomb/hexagonal infill pattern printed at 190°C and 220°C produced the highest standard deviations of 2.57 and 2.23, respectively (Fig. 7.14).

The 35% infill density yielded specimens with more uniform hardness, as expected, with a low standard deviation of approximately 0.34 for specimen 1 at 240°C and 0.52 for specimen 3 at 190°C, gyroid (Fig. 7.15). The explanation is that as the infill density increases, it becomes less likely to measure Shore A hardness in the voids created by the infill pattern. Thus, the 45% infill density produced the most stable specimens, with a standard deviation of 0.39 for 190°C, gyroid (Fig. 7.16).

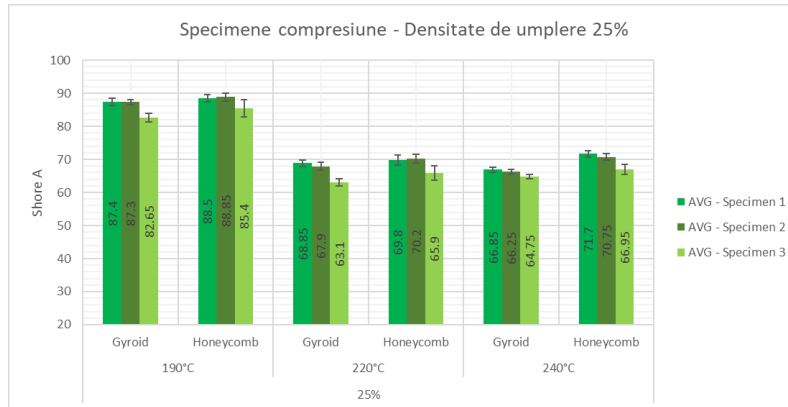


Fig.7.14. Hardness measurements for the 25% infill density samples (average values per sample)

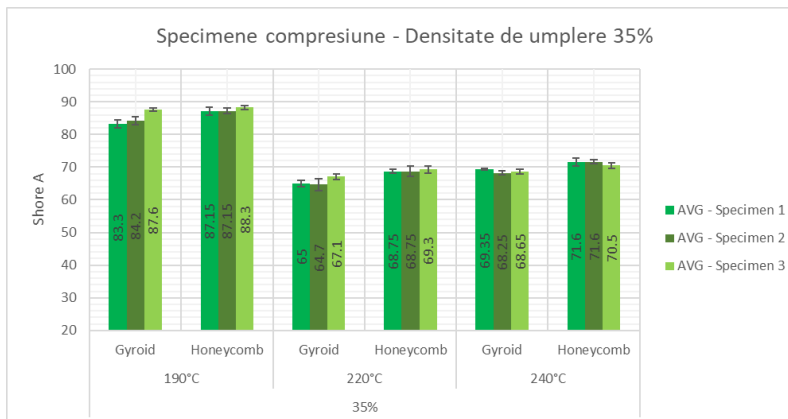


Fig.7.15. Hardness measurements for the 35% infill density samples (average values per sample)

Table 7.7 presents a synthesis of the data obtained from the hardness measurements using the average values for three specimens with the same process parameter configuration. The p-value calculated using one-way ANOVA showed a very low value for the printing temperature data (significant level 0.05), indicating a statistically significant difference in hardness depending on the printing temperature/nozzle.

At 190°C, the resulting hardness exceeds that at 220°C and 240°C because the base hardness of the material is Shore 92A (the hardness of the filament on the spool). At 190°C, no foaming occurs, thus preserving the original hardness of the filament, which was confirmed during the 3D printing process and in the SEM investigations. As the temperature increases to 220°C, the filament demonstrates its foaming capability, resulting in a reduction of its hardness. However, after exceeding a temperature of 220°C, the hardness shows a slight increase again until reaching a temperature of 250°C.

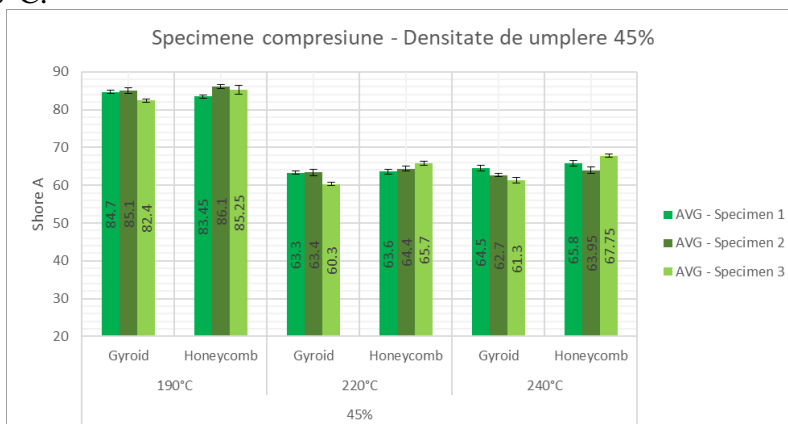


Fig.7.16. Hardness measurements for the 45% infill density samples (average values per sample)

Tabel 7.7. Mean values of hardness for different process parameters configurations

Printing temperature [°C]	Infill density [%]	Infill pattern	Mean hardness
190	25	Gyroid	85.78
		Honeycomb	87.58
	35	Gyroid	85.03
		Honeycomb	87.53
	45	Gyroid	84.06
		Honeycomb	84.93
220	25	Gyroid	66.62
		Honeycomb	68.63
	35	Gyroid	65.60
		Honeycomb	68.93
	45	Gyroid	62.33
		Honeycomb	64.56
220	25	Gyroid	65.95
		Honeycomb	69.80
	35	Gyroid	71.78
		Honeycomb	68.75
	45	Gyroid	62.83
		Honeycomb	65.83

The results regarding the hardness of varioShore could only be compared with two references. In [101] information was found about the relationship between compressive strength and printing temperature for 100% specimens, indicating that higher densities correspond to printing temperatures of 220°C, 205°C, 190°C, and 235°C. However, [101] did not include specific information regarding the number of upper/lower layers of the specimens, as the study primarily focused on compressive testing. Another reference concerning varioShore [106] confirmed the study's results, indicating that the highest hardness value is at 190°C.

From the graphs of the main effects examining the influence of the three analyzed parameters on the hardness of the specimens, it was observed that the extrusion temperature is the most significant influencing factor, followed by the infill density. The least important factor is the infill pattern. The transition from a 35% density to a 45% density produced a greater effect on hardness than a lower density of 35%. In the case of printing temperature, the influence of transitioning from 190°C to 220°C is more significant than that between 220°C and 240°C. Results from [101], but for other types of TPU, showed that the infill pattern does not have a significant influence on compressive strength, and that the honeycomb pattern has a greater compressive strength than gyroid. These observations were also confirmed in the current research for the varioShore.

7.4. Behavior of custom 3D Printed comfort insoles made from varioShore TPU

7.4.1. Analysis of the compressive behavior of varioShore

The compressive-strain characteristics of varioShore specimens were determined in accordance with the standard for compression testing of polymeric materials ISO 7743:2017 [114]. León-Calero et al. tested various types of TPU specimens (but not varioShore) with grid, gyroid, and honeycomb patterns and fill densities of 0%, 20%, 50%, 80%, and 100% [115].

Fig.7.17 presents the specimens for the compression test, manufactured with parameters in Table 7.6., with three specimens made for each configuration. The material flow rate varied depending on different extrusion temperatures, but remained constant for each specific temperature.

Uniaxial compression tests along the Z-axis of the specimens were conducted at the Department of Materials Strength within the Faculty of Industrial Engineering and Robotics at the Polytechnic University of Bucharest, using the Lloyd Instruments LRX Plus device (Ametek, Inc., UK) equipped with a 5 kN load cell (Fig. 7.18). The upper and lower surfaces of the samples were lubricated to reduce friction between the sample and the mounting devices. The testing speed was

set at 10 mm/min for all specimens until 25% of the relative elongation was reached, in accordance with the mentioned standard, after which the load was released at the same speed. The loading (compression) and unloading process was performed a total of four times, resulting in four uninterrupted compression cycles, with the recording done in the form of force-deformation curves from the last trial. These curves were subsequently transformed into stress-relative elongation coordinates by dividing the force by the initial cross-sectional area and the deformation by the initial length.



Fig.7.17. Samples prepared for compression test

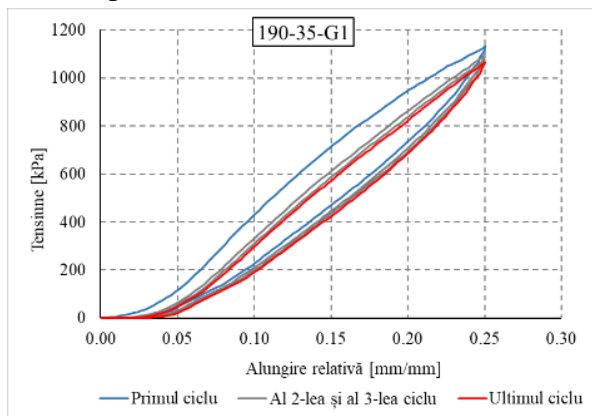


Fig.7.18. Compression testing of a varioShore TPU specimen

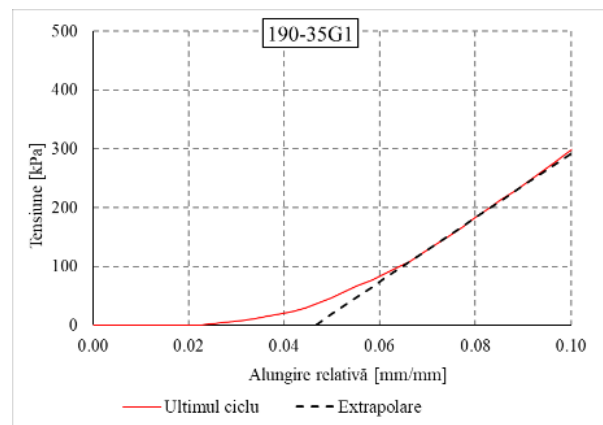
All loading cycles exhibited hysteresis loops and incomplete recovery at the end of each cycle, suggesting a viscoelastic behavior. The secant compression modulus was extracted for the last loading cycle. Due to the formation of a “finger region” at the beginning of the cycle, the actual start of the fourth cycle was determined by extrapolating the loading curve at $0.1 * \sigma_{max}$ and $0.2 * \sigma_{max}$ (Fig.7.19. b), which was found to be linear. Consequently, the modulus were extracted for 10% and 20% strain from the extrapolated starting point, following the relationship:

$$E_i = \frac{\sigma_i}{\varepsilon_i},$$

where: E_i – Compression modulus for 10% and 20% strain, expressed in [MPa]; ε_i – Strain developed during the last loading cycle, expressed in [mm/mm]; σ_i - Recorded stress at which ε_i occurs, expressed in [MPa].



a)



b)

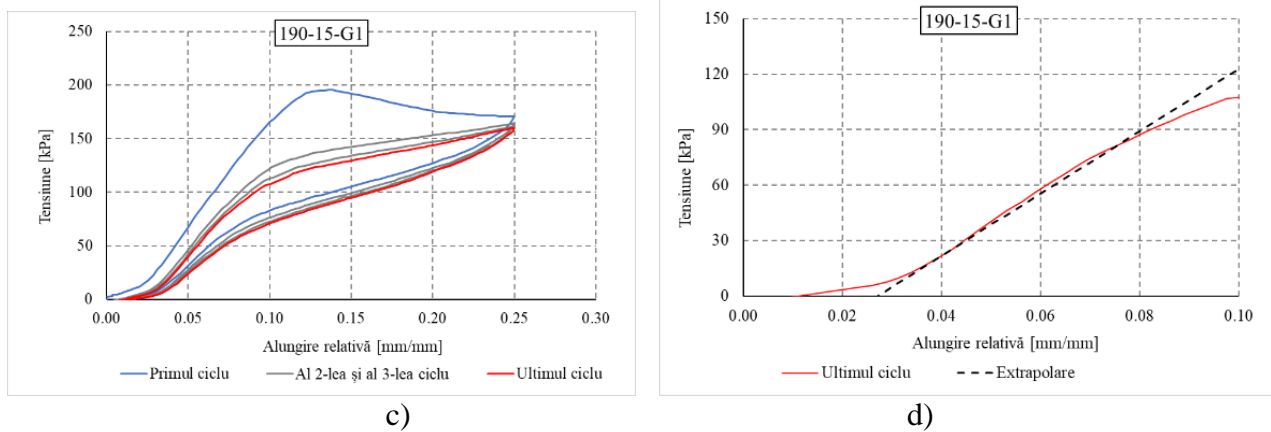


Fig.7.19. Example of derived stress-strain curve, gyroid sample 3D-printed at 190°C, 35% infill; b) Extrapolation of the real start of the fourth cycle; c) Example of stress-strain curve, gyroid sample printed at 190°C, 15% infill; d) Extrapolation of the true start of the fourth cycle.

7.4.2. Results of compression tests for varioShore specimens

Table 7.8 summarizes the experimental data from the compression tests. The specimens are labeled as follows: temperature – infill, meaning that 190-35 indicates a 3D-printed specimen at 190°C with an infill density of 35%, while G or H indicates gyroid or honeycomb.

Tabel. 7.8. Average values of the compression modulus for tested specimens

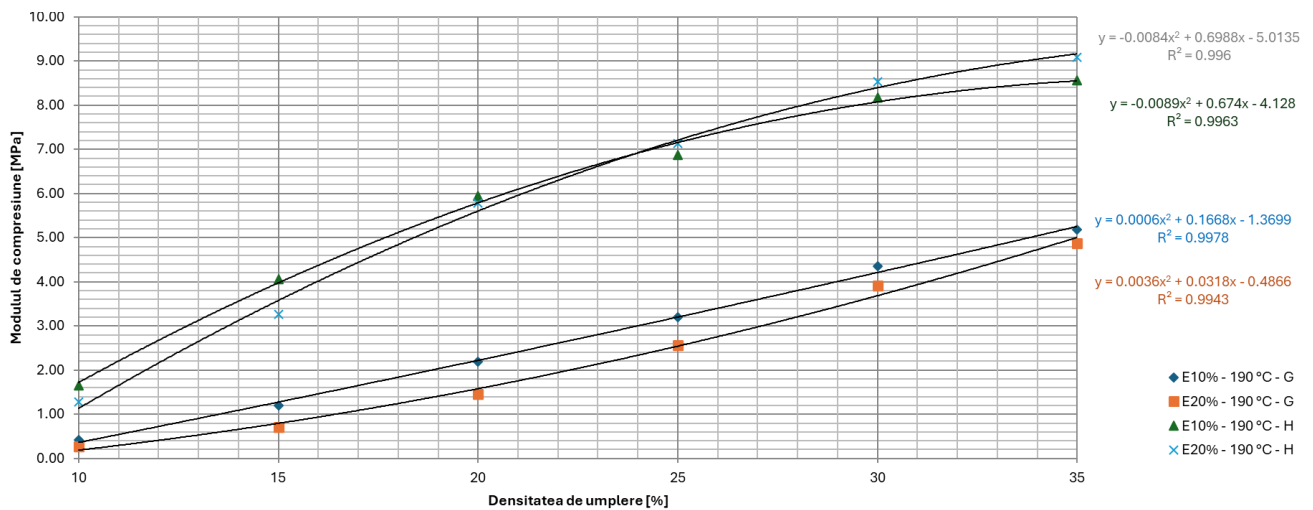
Specimen	Compression modulus [MPa] – mean at 10% strain, G	Compression modulus [MPa] – mean at 20% strain, G	Compression modulus [MPa] – mean at 10% strain, H	Compression modulus [MPa] – mean at 20% strain, H
190-35	5.17 ±0.25	4.88 ±0.25	8.56 ±0.34	9.08 ±0.35
220-35	1.68 ±0.06	1.59 ±0.05	2.6 ±0.10	3.02 ±0.10
240-35	1.82 ±0.03	1.75 ±0.03	2.94 ±0.13	3.19 ±0.13
190-30	4.35 ±0.15	3.91 ±0.15	8.18 ±0.37	8.54 ±0.35
220-30	1.45 ±0.15	1.33 ±0.15	2.38 ±0.37	2.76 ±0.35
240-30	1.47 ±0.09	1.41 ±0.08	2.82 ±0.17	3 ±0.20
190-25	3.2 ±0.12	2.57 ±0.13	6.87 ±0.31	7.14 ±0.30
220-25	1.13 ±0.09	0.97 ±0.07	1.96 ±0.15	2.26 ±0.16
240-25	1.19 ±0.05	1.11 ±0.04	2.25 ±0.29	2.42 ±0.27
190-20	2.19 ±0.07	1.46 ±0.07	5.95 ±0.31	5.79 ±0.33
220-20	0.77 ±0.04	0.59 ±0.03	1.62 ±0.17	1.79 ±0.21
240-20	0.84 ±0.03	0.75 ±0.03	1.7 ±0.27	1.84 ±0.23
190-15	1.19 ±0.03	0.71 ±0.04	4.06 ±0.28	3.26 ±0.23
220-15	0.43 ±0.03	0.31 ±0.02	1.47 ±0.27	1.59 ±0.31
240-15	0.51 ±0.02	0.4 ±0.02	1.36 ±0.19	1.46 ±0.19
190-10	0.42 ±0.03	0.27 ±0.03	1.65 ±0.07	1.28 ±0.05
220-10	0.2 ±0.02	0.14 ±0.01	0.64 ±0.06	0.54 ±0.05
240-10	0.18 ±0.01	0.14 ±0.01	0.74 ±0.10	0.69 ±0.11

As shown in Fig. 7.19, varioShore, like other TPUs, exhibits a significant viscoelastic response to relative elongation, characterized by hysteresis in their stress-strain behavior. Examination of the compression process of varioShore specimens indicated that buckling and bending were the primary mechanisms responsible for the deformation of the structures, rather than cracking or permanent deformations, as observed in [116]. It can also be noted that the compressive strength is highest for specimens printed at 190°C, followed by those printed at 240°C and 220°C. The difference in compressive strength between specimens printed at 220°C and 240°C is considerably smaller compared to that between specimens printed at 190°C and 240°C. This indicates that the highest percentage of foaming is achieved at 220°C, while specimens printed at 190°C remain unfoamed.

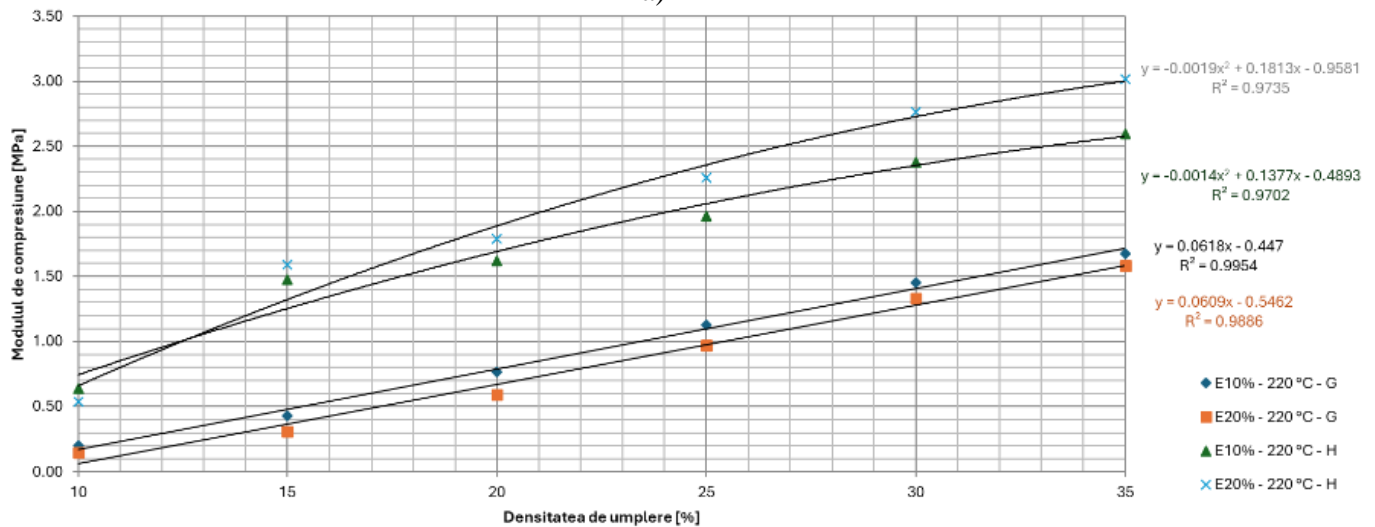
Studies have indicated that the honeycomb infill pattern exhibits superior compressive strength compared to the gyroid pattern, regardless of the printing temperature, although the printing times for both patterns are nearly identical. For instance, at 190°C and 10% infill density, the honeycomb

pattern required 29 minutes, while the gyroid pattern took 27 minutes to print. Although specific research on TPU with blowing agents for MEX technology is lacking in the literature, broader studies on TPUs have confirmed that the gyroid pattern has lower compressive strength than other fill patterns, such as cubic, triangular, or rectilinear ones. Another influential factor on the mechanical behavior of the specimens is the printing temperature, especially for TPU with thermally activated blowing agents. At high strain rates, TPU with full infill density demonstrated excellent durability, remaining unaffected even at the highest compressive strains tested. Thus, it is concluded that TPUs with blowing agents, when correctly used in the printing process, can provide effective solutions for applications requiring mechanical durability, with significant compressive strength and an extended lifecycle, especially in honeycomb-type configurations.

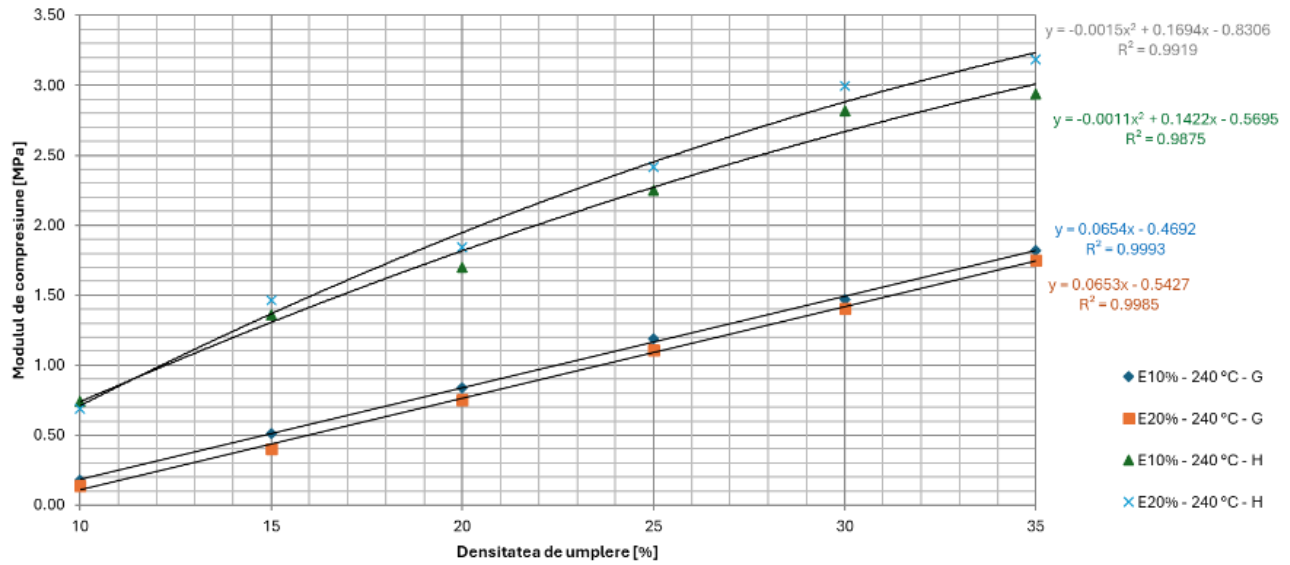
The results of the compression tests are graphically represented in Fig. 7.20. These data can be used to predict the value of the compression modulus at different infill densities and printing temperatures, with correlation coefficients exceeding 0.97. There is an almost linear relationship between infill density and the compression modulus. The highest compression modulus was 9.08 MPa for specimens of 190-35H, while the lowest values were obtained for 10% and 15% infill densities at temperatures of 220°C and 240°C. When the infill is below 15% and the printing temperature is above 220°C, the type of infill pattern is not relevant (the interaction graphs further support this observation).



a)



b)



c)

Fig.7.20. Compression moduli for different process parameter configurations: a) 190°C samples; b) 220°C samples; c) 240°C samples.

Table 7.9 provides data on the density of the samples, indicating that specimens with the honeycomb infill pattern exhibit a higher density. Additionally, it shows that the printing temperature influences the level of foaming in each sample, which affects the compressive strength. To characterize the material behavior over time, the density of the samples was measured two months after the compression resistance testing, and differences were analyzed. The specimen coding was as follows: the first number indicates printing temperature, and the second infill density.

Table 7.9. Samples' mean density before testing and 2 months after testing, and 3D printing time

Specimen	Mean density (kg/cm ³)				3D printing time (min)	
	G		G		G	H
	Before test	2 months after	Before test	2 months after		
190-35	0.532	0.532	0.620	0.621	49	57
220-35	0.295	0.300	0.339	0.345	49	57
240-35	0.330	0.331	0.377	0.381	49	57
190-30	0.484	0.487	0.568	0.569	44	53
220-30	0.266	0.272	0.317	0.321	44	53
240-30	0.307	0.307	0.359	0.362	44	53
190-25	0.437	0.438	0.510	0.510	41	47
220-25	0.255	0.246	0.281	0.284	41	47
240-25	0.273	0.275	0.321	0.321	41	47
190-20	0.390	0.391	0.453	0.453	36	42
220-20	0.215	0.219	0.240	0.242	36	42
240-20	0.246	0.248	0.289	0.292	36	42
190-15	0.342	0.344	0.401	0.402	31	37
220-15	0.186	0.188	0.230	0.232	31	37
240-15	0.214	0.217	0.247	0.250	31	37
190-10	0.303	0.304	0.326	0.327	27	29
220-10	0.165	0.166	0.179	0.181	27	29
240-10	0.193	0.193	0.205	0.206	27	29

A one-way ANOVA analysis was conducted (Table 7.10), with a significance level of 0.05, to evaluate the influence of parameters on the compression modulus. It was observed that the values of the compression modulus at relative elongations of 10% and 20% were similar for similar fill types but differed between G and H. Table 7.10 also presents the ANOVA results for the 3D printing time of specimens with fill patterns G vs. H, and for assessing whether there is a significant difference between the densities of the samples before testing and two months after the expiration date. The

results indicated a statistically significant difference between the densities of specimens G and H. At the same time, there was no significant difference between the densities of the samples before and two months after testing, indicating that the structure of the samples was not affected during testing. For relative elongation values of 20%, the difference in the influence of the variables is not as evident as for the 10% deformation. This shows that, as specimens become more compressed, the importance of their fill structure decreases.

Tabel 7.10. ANOVA analyses

Factors	p-value
10% compression modulus at for gyroid and 20% compression modulus for gyroid	0.632
10% compression modulus at for honeycomb and 20% compression modulus for honeycomb	0.901
10% compression modulus at for gyroid and 10% compression modulus for honeycomb	0.0199
20% compression modulus at for gyroid and 20% compression modulus for honeycomb	0.0067
3D printing times for gyroid and honeycomb samples	0.043
Means density of gyroid vs. honeycomb samples	0.232
Mean density before and 2 months after testing for gyroid samples	0.968
Mean density before and 2 months after testing for gyroid honeycomb	0.960

From the investigations presented in Section 7.3, the user’s evaluation of the 3D-printed varioShore insoles, with uniform fill density but printed at 220°C and 240°C, revealed a higher level of comfort for the insoles produced at 220°C. Fig.7.21 presents the stress-relative elongation curves for different densities at 220°C. These were considered to establish variable fill densities. To this end, correlations were established between the values of the maximum plantar pressure and the fill densities, aimed at reducing and equalizing the static peak plantar pressures.

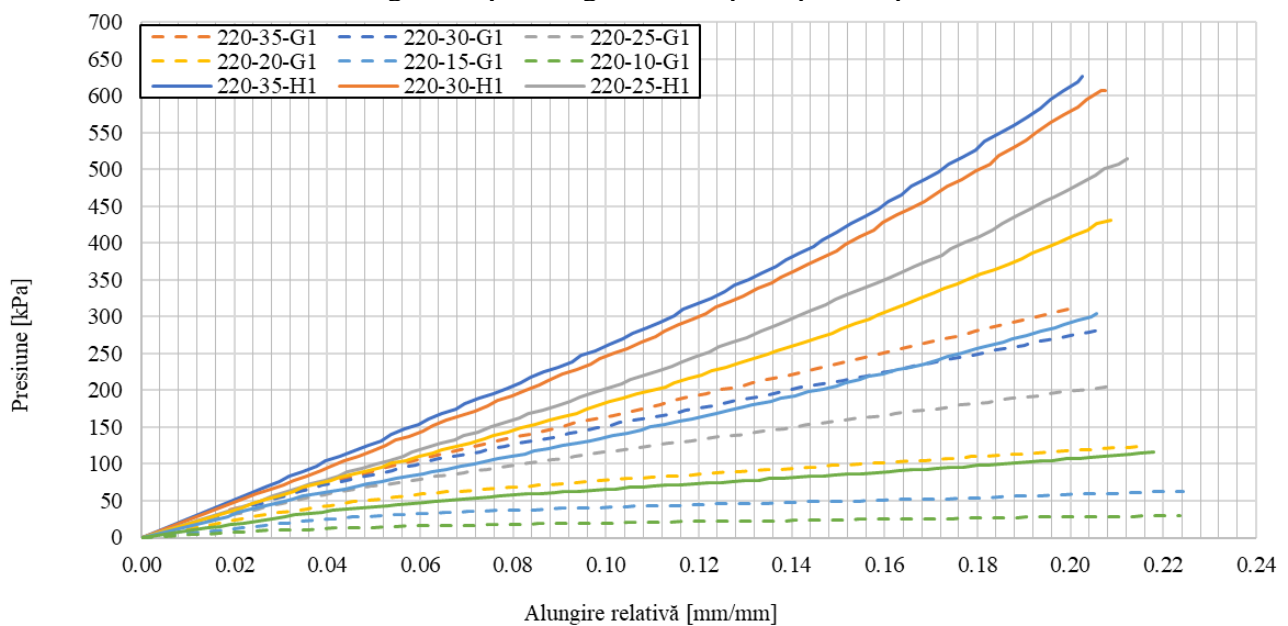


Fig.7.21. Stress-strain curves for the last loading cycle

7.4.3. Evaluation of plantar pressure using sensor-equipped insoles

A user of 48 kg participated in the tests conducted in this section to demonstrate how previous results from mechanical tests can be applied. A similar methodology can be used for individuals with varying weights and plantar pressure characteristics, following the proposed workflow. Based on data obtained from experimental studies with sensor-equipped insole (Chapter 4), an initial measurement of barefoot plantar pressure was performed (Fig. 7.22). Three configurations of the fill pattern with different fill densities (V1-V3) were selected based on the experimentally determined compression values, corresponding to three target peak plantar pressure values: 161.84 kPa, 91.67 kPa, and 53.47 kPa. Additionally, two other insoles with uniform infill density and medium

stiffness were 3D printed for use as references: 20% fill pattern G (gyroid) (V4) and 20% fill pattern H (honeycomb) (V5). The printing times for insoles V1-V5 (for each foot) were as follows: V1 - 3h 15 min, V2 - 3h 13 min, V3 - 2h 58 min, V4 - 3h 13 min, V5 - 2h 43 min.

Given that this study focused on the development of static comfort insoles, a variety of displacement values were selected: 0.06 mm, 0.08 mm, and 0.2 mm (Fig. 7.23). These values represent the degree of height reduction of the insoles under the weight of the user. However, it is important to note that the podiatrist must set these values based on a detailed analysis of the patient's pathology and individual characteristics.

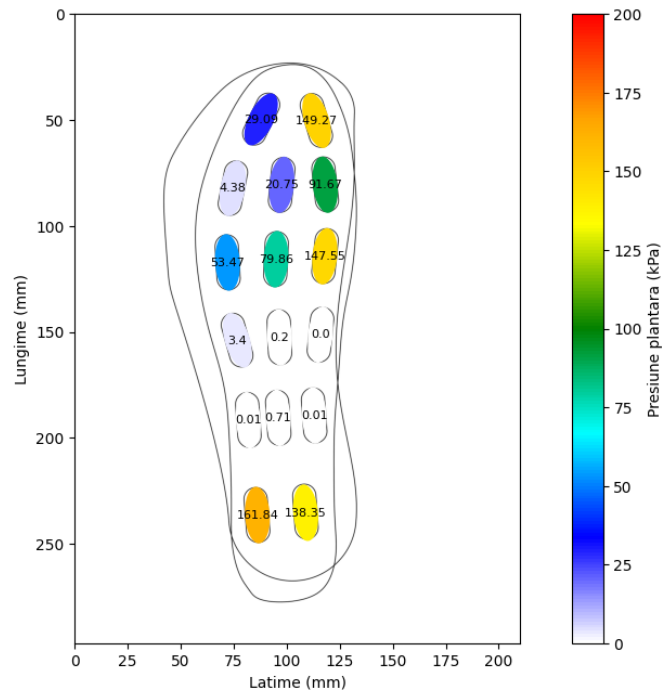


Fig.7.22. Values of peak plantar pressure with user's bare foot

Table 7.11. Pattern and infill density used for 3D printed insoles

Plantar pressure value [kPa]	Infill pattern and infill density				
	Insole V1	Insole V2	Insole V3	Insole V4	Insole V5
161.84	H30	H25	G25	G20	H20
91.67	G25	H15	H10		
53.47	H10	G20	G15		

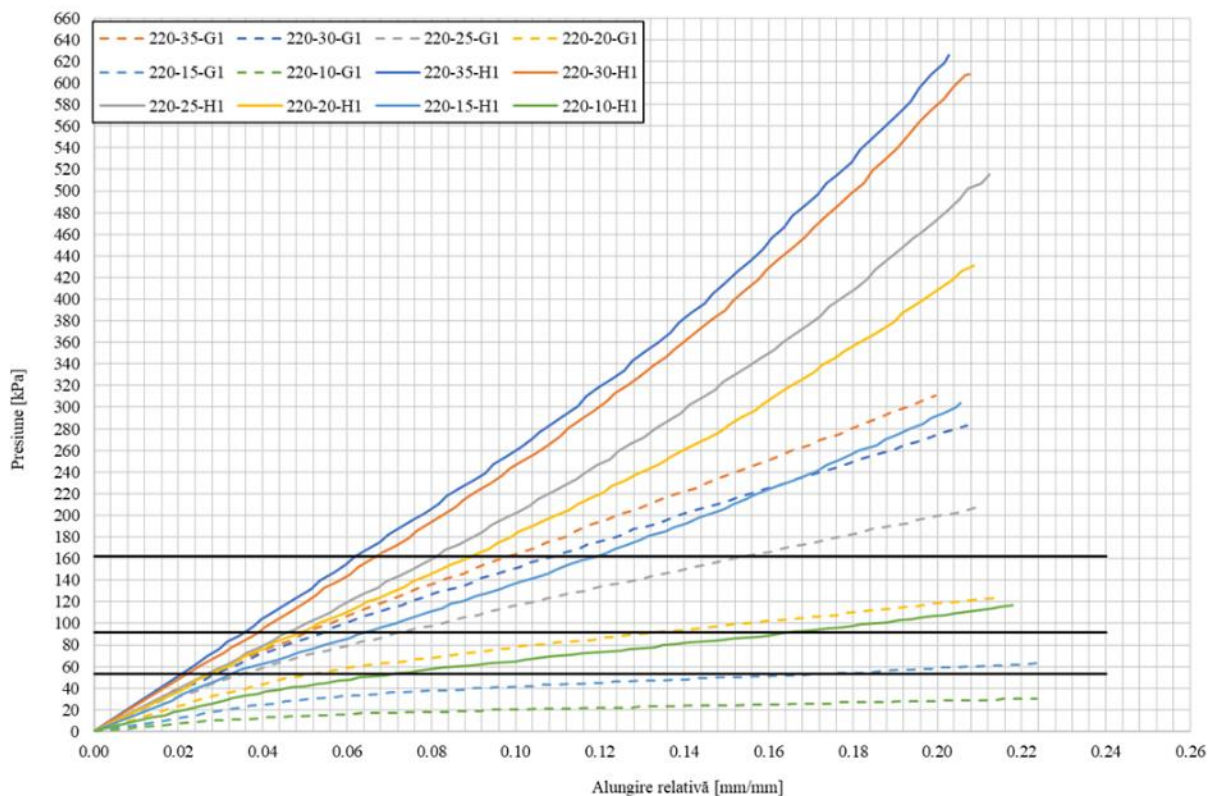


Fig.7.23. Selecting the configuration pattern-infill density for different plantar pressures (the horizontal lines indicate the plantar pressure of interest)

Data in Fig.7.23 was used to select the appropriate fill pattern and density combinations corresponding to different areas of plantar pressure. The fill pattern and density were chosen based on the areas where the horizontal lines of plantar pressure intersect the stress-strain curves and the corresponding vertical lines for different displacement values. Fig. 7.24 captures various stages of manufacturing the insoles with variable fill density to illustrate the structure in different areas of the insoles, also highlighting regions with diverse fill configurations. All insoles were 3D printed at 220°C, as this printing temperature provides the best comfort reported by users [16].

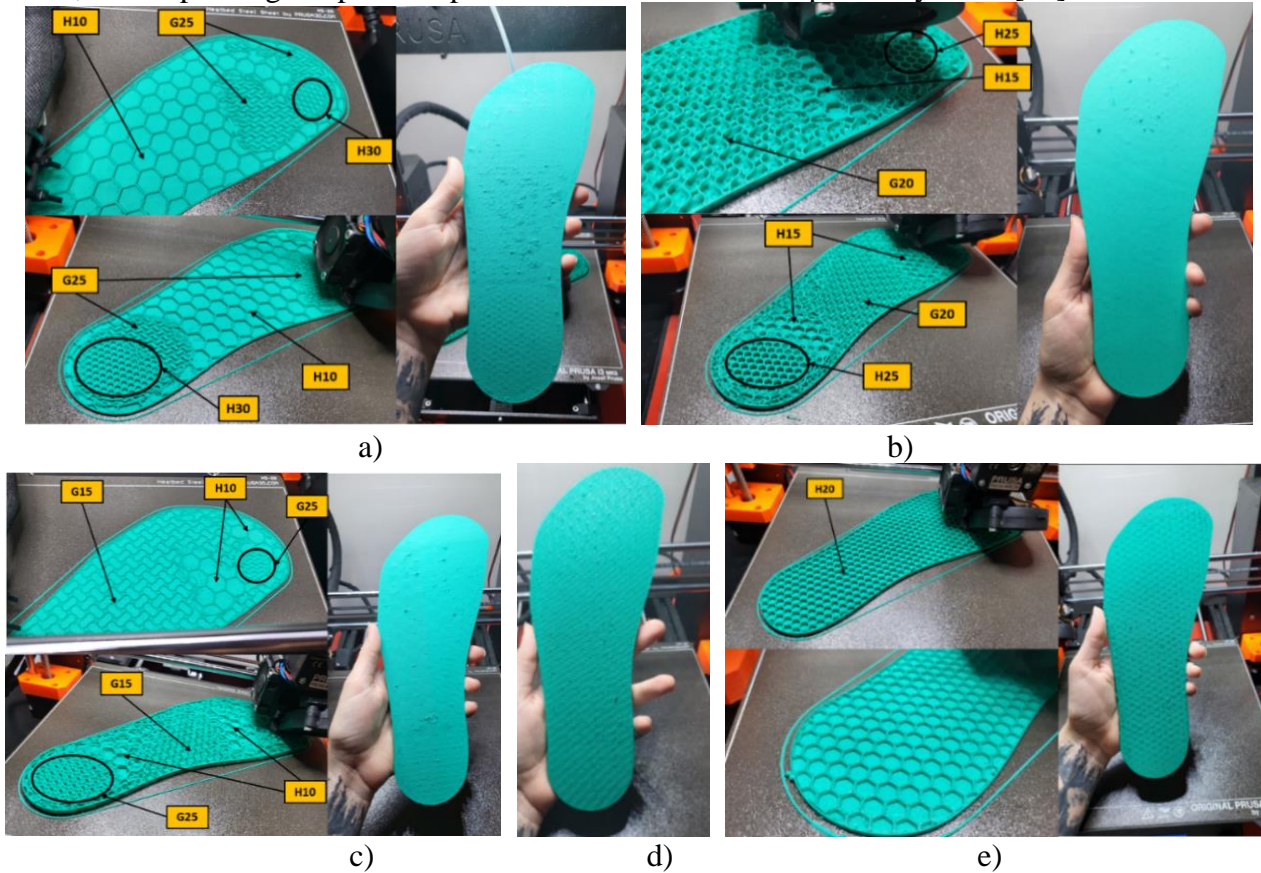


Fig.7.24. 3D printed insoles: a) V1; b) V2; c) V3; d) V4; e) V5.

The 3D-printed insoles were tested using the pressure sensors, showing a significant reduction in peak plantar pressure (Fig. 7.25). The results were summarized to compare the maximum plantar pressure of the bare foot in two important areas: the posterior foot (heel) and the forefoot. Conducting ANOVA for the values in Table 7.12 (p -value = 0.677 for V1-V5, p -value = 0.876 for the V1-V3 insoles with variable fill), it was found that there is a significant difference between the peak plantar pressures. This underscores the importance of correctly setting the infill parameters.

The plantar pressure values were higher when V3 was used, as this insole included two areas with the gyroid fill pattern (G25, G15)—the gyroid pattern was less rigid than the honeycomb, along with one area featuring a low-density honeycomb fill (H10). This explains the peak pressure values exceeding 90 kPa, compared to the V1 or V2 insoles.

The V3 insole recorded higher pressure around the toe (on one sensor) and heel (on two sensors), while for the other insoles, the pressure was distributed across the remaining sensors in the forefoot area. Interesting conclusions can be drawn when comparing the V3 insole with V4 (G20). In this case, we considered that the uniform fill of the gyroid allowed for better pressure distribution due to the nearly isotropic behavior of this pattern [117]. In comparison, V1 and V2 insoles felt similarly regarding the pressure distribution. However, V2 was perceived as softer due to a larger surface area filled with gyroid pattern. In areas with high plantar pressure, V2 felt firmly due to the vertical walls characteristic of the honeycomb pattern. Comparatively, V3 was significantly softer,

allowing the feet to comfortably settle onto the insoles. The peak pressure areas addressed with the gyroid fill pattern felt softer, contributing to increased comfort, even though plantar pressure was not completely reduced (approximately 35% of the initial plantar pressure). V4 and V5 were quite distinct: V4 was comfortable and soft, creating the sensation that the insole conformed to the foot's sole. In contrast, V5 was stiffer, conveying the impression that the fill pattern underwent minimal deformation under the user's weight. The V3 insole received the most favorable feedback for achieving optimal comfort through pressure reduction. The gyroid-patterned insole for areas with high and low pressure effectively supports weight distribution and provides the user with a comfortable standing position.

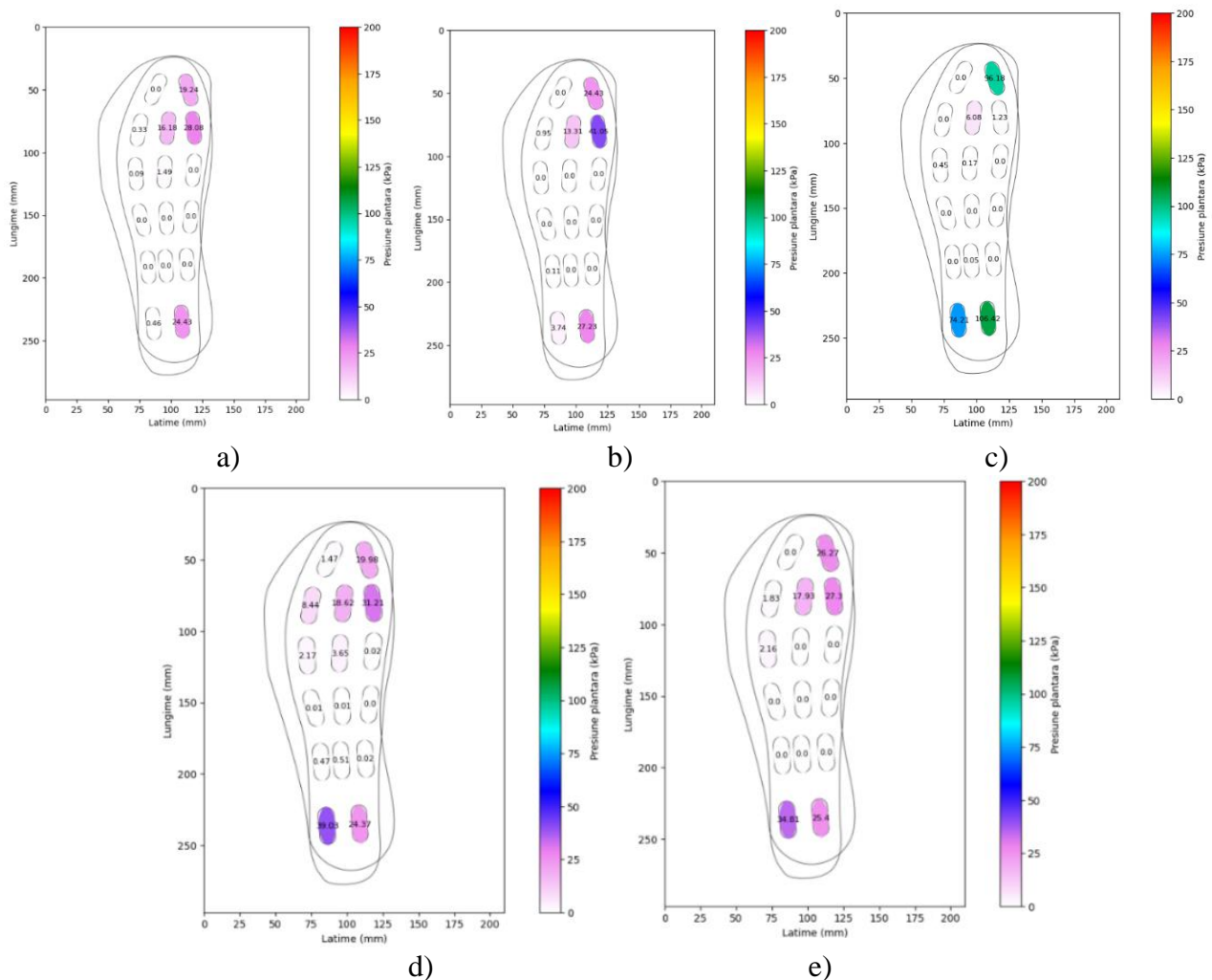


Fig.7.25. Static plantar pressure results when using: a) V1; b) V2; c) V3 d) V4; e) V5.

Conclusions and contributions

Contributions

- Calibration and optimization of the 3D printing process for all studied TPU filaments (Filaflex 60A, 70A, 82A, PolyFlex 90A, varioShore);
- Testing TPU insoles with different shore A hardness in both real conditions and flexural fatigue testing on the dedicated testing device;
- Collecting and analyzing user feedback regarding the use of TPU insoles;
- Investigating varioShore TPU filament with active foaming agent to determine hardness based on process parameters (printing temperature, material flow);
- Conducting SEM investigations to analyze the internal structure of varioShore and evaluate the impact of printing temperature on pore size and shape;

- Investigating several methods for determining plantar pressure and using the data for manufacturing different types of insoles;
- Comparative analysing the hardness of TPU and varioShore insoles, manufactured at different 3D printing temperatures and with uniform infill density;
- Developing a method for customizing insoles, adapting density and infill pattern based on individual plantar pressures, thus improving their functionality and efficiency;
- Testing the comfort and pressure distribution provided by varioShore insoles with variable infill density, using insoles equipped with sensors.

Chapter 7 conclusions:

- Investigations have demonstrated the capability of varioShore TPU to produce parts with different hardness levels, using a single extrusion head on a low-cost 3D printer. Examples of 3D-printed parts, including customized insoles, highlight the flexibility and versatility of this filament in creating products tailored to individual needs;
- Customization of insoles, especially regarding rigidity (hardness/compressive strength), is essential for cushioning, being particularly important for individuals with conditions such as diabetes, flexible flat feet, etc., as well as for those who stand for long periods;
- Adjusting rigidity based on plantar pressure has improved the comfort of varioShore insoles by ensuring evenly distributed plantar pressure;
- TPU printed insoles withstand at least 700,000 lab cycles and 1.4 million real-life steps, without significant degradation, confirming their durability and effectiveness;
- Mechanical tests conducted on varioShore specimens showed that printing temperature plays a crucial role in determining material hardness. Statistical analysis did not reveal a significant difference in compression modulus between relative elongations of 10% and 20%. It is noteworthy that there were only minor variations in the effects of compression modulus at temperatures of 220°C and 240°C, while a substantial difference was observed at 190°C. These tests not only identified the most influential factor but also facilitated the establishment of correlations between plantar pressure values and different infill density configurations to achieve specific displacements;
- Insoles 3D printed from varioShore at 220°C withstood over 300,000 flexural cycles without affecting their internal structure;
- Mechanical tests demonstrated that the printing temperature has the greatest influence on compressive behavior, a result also confirmed by SEM investigations. Additionally, compression tests helped create stress-relative elongation curves that provided insights into the process parameters necessary for 3DP.

Chapter 8. Results, contributions, conclusions and directions for further research

This doctoral thesis aimed to investigate and optimize MEX process for producing customized insoles using flexible and innovative materials, such as TPU with varying hardness levels (Filaflex 60A, 70A, 82A, PolyFlex 90A) and varioShore TPU. Through an interdisciplinary approach that combines plantar pressure analysis, 3D scanning, mechanical simulations, and experimental compression and flexural fatigue tests, the research makes significant contributions to the field of 3DP applied for orthotic and comfort purposes. The project explored both the mechanical performance of the materials and how they can be adjusted by varying printing parameters like temperature, density and pattern to produce customized products with optimal comfort and support.

Another innovative aspect of the research was the development and use of specialized equipment for testing the strength and mechanical behavior of the insoles, including a customized system for cyclic flexural load monitoring. This equipment enabled the evaluation of the insoles' durability under real wear conditions, significantly contributing to the validation of the proposed solutions.

At the same time, the research explored how variations in printing parameters (extrusion temperature, infill density and pattern) are influencing the flexibility and hardness of the insoles. The varioShore TPU material stood out for its ability to allow adjustments in flexibility and hardness based on user's requirements, opening new perspectives for the 3D printed customized orthopedic solutions. Additionally, SEM investigations were conducted to analyze the microstructure and better understand the impact of MEX process parameters on the mechanical properties of the produced insoles.

Throughout the thesis, particular emphasis was placed on the testing and practical evaluation of the insoles, utilizing advanced plantar pressure measurement equipment and wear simulations, which allowed the validation of the proposed solutions, as well as comfort testing through users' feedback. Customizing the insoles according to the plantar pressure distribution, through scanning and modeling was essential for optimizing their comfort and effectiveness. Thus, this research contributes to the understanding of how 3DP technology can advance the orthopedic field, providing accessible and effective solutions for users with specific needs, such as individuals with diabetic foot or other complex orthotic conditions.

8.1. Contributions

The personal contributions of this thesis are numerous, detailed in each chapter, including a series of innovations in the field of MEX-based customized insoles with variable stiffness by investigating new materials and developing dedicated methods and equipment. This research highlighted the need for an integrated approach to the design, manufacturing, and testing of insoles, considering both medical aspects and the technical challenges of 3DP with various materials.

A key aspect was the development of a methodology for personalizing insoles, starting from 3D scans of the foot to obtain digital models. This methodology was integrated with plantar pressure measurements and computer-aided design, allowing for the creation of insoles tailored to individual needs. This represents a significant contribution to the personalization of insoles for comfort.

Another major contribution of the thesis is the development of two equipment for evaluating flexural fatigue and plantar pressures. These were essential for testing the durability of the produced 3D-printed insoles. The experiments demonstrated that insoles made from TPU and varioShore can withstand prolonged use, providing long-term support and comfort. Using the Pedar in-shoe pressure measurement system, relevant data were collected that enabled the evaluation and optimization of the insoles' performance.

The technological contribution is also reflected in the investigation of new materials for 3DP, such as PCL and varioShore TPU. The study of varioShore demonstrated its ability to provide insoles with variable stiffness by adjusting process parameters such as printing temperature, infill pattern, and density. This material flexibility allows for the creation of insoles tailored to various medical conditions, such as diabetic foot or plantar fasciitis.

Additionally, the thesis brought contributions through a comparative analysis of several infill patterns and densities for 3DP, highlighting how these variables influence the compressive strength and mechanical behavior of the insoles. It was demonstrated that the extrusion temperature has the most significant impact on hardness and compressive behavior, thereby establishing an optimal set of process parameters for producing durable and comfortable products.

8.2. Main results achieved

The main results of the thesis and their correspondence with specific theoretical and experimental objectives can be summarized as follows:

1. Literature review analysis:

- The literature review included foot biomechanics, common foot pathologies, existing technologies in the manufacture of orthotic devices for the feet, and a systematic study of the latest research in the use of 3DP technology for producing customized insoles. These theoretical aspects contributed to achieving objectives **OS1** and **OS2**.

2. Personalization and adaptation of insoles:

- The study successfully demonstrated the development of personalized insoles using 3D scanning and specialized design software. This result corresponds to **OS3** and **OS4**.

3. Development of testing equipment:

- A device was developed for testing the flexural fatigue life of insoles, essential for evaluating their performance. This result directly corresponds to objective **OS5**.

4. Development of a plantar pressure measurement system:

- A system for measuring plantar pressure under static conditions was created to evaluate the comfort and effectiveness of customized insoles. This result aligns with objective **OS6**.

5. Materials optimization:

- The research explored the use of new rigid and elastomeric materials and optimized process parameters (temperature, infill density) to adjust the hardness and flexibility of the insoles. This result aligns with **OS7-OS9**.

6. Printability and durability assessment:

- The study tested various materials and evaluated their printability using MEX technology, ensuring that the final products are durable and long-lasting. This result corresponds to objective **OS10**.

7. Performance of insoles:

- The research validated the comfort and durability of the insoles through both subjective feedback and objective measurements, corresponding to objective **OS11**.

8.3. Main conclusions

The detailed synthesis of conclusions for each chapter is presented as follows:

- The research demonstrated that 3DP offers flexibility and efficiency in the production of customized insoles, effectively providing solutions tailored to plantar pressure and individual comfort, in contrast to conventional methods. The 3DP technology allowed the adjustment of the shape and hardness of insoles through the use of elastomeric materials and variable infill settings;

- The use of advanced 3D scanning techniques and design software, such as Gensole, enabled the development of complex custom designs. These were designed to support the plantar arch and redistribute pressure in critical areas, contributing to alleviating discomfort for users who spend long periods on their feet or suffer from orthopedic conditions. The parametrized design of the internal structure of the insoles allowed for the adjustment of flexibility and hardness according to specific pathologies and usage requirements;

- A detailed analysis of insoles printed from various materials, such as Filaflex 60A, 70A, 82A, and PolyFlex 90A, evaluated their hardness and comfort. Tests showed that the hardness of the insoles could be adjusted by modifying the MEX process parameters, with more flexible materials, such as Filaflex 60A, providing greater comfort but with slightly reduced mechanical durability compared to the stiffer ones;

- The analyzed elastomeric materials proved suitable to produce customized insoles. Flexural fatigue tests conducted on an in-house equipment showed the resistance and durability of the insoles to intense mechanical wear, including over 700,000 cycles in the lab and 1.4 million steps in real conditions;

- Special attention was focused on investigating a new TPU filament, varioShore, with foaming agents, demonstrating that it offer additional adjustment options for hardness and flexibility, and can offer solutions for users with diverse podiatric conditions. Process parameters, such as temperature, infill density, and infill pattern, had a significant impact on the durability and comfort of varioShore insoles. 3DP at 220°C provided a balance between comfort and durability, and the honeycomb infill proved to be stiffer than gyroid for higher densities;

- The subjective evaluation of the comfort of variable-density varioShore insoles highlighted that the insoles with gyroid infill provide comfort and pressure cushioning;

- The correlation of collected data regarding the plantar pressure distribution of a user with the variable infill density of the insoles demonstrated the effectiveness of such an approach from the perspective of comfort and cushioning. Such a manufacturing approach is currently only possible through the use of 3DP;
- The research included the development of dedicated, cost-effective equipment for testing the fatigue life of the insoles and monitoring plantar pressure.

8.4. Directions for further research

- Future research targets the collection of more experimental data for developing a finite element model of the insole, which will facilitate semi-automated customization of infill variability. This model will integrate essential information about plantar pressure distribution, peak dynamic pressure values, maximum allowable plantar pressure, and displacements based on specifications provided by the podiatrist and the pathology of each patient. The goal of this model is to optimize insole manufacturing by adjusting stiffness and comfort according to individual needs;
- In addition, future research will expand the applicability of using MEX for producing other comfort products, such as custom seat supports or ergonomic cushions, which require variable properties of flexibility and durability. Studies will also explore other expandable filaments, assessing their suitability not only for insoles, but also for other comfort solutions. The investigation will include tests on hardness, comfort during prolonged use, fatigue life and breathability;
- Furthermore, new aspects regarding the performance of insoles in humid conditions will be tested to evaluate the materials' resistance and the impact on thermal comfort. This will provide additional information for the optimal selection of filament, aiming to develop personalized and accessible solutions for comfort and health;
- A future research direction will address the sustainability of the materials used, exploring biodegradable or recyclable filaments for insoles and other comfort products. These materials will be evaluated for printability, mechanical performance, and comfort, contributing to reducing ecological impact and promoting innovative, personalized, and sustainable solutions.
- An important future research direction may involve automating insole customization through artificial intelligence and machine learning. These technologies will correlate plantar pressure data with material variability and process parameters, optimizing design and production for each user.

Bibliography

1. Asociația de Podiatrie Available online: <https://podiatrie.ro/despre-podiatrie/> (accessed on 7 April 2024).
2. Pedorthic Association Of Australia Available online: <https://pedorthics.org.au/about-pedorthics/> (accessed on 7 April 2024).
3. Foot Orthotic Insoles Market - Fortune Business Insights Available online: <https://www.fortunebusinessinsights.com/industry-reports/foot-orthotic-insoles-market-100348> (accessed on 22 July 2024).
4. Global Market Size, Forecast, and Trend Highlights Over 2024 - 2036 Available online: <https://www.researchnester.com/reports/foot-orthotic-insoles-market/4528> (accessed on 22 July 2024).
5. Grand View Research - Foot Orthotic Insoles Market Size, Share & Trends Analysis Report By Material (Thermoplastic, Composite Carbon Fiber, Others), By Type (Pre-Fabricated, Custom-Made), By Distribution Channel, By Region, And Segment Forecasts, 2023 - 2030 Available online: <https://www.grandviewresearch.com/industry-analysis/foot-orthotic-insoles-market> (accessed on 30 April 2024).
6. Amer, A.O.; Jarl, G.M.; Hermansson, L.N. The Effect of Insoles on Foot Pain and Daily Activities. *Prosthet Orthot Int* **2014**, *38*, 474–480, doi:10.1177/0309364613512369.
7. Nagano, H.; Begg, R. Shoe-Insole Technology for Injury Prevention in Walking. *Sensors* **2018**, *18*, 1468, doi:10.3390/s18051468.
8. Park, J.-H.; Jeon, H.-S.; Kim, J.-H.; Yoon, H.-B.; Lim, O.-B.; Jeon, M. Immediate Effect of Insoles on Balance in Older Adults. *The Foot* **2021**, *47*, 101768, doi:10.1016/j.foot.2020.101768.
9. Hatton, A.L.; Gane, E.M.; Maharaj, J.N.; Burns, J.; Paton, J.; Kerr, G.; Rome, K. Textured Shoe Insoles to Improve Balance Performance in Adults with Diabetic Peripheral Neuropathy: Study Protocol for a Randomised Controlled Trial. *BMJ Open* **2019**, *9*, doi:10.1136/bmjopen-2018-026240.
10. Ahmed, S.; Barwick, A.; Butterworth, P.; Nancarrow, S. Footwear and Insole Design Features That Reduce Neuropathic Plantar Forefoot Ulcer Risk in People with Diabetes: A Systematic Literature Review. *J Foot Ankle Res* **2020**, *13*, doi:10.1186/s13047-020-00400-4.
11. Huang, Y.; Peng, H.-T.; Wang, X.; Chen, Z.-R.; Song, C.-Y. The Arch Support Insoles Show Benefits to People with Flatfoot on Stance Time, Cadence, Plantar Pressure and Contact Area. *PLoS One* **2020**, *15*, e0237382, doi:10.1371/journal.pone.0237382.
12. Zhang, Z.; Dai, Y.; Xu, Z.; Grimaldi, N.; Wang, J.; Zhao, M.; Pang, R.; Sun, Y.; Gao, S.; Boyi, H. Insole Systems for Disease Diagnosis and Rehabilitation: A Review. *Biosensors (Basel)* **2023**, *13*, 833, doi:10.3390/bios13080833.

13. Anderson, J.; Williams, A.E.; Nester, C. Development and Evaluation of a Dual Density Insole for People Standing for Long Periods of Time at Work. *J Foot Ankle Res* **2020**, *13*, doi:10.1186/s13047-020-00402-2.
14. Ko, M.; Ma, T.; Xiong, S. Acute Effects of Carbon Fiber Insole on Three Aspects of Sports Performance, Lower Extremity Muscle Activity, and Subjective Comfort. *Sensors* **2023**, *23*, 2154, doi:10.3390/s23042154.
15. Wang, Y.; Lam, W.-K.; Cheung, C.-H.; Leung, A.K.-L. Effect of Red Arch-Support Insoles on Subjective Comfort and Movement Biomechanics in Various Landing Heights. *Int J Environ Res Public Health* **2020**, *17*, 2476, doi:10.3390/ijerph17072476.
16. Iacob, M.C.; Popescu, D.; Petcu, D.; Marinescu, R. Assessment of the Flexural Fatigue Performance of 3D-Printed Foot Orthoses Made from Different Thermoplastic Polyurethanes. *Applied Sciences* **2023**, *13*, 12149, doi:10.3390/app132212149.
17. Prakotmongkol, V.; Chaemkhuntod, C.; Nutchamong, Y.; Charoenvitvorakul, T.; Tongchai, S.; Janvikul, W.; Thavornnyutikarn, B.; Kosorn, W.; Praewpipat, B. Comparison of Effectiveness, Patient Satisfaction, and Durability between 3D-Printed Customized Insoles and Conventional Custom-Made Insoles for Flat Feet: A Randomized Controlled Trial. **2023**.
18. EVO Laboratoire Available online: <https://laboratoirevo.com/en/benefits-of-orthosis-made-by-3d-printing> (accessed on 7 April 2024).
19. Alina Dragomir *Confortul Pictorului*; 2022;
20. Mariana Cristiana, I.; Diana, P.; Tudor George, A. Printability of Thermoplastic Polyurethane with Low Shore A Hardness in the Context of Customized Insoles Production. *UPB Scientific Bulletin, Series D* **2024**, *86*.
21. Iacob, M.C.; Popescu, D.; Stochioiu, C.; Baciu, F.; Hadar, A. Compressive Behavior of Thermoplastic Polyurethane with an Active Agent Foaming for 3D-Printed Customized Comfort Insoles. *Polym Test* **2024**, *137*, 108517, doi:10.1016/j.polymertesting.2024.108517.
22. Giza, E.; Cush, G.; Schon, L.C. The Flexible Flatfoot in the Adult. *Foot Ankle Clin* **2007**, *12*, 251–271, doi:10.1016/j.fcl.2007.03.008.
23. Francisco, R.; Chiodo, C.P.; Wilson, M.G. Management of the Rigid Adult Acquired Flatfoot Deformity. *Foot Ankle Clin* **2007**, *12*, 317–327, doi:10.1016/j.fcl.2007.03.013.
24. Michaud, T.C. Foot Orthoses and Other Forms of Conservative Foot Care.; 1997.
25. Jeffcoate, W.J.; Harding, K.G. Diabetic Foot Ulcers. *The Lancet* **2003**, *361*, 1545–1551, doi:10.1016/S0140-6736(03)13169-8.
26. Ma, Z.; Lin, J.; Xu, X.; Ma, Z.; Tang, L.; Sun, C.; Li, D.; Liu, C.; Zhong, Y.; Wang, L. Design and 3D Printing of Adjustable Modulus Porous Structures for Customized Diabetic Foot Insoles. *International Journal of Lightweight Materials and Manufacture* **2019**, *2*, 57–63, doi:10.1016/j.ijlmm.2018.10.003.
27. Shaikh, S.; Jamdade, B.; Chanda, A. Effects of Customized 3D-Printed Insoles in Patients with Foot-Related Musculoskeletal Ailments—A Survey-Based Study. *Prosthesis* **2023**, *5*, 550–561, doi:10.3390/prosthesis5020038.
28. Segal, A.; Rohr, E.; Orendurff, M.; Shofer, J.; O'Brien, M.; Sangeorzan, B. The Effect of Walking Speed on Peak Plantar Pressure. *Foot Ankle Int* **2004**, *25*, 926–933, doi:10.1177/107110070402501215.
29. Buldt, A.K.; Forghany, S.; Landorf, K.B.; Levinger, P.; Murley, G.S.; Menz, H.B. Foot Posture Is Associated with Plantar Pressure during Gait: A Comparison of Normal, Planus and Cavus Feet. *Gait Posture* **2018**, *62*, 235–240, doi:10.1016/j.gaitpost.2018.03.005.
30. Gupta, S.; Jayaraman, R.; Sidhu, S.; Malviya, A.; Chatterjee, S.; Chhikara, K.; Singh, G.; Chanda, A. Diabetic Development of a Diabetic Foot Pressure Tracking Device. *J (Basel)* **2023**, *6*, 32–47, doi:10.3390/j6010003.
31. Bacarin, T.A.; Sacco, I.C.N.; Hennig, E.M. Plantar Pressure Distribution Patterns During Gait in Diabetic Neuropathy Patients with a History of Foot Ulcers. *Clinics* **2009**, *64*, 113–120, doi:10.1590/S1807-59322009000200008.
32. Surmen, H.; Ortes, F.; Arslan, Y.Z. Design and Production of Subject Specific Insole Using Reverse Engineering and 3D Printing Technology. **2016**, *5*, 11–15, doi:10.6084/m9.figshare.19729495.
33. Choo, Y.J.; Boudier-Revéret, M.; Chang, M.C. 3D Printing Technology Applied to Orthosis Manufacturing: Narrative Review. *Ann Palliat Med* **2020**, *9*, 4262–4270, doi:10.21037/apm-20-1185.
34. Hastings, M.K.; Mueller, M.J.; Woodburn, J.; Strube, M.J.; Commear, P.; Johnson, J.E.; Cheuy, V.; Sinacore, D.R. Acquired Midfoot Deformity and Function in Individuals with Diabetes and Peripheral Neuropathy. *Clinical Biomechanics* **2016**, *32*, 261–267, doi:10.1016/j.clinbiomech.2015.11.001.
35. Ferreira, R.C.; Gonçalves, D.H.; Filho, J.M.F.; Costa, M.T.; Santin, R.A.L. Midfoot Charcot Arthropathy In Diabetic Patients: Complication Of An Epidemic Disease. *Revista Brasileira de Ortopedia (English Edition)* **2012**, *47*, 616–625, doi:10.1016/S2255-4971(15)30013-6.
36. Najafi, B.; Wrobel, J.S.; Burns, J. Mechanism of Orthotic Therapy for the Painful Cavus Foot Deformity. *J Foot Ankle Res* **2014**, *7*, doi:10.1186/1757-1146-7-2.
37. Shaikh, S.; Jamdade, B.; Chanda, A. Effects of Customized 3D-Printed Insoles in Patients with Foot-Related Musculoskeletal Ailments—A Survey-Based Study. *Prosthesis* **2023**, *5*, 550–561, doi:10.3390/prosthesis5020038.
38. Xu, J.; Ding, L.; Love, P.E.D. Digital Reproduction of Historical Building Ornamental Components: From 3D Scanning to 3D Printing. *Autom Constr* **2017**, *76*, 85–96, doi:10.1016/j.autcon.2017.01.010.
39. Cha, Y.H.; Lee, K.H.; Ryu, H.J.; Joo, I.W.; Seo, A.; Kim, D.-H.; Kim, S.J. Ankle-Foot Orthosis Made by 3D Printing Technique and Automated Design Software. *Appl Bionics Biomech* **2017**, *2017*, 1–6, doi:10.1155/2017/9610468.
40. Schrank, E.S.; Hitch, L.; Wallace, K.; Moore, R.; Stanhope, S.J. Assessment of a Virtual Functional Prototyping Process for the Rapid Manufacture of Passive-Dynamic Ankle-Foot Orthoses. *J Biomech Eng* **2013**, *135*, doi:10.1115/1.4024825.
41. Walbran, M.; Turner, K.; McDaid, A.J. Customized 3D Printed Ankle-Foot Orthosis with Adaptable Carbon Fibre Composite Spring Joint. *Cogent Eng* **2016**, *3*, 1227022, doi:10.1080/23311916.2016.1227022.
42. Aydin, L.; Kucuk, S. A Method for More Accurate FEA Results on a Medical Device Developed by 3D Technologies. *Polym Adv Technol* **2018**, *29*, 2281–2286, doi:10.1002/pat.4339.
43. Woolley, S.M.; Czaja, S.J.; Drury, C.G. An Assessment of Falls in Elderly Men and Women. *J Gerontol A Biol Sci Med Sci* **1997**, *52A*, M80–M87, doi:10.1093/gerona/52A.2.M80.
44. Wojciechowski, E.; Chang, A.Y.; Balassone, D.; Ford, J.; Cheng, T.L.; Little, D.; Menezes, M.P.; Hogan, S.; Burns, J. Feasibility of Designing, Manufacturing and Delivering 3D Printed Ankle-foot Orthoses: A Systematic Review. *J Foot Ankle Res* **2019**, *12*, doi:10.1186/s13047-019-0321-6.
45. Mavroidis, C.; Ranky, R.G.; Sivak, M.L.; Patrilli, B.L.; DiPisa, J.; Caddle, A.; Gilhooly, K.; Govoni, L.; Sivak, S.; Lancia, M.; et al. Patient Specific Ankle-Foot Orthoses Using Rapid Prototyping. *J Neuroeng Rehabil* **2011**, *8*, 1, doi:10.1186/1743-0003-8-1.
46. Creylman, V.; Muraru, L.; Pallari, J.; Vertommen, H.; Peeraer, L. Gait Assessment during the Initial Fitting of Customized Selective Laser Sintering Ankle Foot Orthoses in Subjects with Drop Foot. *Prosthet Orthot Int* **2013**, *37*, 132–138, doi:10.1177/0309364612451269.
47. Faustini, M.C.; Neptune, R.R.; Crawford, R.H.; Stanhope, S.J. Manufacture of Passive Dynamic Ankle-Foot Orthoses Using Selective Laser Sintering. *IEEE Trans Biomed Eng* **2008**, *55*, 784–790, doi:10.1109/TBME.2007.912638.
48. Schrank, E.S.; Stanhope, S.J. Dimensional Accuracy of Ankle-Foot Orthoses Constructed by Rapid Customization and Manufacturing Framework. *The Journal of Rehabilitation Research and Development* **2011**, *48*, 31, doi:10.1682/JRRD.2009.12.0195.
49. Telfer, S.; Pallari, J.; Munguia, J.; Dalgarno, K.; McGeough, M.; Woodburn, J. Embracing Additive Manufacture: Implications for Foot and Ankle Orthosis Design. *BMC Musculoskelet Disord* **2012**, *13*, 84, doi:10.1186/1471-2474-13-84.
50. Deckers, J.P.; Vermandel, M.; Geldhof, J.; Vasiliaskaite, E.; Forward, M.; Plasschaert, F. Development and Clinical Evaluation of Laser-Sintered Ankle Foot Orthoses. *Plastics, Rubber and Composites* **2018**, *47*, 42–46, doi:10.1080/14658011.2017.1413760.

51. Cha, Y.H.; Lee, K.H.; Ryu, H.J.; Joo, I.W.; Seo, A.; Kim, D.-H.; Kim, S.J. Ankle-Foot Orthosis Made by 3D Printing Technique and Automated Design Software. *Appl Bionics Biomech* **2017**, *2017*, 1–6, doi:10.1155/2017/9610468.
52. Shahar, F.S.; Sultan, M.T.H.; Shah, A.U.M.; Safri, S.N.A. A Comparative Analysis between Conventional Manufacturing and Additive Manufacturing of Ankle-Foot Orthosis. *Applied Science and Engineering Progress* **2020**.
53. SR ISO/ASTM 52900:2016 - Fabricație Aditivă. Principii Generale. Terminologie Available online: <https://www.iso.org/obp/ui/#iso:std:iso-astm:52900:ed-2:v1:en> (accessed on 7 April 2024).
54. DE Editors Transforming Ankle Foot Orthosis with 3D Printing Available online: <https://www.digitalengineering247.com/article/transforming-ankle-foot-orthosis-3d-printing/> (accessed on 7 April 2024).
55. Yick, K.L.; Tse, C.Y. Textiles and Other Materials for Orthopaedic Footwear Insoles. In *Handbook of Footwear Design and Manufacture*; Elsevier, 2013; pp. 341–371.
56. Daryabor, A.; Kobayashi, T.; Saeedi, H.; Lyons, S.M.; Maeda, N.; Naimi, S.S. Effect of 3D Printed Insoles for People with Flatfeet: A Systematic Review. *Assistive Technology* **2023**, *35*, 169–179, doi:10.1080/10400435.2022.2105438.
57. Xu, R.; Wang, Z.; Ren, Z.; Ma, T.; Jia, Z.; Fang, S.; Jin, H. Comparative Study of the Effects of Customized 3D Printed Insole and Prefabricated Insole on Plantar Pressure and Comfort in Patients with Symptomatic Flatfoot. *Medical Science Monitor* **2019**, *25*, 3510–3519, doi:10.12659/MSM.916975.
58. Mo, S.; Leung, S.H.S.; Chan, Z.Y.S.; Sze, L.K.Y.; Mok, K.-M.; Yung, P.S.H.; Ferber, R.; Cheung, R.T.H. The Biomechanical Difference between Running with Traditional and 3D Printed Orthoses. *J Sports Sci* **2019**, *37*, 2191–2197, doi:10.1080/02640414.2019.1626069.
59. Walker, K.J.; Przeźralski, B.T.; Kaluf, B.; Driggers, N.H.; Ballard, W.D.; Pruett, T.C.; Hoeffner, S.L.; DesJardins, J.D. Novel 3D-Printed Foot Orthoses with Variable Hardness: A Comfort Comparison to Traditional Orthoses. *Med Eng Phys* **2023**, *115*, 103978, doi:10.1016/j.medengphys.2023.103978.
60. Channasanon, S.; Praewpipat, B.; Duangjinda, N.; Sornchalerm, L.; Tesavibul, P.; Paecharoen, S.; Tanodekaew, S. 3D-Printed Medial Arch Supports of Varying Hardness versus a Prefabricated Arch Support on Plantar Pressure: A 1-Month Randomized Crossover Study in Healthy Volunteers. *Prosthet Orthot Int* **2023**, *47*, 210–217, doi:10.1097/PXR.000000000000178.
61. Jonnala, U.K.; sankineni, R.; Ravi Kumar, Y. Design and Development of Fused Deposition Modeling (FDM) 3D-Printed Orthotic Insole by Using Gyroid Structure. *J Mech Behav Biomed Mater* **2023**, *145*, 106005, doi:10.1016/j.jmbbm.2023.106005.
62. Rico-Baeza, G.; Pérez-Soto, G.I.; Morales-Hernández, L.A.; Cuan-Urquizo, E.; Camarillo-Gómez, K.A. Additively Manufactured Foot Insoles Using Body-Centered Cubic (BCC) and Triply Periodic Minimal Surface (TPMS) Cellular Structures. *Applied Sciences* **2023**, *13*, 12665, doi:10.3390/app132312665.
63. Siegkas, P.; Lane, C.; Apps, C. Plantar Pressure Distribution Using Personalised 3D Printed Lattice Insoles with Distributed Stiffness. *Engineering Research Express* **2024**, *6*, 025529, doi:10.1088/2631-8695/ad4435.
64. Kang, L.-P.; Gong, T.-S. Design of 3D Printed Pressure-Reducing Insoles Based on Changes in Parameters of Lattice Structure. *Advances in Mechanical Engineering* **2023**, *15*, doi:10.1177/16878132231216609.
65. Kumar, R.; Sarangi, S.K. 3D Printed Customized Diabetic Foot Insoles with Architecture Designed Lattice Structures – a Case Study. *Biomed Phys Eng Express* **2024**, *10*, 015019, doi:10.1088/2057-1976/ad1732.
66. Hudak, Y.F.; Li, J.-S.; Cullum, S.; Strzelecki, B.M.; Richburg, C.; Kaufman, G.E.; Abrahamson, D.; Heckman, J.T.; Ripley, B.; Telfer, S.; et al. A Novel Workflow to Fabricate a Patient-Specific 3D Printed Accommodative Foot Orthosis with Personalized Latticed Metamaterial. *Med Eng Phys* **2022**, *104*, 103802, doi:10.1016/j.medengphys.2022.103802.
67. Zoboli, L.; Bianchi, D.; Falcinelli, C.; Gizzi, A. Improving the Manufacturing of 3D Printed Insoles through a Combined Experimental and Topology Optimization Approach. *Mechanics of Advanced Materials and Structures* **2024**, 1–15, doi:10.1080/15376494.2024.2326667.
68. Ning, K.; Yick, K.-L.; Yu, A.; Yip, J. Effects of Textile-Fabricated Insole on Foot Skin Temperature and Humidity for Enhancing Footwear Thermal Comfort. *Appl Ergon* **2022**, *104*, 103803, doi:10.1016/j.apergo.2022.103803.
69. Ning, K.; Yick, K.-L.; Yu, A.; Yip, J. Effects of Textile-Fabricated Insole on Foot Skin Temperature and Humidity for Enhancing Footwear Thermal Comfort. *Appl Ergon* **2022**, *104*, 103803, doi:10.1016/j.apergo.2022.103803.
70. Leung, M.S.; Yick, K.; Sun, Y.; Chow, L.; Ng, S. 3D Printed Auxetic Heel Pads for Patients with Diabetic Mellitus. *Comput Biol Med* **2022**, *146*, 105582, doi:10.1016/j.compbiomed.2022.105582.
71. Rico-Baeza, G.; Pérez-Soto, G.I.; Morales-Hernández, L.A.; Cuan-Urquizo, E.; Camarillo-Gómez, K.A. Additively Manufactured Foot Insoles Using Body-Centered Cubic (BCC) and Triply Periodic Minimal Surface (TPMS) Cellular Structures. *Applied Sciences* **2023**, *13*, 12665, doi:10.3390/app132312665.
72. Geiger, F.; Keibach, M.; Vogel, D.; Weissmann, V.; Bader, R. Efficient Computer-Based Method for Adjusting the Stiffness of Subject-Specific 3D-Printed Insoles during Walking. *Applied Sciences* **2023**, *13*, 3854, doi:10.3390/app13063854.
73. Ebrahim, M. 3D Laser Scanners: History, Applications, And Future. **2014**, doi:10.13140/2.1.3331.3284.
74. Gensole Available online: <http://gensole.com/> (accessed on 7 April 2024).
75. SATRA Performance Footwear Testing Available online: https://www.youtube.com/watch?v=V-Tag1Gc8tY&ab_channel=SatraTechnologyCentre (accessed on 2 June 2024).
76. Whole Shoes Flexing Tester GT-KA01-2B Available online: https://www.youtube.com/watch?v=T2NDCQfkJyQ&ab_channel=GesterInstruments (accessed on 2 June 2024).
77. International Standard ISO 17707:2005 - Footwear - Test Methods for Outsoles - Flex Resistance Available online: <https://cdn.standards.iteh.ai/samples/31478/e04fdf9b056347b4bb0a39e85e9541e6/ISO-17707-2005.pdf> (accessed on 7 April 2024).
78. Popescu, D.; Gheorghe Amza, C.; Marinescu, R.; Cristiana Iacob, M.; Luminița Căruțașu, N. Investigations on Factors Affecting 3D-Printed Holes Dimensional Accuracy and Repeatability. *Applied Sciences* **2022**, *13*, 41, doi:10.3390/app13010041.
79. Nancharaiah, T.; Raju, D.; Raju, V. An Experimental Investigation on Surface Quality and Dimensional Accuracy of FDM Components. *Int J Emerg Technol* **2010**, *1*.
80. Zhu, Q.; Liu, Y.; Cai, Y.; Wu, M. Research on the Shrinkage of Model with Hole in PLA Material Based on the FDM 3D Printing. In Proceedings of the Proceedings of the 2017 6th International Conference on Measurement, Instrumentation and Automation (ICMIA 2017); Atlantis Press: Paris, France, 2017.
81. Buj-Corral, I.; Bagheri, A.; Sivatte-Adroer, M. Effect of Printing Parameters on Dimensional Error, Surface Roughness and Porosity of FFF Printed Parts with Grid Structure. *Polymers (Basel)* **2021**, *13*, 1213, doi:10.3390/polym13081213.
82. Hernandez, D. Factors Affecting Dimensional Precision of Consumer 3D Printing. *International Journal of Aviation, Aeronautics, and Aerospace* **2015**, doi:10.15394/ijaaa.2015.1085.
83. Amza, C.G.; Zapciu, A.; Baciu, F.; Vasile, M.I.; Popescu, D. Aging of 3D Printed Polymers under Sterilizing UV-C Radiation. *Polymers (Basel)* **2021**, *13*, 4467, doi:10.3390/polym13244467.
84. Lin, W.; Xie, G.; Qiu, Z. Effects of Ultraviolet Aging on Properties of Wood Flour–Poly(Lactic Acid) 3D Printing Filaments. *Bioresources* **2019**.
85. Amza, C.G.; Zapciu, A.; Baciu, F.; Vasile, M.I.; Nicoară, A.I. Accelerated Aging Effect on Mechanical Properties of Common 3D-Printing Polymers. *Polymers (Basel)* **2021**, *13*.

86. Hernandez, D. Factors Affecting Dimensional Precision of Consumer 3D Printing. *International Journal of Aviation, Aeronautics, and Aerospace* **2015**, doi:10.15394/ijaaa.2015.1085.
87. Herath, H.M.D.B.; Thalagala, S.; Gamage, P. Enhancing the Dimensional Accuracy of Components Fabricated Using Rapid Prototyping Technique by Optimizing Machine Parameters of a 3D Printer. In Proceedings of the 2019 IEEE International Conference on Industrial Engineering and Engineering Management (IEEM); IEEE, December 2019; pp. 1379–1383.
88. Zhu, Q.; Liu, Y.; Cai, Y.; Wu, M. Research on the Shrinkage of Model with Hole in PLA Material Based on the FDM 3D Printing. In Proceedings of the Proceedings of the 2017 6th International Conference on Measurement, Instrumentation and Automation (ICMIA 2017); Atlantis Press: Paris, France, 2017.
89. Pearson, E.J.M. Comfort and Its Measurement – A Literature Review. *Disabil Rehabil Assist Technol* **2009**, *4*, 301–310, doi:10.1080/17483100902980950.
90. Kromołowska, K.; Kluza, K.; Kańtoch, E.; Sulikowski, P. Open-Source Strain Gauge System for Monitoring Pressure Distribution of Runner's Feet. *Sensors* **2023**, *23*, 2323, doi:10.3390/s23042323.
91. Pressure Mapping FS-INS-16Z Foot Pressure Distribution. LEGACT - Leading Force Sensing Technology Solution Provider Available online: <https://film-sensor.com/product/pressure-mapping-fs-ins-16z> (accessed on 7 April 2024).
92. McKeen, L.W. Environmentally Friendly Polymers. In *Permeability Properties of Plastics and Elastomers*; Elsevier, 2012; pp. 287–304.
93. Reshmy, R.; Philip, E.; Vaisakh, P.H.; Sindhu, R.; Binod, P.; Madhavan, A.; Pandey, A.; Sirohi, R.; Tarafdar, A. Biodegradable Polymer Composites. In *Biomass, Biofuels, Biochemicals*; Elsevier, 2021; pp. 393–412.
94. TPU Filament Filaflex 60A, Flexible Filament for 3d Printing. Recreus. Available online: <https://recreus.com/gb/filaments/1-filaflex-60a.html> (accessed on 7 April 2024).
95. TPU Filament Filaflex 70A, Flexible Filament for 3D Printing. Recreus Available online: <https://recreus.com/gb/filaments/6-filaflex-70a.html> (accessed on 7 April 2024).
96. TPU Filament Filaflex 82A, Flexible Filament for 3D Printing. Recreus. Available online: <https://recreus.com/gb/filaments/9-684-filaflex-82a.html> (accessed on 7 April 2024).
97. MerchantPro. Filament Polymaker PolyFlex TPU-90A Teal (Turcoaz) 750g. Filamente 3D. Available online: <https://www.filamente3d.ro/filamente/filament-polymaker-polyflex-tpu-90a-teal-turcoaz-750g> (accessed on 7 April 2024).
98. Damanpack, A.R.; Sousa, A.; Bodaghi, M. Porous PLAs with Controllable Density by FDM 3D Printing and Chemical Foaming Agent. *Micromachines (Basel)* **2021**, *12*, 866, doi:10.3390/mi12080866.
99. Crowe, S.; Maxwell, S.; Brar, H.; Yu, L.; Kairn, T. Use of Light-Weight Foaming Poly(lactic acid) as a Lung-Equivalent Material in 3D Printed Phantoms. *Phys Eng Sci Med* **2023**, *46*, 1811–1817, doi:10.1007/s13246-023-01318-4.
100. Kalaycıoğlu, Ş.G. Mechanical Behaviour Of Polymeric Lattice Structures Produced By Additive Manufacturing. Master of Science, Middle East Technical University, 2022.
101. Hermann, S. Testing ColorFabb VarioShore TPU - Foaming 3D Printing Filament. Available online: <https://www.cnkitchen.com/blog/testing-colorfabb-varioshore-tpu-foaming-3d-printing-filament> (accessed on 7 April 2024).
102. Popescu, D.; Lăptoiu, D.; Marinescu, R.; Botezatu, I. Design and 3D Printing Customized Guides for Orthopaedic Surgery – Lessons Learned. *Rapid Prototyp J* **2018**, *24*, 901–913, doi:10.1108/RPJ-05-2017-0099.
103. Wang, Z.; Dubrowski, A. A Semi-Automatic Method to Create an Affordable Three-Dimensional Printed Splint Using Open-Source and Free Software. *Cureus* **2021**, doi:10.7759/cureus.13934.
104. Chatzistergos, P.E.; Gatt, A.; Formosa, C.; Farrugia, K.; Chockalingam, N. Optimised Cushioning in Diabetic Footwear Can Significantly Enhance Their Capacity to Reduce Plantar Pressure. *Gait Posture* **2020**, *79*, 244–250, doi:10.1016/j.gaitpost.2020.05.009.
105. Pivar, M.; Gregor-Svetec, D.; Muck, D. Effect of Printing Process Parameters on the Shape Transformation Capability of 3D Printed Structures. *Polymers (Basel)* **2021**, *14*, 117, doi:10.3390/polym14010117.
106. ColorFabb VarioShore TPU Available online: https://colorfabb.com/media/datasheets/tds/colorfabb/TDS_E_ColorFabb_varioShore_TPU.pdf (accessed on 7 April 2024).
107. Nofar, M.; Utz, J.; Geis, N.; Altstädt, V.; Ruckdäschel, H. Foam 3D Printing of Thermoplastics: A Symbiosis of Additive Manufacturing and Foaming Technology. *Advanced Science* **2022**, *9*, doi:10.1002/advs.202105701.
108. Sun, B.; Wu, L. Research Progress of 3D Printing Combined with Thermoplastic Foaming. *Front Mater* **2022**, *9*, doi:10.3389/fmats.2022.1083931.
109. Popescu, D.; Iacob, M.C.; Tarbă, C.; Lăptoiu, D.; Cotruț, C.M. Exploring a Novel Material and Approach in 3D-Printed Wrist-Hand Orthoses. *Journal of Manufacturing and Materials Processing* **2024**, *8*, 29, doi:10.3390/jmmp8010029.
110. Paluch, A.E.; Gabriel, K.P.; Fulton, J.E.; Lewis, C.E.; Schreiner, P.J.; Sternfeld, B.; Sidney, S.; Siddique, J.; Whitaker, K.M.; Carnethon, M.R. Steps per Day and All-Cause Mortality in Middle-Aged Adults in the Coronary Artery Risk Development in Young Adults Study. *JAMA Netw Open* **2021**, *4*, e2124516, doi:10.1001/jamanetworkopen.2021.24516.
111. ISO 7619-1:2004 - Rubber, Vulcanized or Thermoplastic — Determination of Indentation Hardness — Part 1: Durometer Method (Shore Hardness). Available online: <https://www.iso.org/standard/31078.html> (accessed on 7 April 2024).
112. Birke, J.A.; Foto, J.G.; Pfeifer, L.A. Effect of Orthosis Material Hardness on Walking Pressure in High-Risk Diabetes Patients. *JPO: Journal of Prosthetics and Orthotics* **1999**, *11*.
113. Brodsky, J.W.; Pollo, F.E.; Cheleuitte, D.; Baum, B.S. Physical Properties, Durability, and Energy-Dissipation Function of Dual-Density Orthotic Materials Used in Insoles for Diabetic Patients. *Foot Ankle Int* **2007**, *28*, 880–889, doi:10.3113/FAI.2007.0880.
114. Rubber, Vulcanized or Thermoplastic - Determination of Compression Stress-Strain Properties ISO 7743:2017. Available online: <https://www.iso.org/standard/72784.html> (accessed on 7 April 2024).
115. León-Calero, M.; Reyburn Valés, S.C.; Marcos-Fernández, Á.; Rodríguez-Hernandez, J. 3D Printing of Thermoplastic Elastomers: Role of the Chemical Composition and Printing Parameters in the Production of Parts with Controlled Energy Absorption and Damping Capacity. *Polymers (Basel)* **2021**, *13*, 3551, doi:10.3390/polym13203551.
116. Płatek, P.; Rajkowski, K.; Cieplak, K.; Sarzyński, M.; Małachowski, J.; Woźniak, R.; Janiszewski, J. Deformation Process of 3D Printed Structures Made from Flexible Material with Different Values of Relative Density. *Polymers (Basel)* **2020**, *12*, 2120, doi:10.3390/polym12092120.
117. Bean, P.; Lopez-Anido, R.A.; Vel, S. Numerical Modeling and Experimental Investigation of Effective Elastic Properties of the 3D Printed Gyroid Infill. *Applied Sciences* **2022**, *12*, 2180, doi:10.3390/app12042180.